# Engineered Materials Characterization Report for the Yucca Mountain Site Characterization Project

Volume 3 Revision 1
Corrosion Data and Modeling

R. Daniel McCright

April 1, 1997

Engineered Materials Characterization Report for the Yucca Mountain Site Characterization Project

Volume 3
Revision 1
Corrosion Data and Modeling

by R. Daniel McCright
Lawrence Livermore National Laboratory
April 1997

Volume 3 (Rev. 1 April 1997)

Table of Contents

Preface (April 30, 1997)

This report of the revised Volume 3 of the Engineered Materials Characterization Report (EMCR) is a Yucca Mountain Project deliverable. This report will also be published as a UCRL report. The present report is similar to the one made as an August 1996 project deliverable with additional test results and descriptions made since that time. The present report includes responses to review comments made by the DOE and other M&O organization members on the August 1996 draft. The Performance Assessment group reviewed this material in February 1997 and an additional review was conducted on the new material by DOE/YMSCO in March 1997. Further revision is scheduled to be made to the EMCR as test data becomes available and as model development proceeds in succeeding years.

This report generally reflects the level of effort in each WBS element and in each technical activity. There is some unevenness, because more progress has been made in some activities than in others. For instance in Section 2.6, a great deal of effort has been made in cataloguing the microbial species that will be used in corrosion studies, most of which are just getting underway. Also, as discussed in Section 2.4 much time and effort has been expended in building the test facility. Testing is underway but the first results will come after six-months of exposure. Some of the technical activities require a large outlay of expenditures to purchase specimens, equipment, and instrumentation. Restricted funding has delayed some of the progress. These activities also require a great amount of time in setting up the equipment. Therefore, certain "thin" sections of this report act as a sort of "place holder" where planned work will eventually fill these sections in future revisions.

While modeling of all the pertinent corrosion phenomena is planned, to date the effort has centered on low temperature oxidation modeling of the outer barrier (Section 2.10) and pitting corrosion of the inner barrier (Section 2.11). A series of Performance Assessment workshops was organized in the late 1996 - early 1997 time period. During these workshops, some rethinking of the organization of the corrosion modeling effort occurred, mainly to establish more integrated models between the different modes of corrosion. This effort will be reflected in the work reported in future revisions of the EMCR.

1.0 Introduction

The Engineered Materials Characterization Report (EMCR) serves as a source of information on the properties of materials proposed as elements in the engineered barrier system (EBS) for the Yucca Mountain nuclear waste repository. The initial version of this report was compiled in December 1994. In the initial version, the report was divided into three volumes: Volume 1 covered the background and history of the materials effort. Volume 2 covered the properties of materials of paramount interest to the waste package design effort. Volume 3 covered the corrosion data and modeling efforts. The present report is a revision to Volume 3 and updates information on the corrosion (and other degradation modes) behavior of candidate materials for the various components of the EBS. It also includes work on the performance modeling of these materials. The contents of Volumes 1 and 2 are not being revised at this time. Most of the effort has historically been and continues to emphasize the metallic barrier materials for the waste package container. However, work was begun in FY-95 on the "basket" materials that will control criticality in the large, multiple-assembly spent nuclear fuel waste packages. In FY-96, work was begun on evaluating materials that would be emplaced outside the waste package, but which would function as part of the EBS. These materials have generally been placed under the category of "backfill", although they may properly be serving as a packing, backfill, or invert materials, as will be explained later. Some work was funded in FY-94 on non-metallic barriers, but has not been actively funded since that time. The accomplishments of the FY-94 were written in a survey report. A summary of that report is included in this revision of EMCR Volume 3.

The current waste package design focuses on a multiple barrier container, consisting of an outer barrier made from a corrosion allowance material and an inner barrier made from a corrosion resistant material. Multiple barrier containers will be used for packages containing spent nuclear fuel and for those containing high level vitrified waste. The principle is that the different types of barrier materials will respond quite differently to the changes of environments that will occur over the very long time periods of concern for waste containment. An important part of the waste isolation strategy at Yucca Mountain is to design the waste package repository so that the environment surrounding the waste packages remains warm and dry for a very lengthy period. The thick outer barrier of the waste package (on the order of 10 cm thick) is expected to slowly oxidize under these conditions. As the temperature drops and conditions become progressively more humid, a point is reached where aqueous corrosion effects may develop. Corrosion allowance materials, such as carbon steel, are proposed for the outer barrier, and these materials would withstand the low temperature oxidation and would corrode at moderate rates once they are wet.

Depending on how aggressive the water is to the steel (and this depends largely on the chemical composition of the water), the outer barrier would eventually be breached in places, exposing the inner barrier to the environment. The inner barrier is proposed to be made from a highly corrosion resistant material. Currently, a number of nickel-base and titanium-base materials are under consideration for the inner barrier. The individual

electrochemical corrosion potentials of the inner and outer barriers are expected to be quite different, such that the outer barrier will be the anode and the inner barrier, the cathode when the metals are in electrical contact with one another. Thus, the outer barrier is expected to "cathodically protect" (same meaning as galvanically protect) the inner barrier for as long as some of the outer barrier material remains. The efficiency of the protection depends on how the two materials are bonded or otherwise connected and characteristics of the environment to distribute the electrolytic current between the two metals. The cathodic protection protects against general corrosion (rate of general corrosion is expected to be very small even without cathodic protection), and, more importantly, against localized corrosion. However, there are some complications that may arise, and these are discussed in the section on galvanic interactions.

Once the outer barrier is corroded away, the inner barrier is subject to attack by the environment. The inner barrier is designed to be around 2 cm in thickness. Again, depending on the severity of the water chemistry and choice of material, the corrosive attack may be extremely modest and provide for a very long life, but of greater concern is the possibility of localized corrosion (e.g. pitting or crevice attack) or stress corrosion cracking. Several activities in the testing program are directed to determining whether these forms of corrosion will limit the container performance.

In much the same way that the appearance of a water film on a metal surface exposed in a sufficiently humid atmosphere marks the beginning of the electrolytic processes of aqueous corrosion, the water film also supports microbiological life. In the hot, dry repository, microbiologically influenced corrosion (MIC) seems an impossibility, but as temperatures cool and humidities rise, MIC becomes a real possibility. As will be discussed in the section on MIC, several different microbial species attack corrosion allowance materials, like carbon steel. There are fewer kinds attacking the corrosion resistant materials, but MIC evaluation remains one of the important areas of study in evaluating candidate materials.

Potential problems associated with the welds or with embrittled microstructures can occur throughout the containment period. Phase instability leading to embrittlement is one such cause, and many times the brittle phases preferentially form in and around the welds. Also, undetected weld cracks may grow after container emplacement in the repository. Temperature and strain in the metal may affect the propensity toward brittle phase formation. Unrelieved residual stress in the welded areas is a source of strain that may affect metallurgical transformations. Environmental factors, such as hydrogen production during electrochemical reactions, may also play a role in affecting cracking in and around the welds.

The sequence of *possible* container degradation events is shown in Figure 1 - 1. Efforts in waste package design, container materials selection, and container fabrication/welding process specifications have the obvious goal to eliminate some of these degradation modes or to reduce their probability to within the limits of "substantially complete containment". The waste package container materials testing and modeling work is

organized to resolve the technical issues surrounding corrosion and other degradation modes. This has been the basis of the Metallic Barriers Scientific Investigation Plan (SIP), which is the main planning document for the various technical activities supporting materials evaluation. The SIP is briefly described in the next section, and then the progress made on the individual activities is detailed. Most of the effort to date has been in the Metallic Barriers task dealing with the waste package multi-barrier container, and this work is discussed in Section 2.0 Then, the materials work on other parts of the engineered barrier system is discussed, in Sections 3.0, 4.0, and 5.0.

Figure 1-1 Schematic illustrating temperature regimes within which various degradation modes could *potentially* affect the two-barrier waste package container. The temperature and time scales represent a high mass load (>80 MTU/acre) case for the projection of the thermal profile of a spent fuel waste package. The particular time frame of interest is the time when the container surface temperature reaches the boiling point of water. This is estimated to occur sometime between 1000 and 10,000 years after emplacement of the waste package.

2.0 Waste Package Container Materials

2.1 Metallic Barriers Scientific Investigation Plan

A completely revised metallic barriers Scientific Investigation Plan (SIP) was prepared in December 1994. This revision was necessary because of the change in the waste package container design from a single-metal, thin-walled container to a multiple barrier, thick waste package. All of the planned technical activities were reorganized and rather detailed descriptions were written for each activity. The SIP further discusses the interfaces between the metallic barrier work and the work proceeding in other parts of the project, particularly Waste Package Design (WBS 1.2.2.3), Performance Assessment,(1.2.5.4), Near-Field Environment (1.2.3.10), and Waste Form (1.2.2.4) and the kinds of information transmitted from one part of the project to another. The EMCR is one of the vehicles of transmission of information from the Metallic Barriers work, as well as work on the other EBS materials, to the other parts of the project. The waste form work [1] and the near-field environment work [2] also produce similar types of comprehensive reports transmitting information, and like the EMCR they are periodically revised. The waste package design effort also produces periodic reports [3], summarizing and detailing the many aspects of its work. Of particular interest to the waste package materials work is the processes that will be used to fabricate and weld the multiple barrier container.

The SIP was then again revised in June 1995, but this revision was relatively minor and involved some rearrangement of the technical activities. The current version is SIP CM-01, Rev 3 [4]. There are four major categories of activities in the SIP.

(1) Degradation Mode Surveys (DMS) and Information Bases (IB)

This group of activities is a consolidation of available information related to the expected performance of candidate materials. Degradation mode surveys center on the collection of information on failure modes of materials, notably the various forms of corrosion, but also include oxidation and embrittlement phenomena and evaluate this information as it pertains to Yucca Mountain. Information bases are collections of information on properties of candidate materials, such as physical and mechanical properties, that are important to the waste package design and materials evaluation activities.

(2) Corrosion Testing and Physical Properties Evaluation

This area comprises the largest effort in the Metallic Barrier task. Because of the multiple barrier nature of the waste package design and a number of options for design of the repository, a comprehensive testing program is needed to evaluate the performance of materials under a wide range of repository environmental conditions. Several candidate materials are under consideration for the container. Multiple barriered configurations of the waste package container are comprised of an outer barrier made of a corrosion

2.0 Waste Package Container Materials

2.1 Metallic Barriers Scientific Investigation Plan

A completely revised metallic barriers Scientific Investigation Plan (SIP) was prepared in December 1994. This revision was necessary because of the change in the waste package container design from a single-metal, thin-walled container to a multiple barrier, thick waste package. All of the planned technical activities were reorganized and rather detailed descriptions were written for each activity. The SIP further discusses the interfaces between the metallic barrier work and the work proceeding in other parts of the project, particularly Waste Package Design (WBS 1.2.2.3), Performance Assessment,(1.2.5.4), Near-Field Environment (1.2.3.10), and Waste Form (1.2.2.4) and the kinds of information transmitted from one part of the project to another. The EMCR is one of the vehicles of transmission of information from the Metallic Barriers work, as well as work on the other EBS materials, to the other parts of the project. The waste form work [1] and the near-field environment work [2] also produce similar types of comprehensive reports transmitting information, and like the EMCR they are periodically revised. The waste package design effort also produces periodic reports [3], summarizing and detailing the many aspects of its work. Of particular interest to the waste package materials work is the processes that will be used to fabricate and weld the multiple barrier container.

The SIP was then again revised in June 1995, but this revision was relatively minor and involved some rearrangement of the technical activities. The current version is SIP CM-01, Rev 3 [4]. There are four major categories of activities in the SIP.

(1) Degradation Mode Surveys (DMS) and Information Bases (IB)

This group of activities is a consolidation of available information related to the expected performance of candidate materials. Degradation mode surveys center on the collection of information on failure modes of materials, notably the various forms of corrosion, but also include oxidation and embrittlement phenomena and evaluate this information as it pertains to Yucca Mountain. Information bases are collections of information on properties of candidate materials, such as physical and mechanical properties, that are important to the waste package design and materials evaluation activities.

(2) Corrosion Testing and Physical Properties Evaluation

This area comprises the largest effort in the Metallic Barrier task. Because of the multiple barrier nature of the waste package design and a number of options for design of the repository, a comprehensive testing program is needed to evaluate the performance of materials under a wide range of repository environmental conditions. Several candidate materials are under consideration for the container. Multiple barriered configurations of the waste package container are comprised of an outer barrier made of a corrosion

allowance material and an inner barrier made of a corrosion resistant material. Different concerns are addressed for each barrier in the testing program.

(3) Model Development of Performance Behavior

This group of activities serves two major purposes. One major purpose is to support the materials recommendations. A key selection criterion is the predictability of the performance of the material. The second major purpose is to furnish the performance assessment effort with our best understanding of how the selected material will perform in the repository environment. To these ends, it is important to obtain repository-relevant data from the testing activities and to interpret these data with an understanding of the mechanisms of materials behavior.

(4) Materials Recommendations

Materials recommendations are one of the two primary applications of the work in this WBS. The recommendations are based on results of the other three groups of activities and on information and results obtained by other WBS elements, especially Waste Package Design.

The work discussed in the next sections is organized along these same general lines. Most work to date has been in the testing area, but some effort has been made in the modeling area as well. Preparation of degradation mode surveys is being completed, while most of the work on materials recommendation is in the future.

References for Section 2.1

1. R. B. Stout and H. R. Leider, "Preliminary Waste Form Characteristics Report," LLNL Report UCRL-ID 108314, December 1994

2. D. G. Wilder, "Preliminary Near Field Environment Report", Volumes 1 and 2, LLNL Report UCRL-LR 107476, June 1993

3. T. L. Lotz et al, "Waste Package/Engineered Barrier Segment Conceptual Design Report", TRW Report BBA000000-01717-5705-00006, rev 00A, October 1995

4. R. D. McCright, Metallic Barriers Scientific Investigation Plan, WBS 1.2.2.5.1, SIP CM-01, Revision 3, June 1996

2.2 Degradation Mode Surveys on Container Materials

Surveys of degradation modes of the different candidate materials were first begun for materials under consideration for the Site Characterization Plan -- Conceptual Design (SCP-CD) in 1987-88. This design was centered on a thin-walled container made from a single metal. Wall thicknesses on the order of 1 cm were under consideration, and the waste packages were smaller in diameter. Since some of the candidate materials for the SCP-CD are also candidate materials for the present multiple barrier design, these degradation mode surveys are still useful. The original set of degradation mode surveys comprised an eight volume set covering austenitic alloys (including Alloy 825) and copper-base alloys (including 70/30 copper nickel)[1]. All corrosion-relevant factors considered, Alloy 825 (a Ni-Fe-Cr-Mo alloy) was superior to the austenitic stainless steels, and the 70/30 Cu/Ni was generally superior to the other copper-base alloys. For these reasons, these materials were carried as candidate materials for multiple barrier waste package containers.

Later, a degradation mode survey was prepared on four Ni-Cr-Mo alloys, including Alloys C-22, C-4, C-276, and 625.[2] All of these alloys show exceptional resistance to localized corrosion and stress corrosion cracking because of the high alloy content. The "critical potential" for localized corrosion attack in aggressive acidic chloride solutions increases with the molybdenum content of the alloy. All of these materials show excellent corrosion resistance to general, pitting, and crevice corrosion in sea water and in hot brines. They also appear to be immune from hydrogen embrittlement in the annealed condition, but they may be susceptible when strengthened by cold working or ageing and exposed to aggressive environments and coupled to an active metal (like carbon steel). With regard to phase stability, this survey concluded that Alloy C-4 is superior to Alloys C-22, C-276, and 625. Alloys C-22 and C-276 are susceptible to intermetallic and carbide precipitation. Alloy 625 is susceptible to carbide precipitation and microstructural ordering. Alloy C-4 appears to be the most resistant to adverse microstructural changes. Although the localized corrosion resistance may be similar for these alloys under long term repository conditions, the differences in phase instability and the manifestations of this instability in affecting either a brittle microstructure or one more prone to hydrogen embrittlement may be the most distinguishing feature of these alloys.

More recently, degradation modes of iron-based corrosion allowance materials were surveyed. [3] Based on this literature review, it appears that the addition of chromium significantly enhances the oxidation resistance in these materials. As to general corrosion resistance, the low alloy steels, plain carbon steels, and cast irons seem to corrode at similar rates when exposed to an aqueous environment. However, other factors beside the corrosion resistance are important in distinguishing among the various grades of steel and cast iron. These include several issues in the fabrication and welding of thick-sectioned containers.

Also, a degradation mode survey was compiled on some of the additional nickel-bearing candidate alloys that were not covered in previous literature reviews.[4] This included Alloy 400 (also called Monel 400), a Ni-Cu alloy, and Alloy G, including its derivatives. Alloy G is also called Hastelloy G and is a Ni-Fe-Cr-Mo alloy. Its most current modification is as Alloy G-3. Monel 400 is widely used in sea water applications because of its generally low general corrosion rate and resistance to chloride-induced stress corrosion cracking. When these alloys are compared to Alloy 825, Alloy G-3 shows usually better resistance to localized corrosion in aggressive environments. Lacking a Cr and Mo content, the localized corrosion resistance of Alloy 400 in aggressive media is much inferior to that of Alloys 825 and G-3. However, Alloy 400 merits consideration as an alternative (although more costly) to carbon steel for the outer barrier if environmental conditions corrode the steel at too high a rate. The overall corrosion resistance of Alloy 400 (and also that of 70/30 Cu/Ni) is intermediate between the Fe-base corrosion allowance and highly corrosion resistant materials.

A degradation mode survey was recently prepared on the galvanic corrosion effects between materials proposed as candidate materials for the outer barrier and for the inner barrier.[5] This survey cites references on carbon and low alloy steels, copper-nickel and nickel-copper alloys, stainless steels, nickel-rich stainless alloys, nickel-base alloys, and titanium and its alloys. An important item in determining container performance is whether corrosion of the outer barrier serves to protect the inner barrier, and for how long this protection may operate. The efficiency is also dependent on how the two barriers are fabricated and how they contact one another. The survey also based the discussion on the electrochemical basis for galvanic effects (the Wagner-Traud mixed potential theory) and how this may be used in the demonstration of galvanic effects. This will be more fully explained in Section 2.8 of this report. Finally, the survey pointed out the possible complications between an anodic carbon steel and a cathodic Ni-base or Ti-base couple, including formation of ferric ion corrosion products from the steel and hydrogen evolution on the more cathodic member of the couple.

A degradation mode survey was prepared on fabrication and welding effects on the corrosion performance of the high nickel candidate alloys and the titanium alloys under consideration as candidate materials for the inner barrier.[6] The survey describes the metallurgical structures that develop due to the time-temperature history that occurs during the primary formation of the container material. The survey then discusses the changes in structure that occur in and around the welded areas. In many cases, there are "critical" microstructures that one tries to avoid because these microstructures result in a loss of fracture toughness or result in formation of phases that are more susceptible to certain forms of corrosion. Two of the Ni-base candidate materials, Alloys C-4 and C-22, have extremely low carbon contents, which make these alloys very resistant to grain boundary precipitation in the weld heat affected zone. Also, because of the presence of stabilizing elements and the low carbon content, post-weld thermal treatments are usually not necessary. Wrought forms of these alloys are usually supplied in the solution-annealed condition. With respect to the titanium alloys under consideration, the major

process concern is the care that must be taken to avoid surface contamination and hydrogen pick-up during container fabrication and welding.

The degradation mode surveys on the individual candidate alloys comprise Metallic Barriers SIP Activity E-20-32. The galvanic effects degradation mode survey between the barrier materials is Activity E-20-33. Information bases, in the form of compilation of mechanical and physical properties of the candidate materials were collected and presented in Volume 2 of the original EMCR. These are Activities E-20-35, andE-20-36, respectively. Finally, preparation of the updated EMCR is Activity E-20-39.

References for Section 2.2

1. J. C. Farmer et. Al., "Survey of Degradation Modes of Candidate Materials for High-Level Radioactive Waste Disposal Containers, Volumes 1-8", LLNL Report UCID-21362 (1986)

2. G. E. Gdowski, "Survey of Degradation Modes of Four Nickel-Chromium-Molybdenum Alloys", LLNL Report UCRL-ID-108330, March 1991

3. D. W. Vinson, W. M. Nutt, and D. B. Bullen, "Survey of the Degradation Modes of Candidate Materials for High Level Radioactive Waste Disposal Containers, Iron-Base Corrosion-Allowance Materials" LLNL Report UCRL-CR-120464, June 1995

4. D. W. Vinson and D. B. Bullen, "Survey of Degradation Modes of Candidate Materials for High-Level Radioactive Waste Disposal Container -- Nickel-Copper Alloys", LLNL Report UCRL-CR-122862, Sept. 1995

5. A. K. Roy and D. A. Jones, "Degradation Mode Survey Galvanic Corrosion of Candidate Metallic Materials for High-Level Radioactive Waste Disposal Containers", LLNL Report UCRL-ID-12564 Nov. 1996.

6. A. Goldberg and E. N. Dalder, "Considerations on the Performance and Fabrication of Candidate Materials for the Yucca Mountain Repository Waste Packages: Highly Corrosion Resistant Nickel-Base and Titanium-Base Alloys, in preparation, to be published as an LLNL UCRL report.

2.3 Oxidation/Corrosion Transition

(input for this section of the report was provided by Greg Gdowski)

The presence of water vapor in air can have a significant effect on the corrosivity of that atmosphere [1]. At high vapor pressures of water, water adsorption occurs and the corrosion/oxidation process is "aqueous film electrochemical corrosion" as opposed to "dry oxidation" which occurs at low water vapor pressures. Gaseous and solid state processes that control "dry oxidation" are oxygen adsorption and dissociation, and ionic and electronic diffusion through the oxide layer on the metal surface. Corrosion / oxidation processes are accelerated during "aqueous film electrochemical corrosion" because oxygen reduction is enhanced in the aqueous film and ionic transport also occurs in the aqueous phase.

The water vapor pressure at which water condensation occurs increases with increasing temperature. It is usually more convenient to consider the amount of water in an atmosphere in terms of relative humidity, which is a measure of the degree to which the atmosphere is saturated with water. Relative humidity is defined as the ratio of actual water vapor pressure to the saturated water vapor pressure.

The transitional relative humidity (RH) where corrosion / oxidation changes from "dry oxidation" to "aqueous film electrochemical corrosion" is typically referred to in the corrosion literature as the "critical relative humidity" (CRH). In actuality, there is not usually an abrupt transition at a particular RH. The change occurs continuously, but the corrosion/oxidation rate accelerates with increasing RH. The choice of the CRH is then a somewhat arbitrary choice based on what is defined as an accelerated corrosion rate compared to oxidation in a "water-free" or "dry" atmosphere. The continuous change in the corrosion rate with RH relates to the surface heterogeneity where water adsorption can occur at sites such as structural defects (e.g. porosity), impurities, and contaminants.

The susceptibility of a metal or alloy to "aqueous film electrochemical corrosion" is dependent on the composition of the metal or alloy, and the presence of gaseous and/or surface contaminants. In particular hygroscopic contaminants tend to be aggressive enhancers of aqueous film electrochemical corrosion.

The general characteristics of aqueous film electrochemical corrosion have been established at ambient atmospheric temperatures. The objective of this work is to understand the effect of elevated temperatures on the kinetics and mechanism of aqueous film electrochemical corrosion. In particular, the corrosion / oxidation behavior of carbon steel in air with varying relative humidities over the temperature range of 65°C to 95 °C was studied. The oxidation/corrosion transition is of primary interest for the outer barrier materials.

2.3.1 Corrosion and oxidation processes

Dry oxidation leads to the steady build up of an oxide layer. Oxidation rates can be limited by adsorption and dissociation of oxygen on the oxide layer and / or transport of ions through the oxide layer. In general the thicker the oxide layer, the slower the subsequent oxidation rate; typical corrosion rates are parabolic in time. Less protective oxide layers tend to be porous or cracked. Unless there is spalling of the oxide layer, the oxide layer will continue to grow. Because of the slow oxidation rates at low temperature, studies of the kinetics of oxidation processes are usually obtained at high temperatures

Aqueous film electrochemical corrosion occurs in the aqueous films on metal surfaces. It should be emphasized that "aqueous films" can be localized on surfaces, that is, located at surface defects or contaminants. Depending on the metal or alloy, this type of process can have a greatly enhanced corrosion rate relative to dry oxidation. As discussed below, this type of corrosion is dependent on relative humidity and the presence of deleterious contaminants. Electrochemical corrosion can be very aggressive if the oxide layer formed is porous (that is, nonprotective). In addition to metal loss by formation of the oxide layer, metal can be lost by dripping of water off the material or washing the aqueous film off by water.

In oxidizing atmospheres the controlling chemical reactions in aqueous film electrochemical corrosion are:

$$Fe \rightarrow Fe^{2+} + 2e^- \quad \text{(oxidation)}$$
$$\text{and} \quad O_2 + H_2O \rightarrow 2OH^- \quad \text{(reduction)}.$$
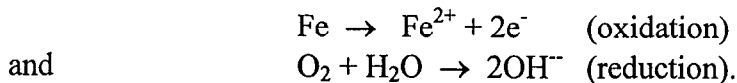
As long as these reactions are operative, corrosion will occur. The corrosion literature indicates that certain conditions must exist in order for these reactions to remain sustainable. 1) Oxygen reduction occurs on metal oxide, and in order for this to occur the oxide must be electrically conductive [2]. From a corrosion point of view the electrically conductive oxides are Fe_3O_4 (magnetite) and a defective g-FeOOH structure. The non-conductive oxides are non-defective g-FeOOH, a-FeOOH, and Fe_2O_3 (hematite). The defective g-FeOOH structure forms under reducing conditions, while the non-defective g-FeOOH structure forms under oxidizing conditions. 2) The metal must be in contact with the water layer.

Corrosion studies have indicated that accelerating factors for sustained aggressive electrochemical corrosion are a film thickness greater than 10 μm [2] and electrolytes in solution. A sufficiently thick film is required because as film thickness decreases the solution will become saturated with iron and hydroxyl ions, and iron oxides will precipitate. The thin film allows rapid resaturation of the film with oxygen; the oxides formed are non-conducting and therefore corrosion rate diminishes. Electrolytes enhance corrosion rates by their hygroscopic nature, that is, water adsorption occurs at RH values

less than saturation, and because of their contribution to the electrical conductivity of the solutions.

2.3.2 Factors affecting "critical relative humidity"

Factors which may affect the "critical relative humidity" of a particular metal include the surface condition, surface contaminants, and gas phase contaminants. Salts affect the CRH by their hygroscopic nature and because they can accelerate electrochemical reactions (i.e. they are electrolytes).

It has been shown that the aggressiveness of salts deposited on a metal surface in humid air is related to the hygroscopic nature of the salts [3,4]. In particular it has been observed that aggressive corrosion occurs at ambient conditions when the relative humidity of the air is near or exceeds the equilibrium relative humidity (or equivalently the water vapor pressure) above a saturated solution of the salt. This has been demonstrated at room temperature for numerous salts on carbon steel [4]. The salts tested included those with high equilibrium relative humidities, Na_2SO_4 (93% RH) and NaCl (78% RH), to those with low equilibrium relative humidities, NaI (43% RH) and LiCl (15% RH).

Duly [3] showed sea salt deposits were corrosive to mild steel even at relative humidities below the equilibrium RH, although at the lower relative humidities the corrosion was limited to the periphery of the salt deposits. Aggressive corrosion occurred when liquid water was visible on the metal surface; this occurred when the relative humidity was greater than or equal to 80%.

It is of interest to know if the relationship between equilibrium RH and aggressiveness of salts deposits extends to higher temperatures. This will in part depend on the hygroscopic property of the salts at high temperature. Greenspan [5] has compiled equilibrium relative humidity data above saturated salt solutions for numerous salts. The data indicates that the equilibrium RH typically are within ± 20% of their value at room temperature. The exceptions are those salts that can decompose into volatile components, such as carbonates. The equilibrium RH were not reported at high temperatures for these salts.

Air contaminated with certain species, such as, SO_2 and CO_2, can also change the critical relative humidity. Brown and Masters [6] showed that steel at room temperature was aggressively attack by SO_2-contaminated air at relative humidities greater than 60%. Corrosion rates were 100 times greater than those at lower relative humidities. In contrast, SO_2-free air at 100% RH corroded at rates less than 10% of that for SO_2-contaminated air at 80% RH.

2.3.3 Thermogravimetic Analysis Apparatus

Testing is being performed in an extensively modified commercial thermogravimetric analyzer (TGA) apparatus, a Cahn model TG-131. A schematic of the modified apparatus and simplified illustration of the reaction chamber are shown in Fig. 2.3 -1. The main components of the apparatus are: a microbalance, a reaction chamber, temperature-humidity sensor, and a humidified air delivery system (not shown). The TGA work comprises Activity E-20-47 in the Metallic Barriers SIP.

The microbalance has a manufacturer stated capacity of 100 grams and a sensitivity of 1.0 μgrams. In practice the sensitivity of the balance is about 20 μgrams. A test specimen is suspended on a wire from one arm of the microbalance. An inert counter weight specimen of nearly equal weight to the test specimen is suspended on a wire from the other arm of the microbalance. The counter weight specimen in this testing is made of platinum. The specimens are suspended vertically from the wires.

The temperature-humidity sensor is a Vaisala Model 230, which is equipped with an RTD temperature sensor and a humidity sensor. The manufacturer stated range of sensor is 0 to 100% RH in the temperature range of -40 to +180 °C. The temperature-humidity sensor is in the reaction chamber and is situated just below the test specimen.

The reaction and reference chambers, and the associated support hardware were custom designed. The reaction and reference chambers are basically doubled-walled glass cylinders with silicon oil flowing through the outer annulus providing temperature control. Temperature of the silicon oil is controlled by a programmable heating/cooling unit. With this arrangement the temperature change across the length of the specimen in the reaction chamber is less than a degree centigrade, and the centerline temperature of the test specimen is maintained within ± 0.5°C. (In the manufacturer supplied furnace the temperature change across the length of the specimen was about 15°C.) The redesign support hardware was necessary to accommodate the added weight due to the chambers, the temperature-humidity sensors, and part of the humid air delivery system. The chambers move vertically in order to allow changing of specimens.

The reactant air delivery system consists of MKS direct liquid injection (DLI) apparatus and flow-rate-controlled, purified-air feed. The purified air is mixed with the water which has been vaporized in a high temperature vaporizer. The water vapor content of the air is controlled by changing the flow rate of de-ionized water to the vaporizer. The water flow rate is controlled by a micropump assembly. Water delivery rates to the vaporizer can be varied between 0.006 and 2 cubic centimeters per minute. (In one set of tests the reactant air was purified house air that was humidified by bubbling it through a heated deionized water bath. Humidity control with this bubbler arrangement was poor and very ineffective for humidifying the air at temperatures greater than 65°C.)

The test specimen and the reaction chamber wall are separated by a glass cylinder that was open at the bottom and vented directly to the laboratory. The reactant gas was feed-in at the top of the reaction chamber. It was, therefore, in contact with the length of the chamber wall before contacting the test specimen. The air flow was vertical across the

length of the specimen. All feed lines to the reaction chamber were heated in order to prevent water condensation.

The test parameters (time, temperature, specimen weight gain, and relative humidity) were recorded and stored electronically. In addition the reaction chambers being made of glass allows visual inspection of the specimens during testing.

The primary test specimens were made of A516 Grade 55 carbon steel and have nominal dimensions of 5.1 cm x 1.3 cm x 0.16 cm. Other specimens used were made of AISI 1020 carbon steel and had nominal dimensions of 4.4 cm x 1.3 cm x 0.16 cm. The specimens were cleaned and degreased in acetone and isopropanol. Sodium chloride (NaCl) was deposited on specimens by immersing the specimens in 50% acetone / 50% water solution saturated with sodium chloride. Non-adherent salt was removed by wiping the specimens with a clean wipe. The amount of salt deposited was recorded and was about 5 milligrams. Care was taken not to inadvertently contaminate the specimens prior to insertion into the reaction chamber.

2.3.4 TGA Results and Discussion

Clean polished surface

In the temperature range 60 to 90°C the oxidation/corrosion of clean and polished specimens at low relative humidities was within the detection limit of the TGA. At relative humidities above 85% some oxidation of the specimens occurred. The weight gain of the specimens as a function of time at various temperatures and at high relative humidities is shown in Fig. 2.3 -2. At each temperature there was an induction period before any detectable weight gain occur. At the lower temperatures the oxidation of the metal started at a point and spread outward from there. At the highest temperature tested (95°C), the oxidized metal was limited to surface imperfections on a certain part of the specimen. In each case the oxide was adherent.

The slopes of the initial oxidation rates on the clean surfaces indicate that the susceptibility to oxidation is greater at lower temperatures. There are several possible explanations for this: 1) oxygen solubility decreases with increasing temperature, 2) the amount of adsorbed water decreases with increasing temperature, 3) an artifact of the surface condition of the specimens (e.g. more defective specimens were tested at lower temperatures). Although the last explanation cannot be ruled out, it would seem that difference in the oxidation rates is due to the amount of adsorbed water on the surface for the following reason. The steady state water film thickness on a metal surface at ambient temperature is less than 2-3 nm at relative humidities less than 95% [7]. Increasing temperatures are expected to decrease the amount of adsorbed water. Due to the relative thinness of the oxide layer it is not expected that oxygen resupply of the water would be limiting.

In any case it must be emphasized that the oxide layer that forms under these conditions is adherent and is therefore "protective" in that the oxidation rate will decrease with time. The planned microstructural examination of the surface oxide formed will give additional information on the "protectiveness" of the oxide formed.

Clean, etched surfaces

AISI 1020 carbon steel specimens (non QA specimens) were used in the initial tuning of the test apparatus. In this capacity the test specimens were reused often. In between tests, the oxide layer that formed on the specimens was removed by chemical etching. It is expected that this process resulted in roughened surfaces relative to a polished surface. However no quantitative measure of the degree of roughening was made. Testing of porous oxide covered specimens is planned for FY-97.

The weight gain of these specimens was recorded as a function of time and relative humidity at 65°C (Fig. 2.3 - 3). (It should be noted that in these tests the humid air was formed with the bubbler arrangement, and RH control was ± 10% around the stated RH value.) At relative humidities of 65 and 75%, weight gains were small and gradual. However at relative humidities above 85%, the weight gain was initially rapid, but then decreased with time as the oxide layer built up on the surface. Maximum weight gain recorded with the 80 hr test period was about 6 mg. Note that these specimens have about 15% less surface area than those used in the other testing.

Visual examination of the specimens showed that those which were exposed to the higher relative humidities were covered with a uniform reddish-brown oxide, while those which were exposed to the lower relative humidities looked to be unoxidized. Examination with an optical microscope at higher magnification showed that for the specimen oxidized at RH > 85%, there were small uniformly scattered regions which were not oxidized to a significant extent. For the specimens oxidized at RH < 75% the faces of the specimens showed little indication of oxidation, however the edges of the specimens tested at 75% RH had characteristics similar to those of the specimens oxidized at the higher RH, that is, the presence of the reddish-brown oxide.

The outer reddish-brown oxide was powdery and non-adherent, and could be easily removed by light brushing of the surface. There appeared to be an inner oxide that was more adherent, that is, it was not removed by light brushing of the surface.

Salt covered surfaces

Contamination of the surfaces with a fixed amount of sodium chloride had a dramatic effect on the susceptibility of the specimens to aqueous film electrochemical corrosion. Figure 2.3 - 4 is a plot of the weight gain of the salt covered specimens versus time at various relative humidities and temperatures near 80°C. Also include in the plot for comparison purposes is the data for clean surface at 85% RH. The offset for the 88% RH

in comparison to the 78% and 63% RH data just reflects the earlier introduction of humid air into the reaction chamber.

Several features of the data in Fig. 2.3 - 4 are worth emphasizing.

1) Note that there is a large increase in the initial corrosion rate with increasing RH. This is discussed in more detail below.

2) After the initial high corrosion rate at high RH, note the decrease in corrosion rate with time. It appears that either a protective layer is forming with time or that the salt somehow becomes incorporated into the oxide and its effectiveness at facilitating the electrochemical reactions decreases. Investigating the surface structure of the oxide will also be useful in determining the reason for the decrease in oxidation rate (FY97 plan). Tests are also planned to redeposit salt on a corroded surface to determine that surface's susceptibility to this additional salt load.

It also appears that for the 78%RH test the weight gain ceases at long times and may even be decreasing. A similar result was seen at 88%RH (not shown). The test run at 63%RH was probably terminated too soon to see this phenomenon. This decrease in weight could be due to spalling of the oxide layer and/or a transformation of the oxide. Unfortunately the test apparatus is not set up to catch particles that may spall from the surface. An oxide transformation from FeOOH to Fe_2O_3 with the loss of volatile water would result in a weight loss.

$$2FeOOH \rightarrow Fe_2O_3 + H_2O$$
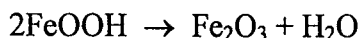
There is a driving force for this reaction because Fe_2O_3 is the thermodynamically stable oxide phase under oxidizing conditions. Again the surface characterization to be performed in FY97 may be able to identify the mechanism responsible for this weight loss.

3) There is significant corrosion at relative humidities below the equilibrium relative humidity of a saturated NaCl solution; the equilibrium RH value is about 76% at 80°C [5]. This is probably due to the strong adsorption of water on the salt particles without the salt necessarily dissolving in the adsorbed water to a significant extant. (The equilibrium RH values are determined for a homogenous system (aqueous solution), while adsorption on the surface is a heterogeneous phenomenon.) Therefore caution must than be exercised in using the equilibrium RH values for determining aggressive corrosion at least at these temperatures. The equilibrium RH are probably still a good qualitative guide to the aggressiveness of a particular salt.

Figure 2.3 -5 is an expanded view of the initial weight gain as function of time. It shows the large increase in the initial oxidation rate with increasing RH. From the plots the initial rate of weight gain was determined and a corrosion rate calculated from the weight

gain rate and assuming hematite (Fe_2O_3) was formed; these calculations are shown in Table 2.3 -1. (Assuming other oxides formed would change the rate by ± 25%.) The results show the rather dramatic increase in initial corrosion rate with adsorbed salt and increasing RH on salt covered surfaces. Compared to a clean surface (95% RH) the initial oxidation rate on the salt covered surface at a comparable RH (88%) increases by factor of 10,000. On salt covered surfaces increasing the RH from 48 to 63% increases the corrosion rate by over a factor of 100. Further increases of RH from 63 to 88% increases the corrosion rate by a factor of 17. The increase in the initial rate in going from 48 to 88% RH is almost a factor of 2000.

Table 2.3 -1. Initial rate of weight gain of sodium chloride covered specimens at various RH and 80°C, except the 95% RH test which was for a clean surface at 75°C. A corrosion rate (or metal consumption rate) was calculated assuming a uniform oxidation of the metal and that hematite (Fe_2O_3) was formed.

Relative Humidity (%)	mg/hr	µm/yr
95*	0.004	6.7
48	0.020	35.
63	2.3	4000.
78	6.2	11000.
88	38.	67000.

* clean surface

In each test the corrosion started at visible salt deposits, but eventually spread across the entire surface. The rapidness of the spreading increased rapidly with increasing RH. The final corrosion product in each case was a reddish brown product. The corrosion product formed at 43% RH was fairly adherent in that some of it could be removed by rubbing with a clean wipe. The corrosion product formed on surfaces at RH values greater than or equal to 63% was brittle and nonadherent; it flaked off with simple touching. Preliminary investigation of the surface structure with scanning electron microscopy revealed a whiskered structure for the outer oxide formed. This is typical of the oxide formed in chloride containing environments. More detailed investigations of the oxide structure and composition are planned for FY-97.

2.3.5 Tentative Conclusions and Future Work

This work investigated the effect of relative humidity on the corrosion / oxidation of carbon steel, both clean and covered with a fixed amount of NaCl. It was found on clean polished surfaces that high relative humidities (> 85%) were necessary so that enhanced corrosion relative to "dry oxidation" could be detected over time periods of about 100 hrs. This is consistent with other studies which showed that significant water adsorption does not occur on polished contaminant-free surfaces at RH less than 95%. Hence the aqueous film electrochemical corrosion occurs only at high RH under these conditions.

Chemical etching of the surface enhances the susceptibility to electrochemical corrosion at lower RH values. This is probably due to a surface roughening although residual etchant on the surface may have enhanced the susceptibility. In either case water adsorption occurred at lower RH values than on a polished surface. At high RH values (85 and 90%), the initially high corrosion rate decreased with increasing time. The outer oxide formed on these surfaces was non-adherent however the inner oxide was not easily removed.

On NaCl covered surfaces the susceptibility to aqueous film electrochemical corrosion was significantly enhanced relative to the clean surfaces. At about 88% RH the initial corrosion rates were up to 10,000 times faster than on a clean surface under similar conditions. The initial corrosion rate decreases with decreasing RH. With increasing time at high RH the corrosion rate decreased and in fact seemed to plateau within the detectable weight measurement. It is expected that the same effect would occur at the lower RH values with time after the corrosion had reach the same extent as at the high RH. The ineffectiveness of the deposited salt at sustaining the corrosion may be due to "incorporation" of the salt in the oxide layer. With redeposition of salt the rate may return to its initial rate. Testing is planned to investigate this hypothesis.

Future studies will extend the characterization to higher and lower temperatures; in particular, the corrosion susceptibility will be studied at temperatures above 100°C where hygroscopic salts will enhance the adsorption of water. Other factors that may affect aqueous film electrochemical corrosion; such as, gas phase contaminants, surface contaminants (such as, salts), and surface condition (e.g. previously oxidized, scratched) will also be investigated. Longer term tests will be performed in controlled temperature and humidity chambers as MB Activity E-20-59. These tests were initiated in January 1997 with the first group of carbon steel weight-loss specimens placed in a large humidity control chamber (Envirotronics, Inc. Grand Rapids, MI) maintained at 80° C and 50% relative humidity at that temperature. Additional test specimens will be placed in this chamber, and another similar chamber has recently been purchased. Environmental control in this second chamber will be the same temperature, 80° C, but at a higher relative humidity, 80%. Thus, the first chamber will operate generally below the "critical" relative humidity conditions for the test specimens, while the second chamber operates above the "critical" relative humidity conditions, as predicted by the short term TGA tests. The full complement of experimental conditions, as well as a full description of the experimental techniques is available in the activity plans prepared for this work.[8, 9]

The planned microstructural investigation of corrosion product formed on the surfaces under the different test conditions will give important information that will help elucidate the mechanism of the corrosion process. This information is necessary for the modeling of the corrosion process. (See Section 2.10 of this report) Planned testing includes identification of the oxide crystal structure and composition, determination of the surface morphology.

References for Section 2.3

1) Ailor, W.J., ed., <u>Atmospheric Corrosion</u>, John Wiley & Sons, New York, 1982.

2) Stratmann, M., H. Streckel, K.T. Kim, S. Crockett, Corrosion Science 30, pp. 715-734, 1990.

3) Duly, S.J., Journal of the Society of Chemical Industry, 69, pp. 304-306, 1950.

4) Kaesche, H., <u>Metallic Corrosion</u>, NACE, Houston, pp. 216-219, 1985.

5) Greenspan, L., Journal of Research of the National Bureau of Standards, **81A**, pp. 89-96, 1977.

6) Brown, P.W., and L.W. Masters, <u>Atmospheric Corrosion</u>, W.J. Ailor, ed., John Wiley & Sons, New York, 1982, p. 31.

7) Eichforn, K.J., and W. Forker, Corrosion Science, 28, pp. 745ff, 1988.

8) Gdowski, G. E., Yucca Mountain Project Activity Plan, Thermogravimetric Analysis Studies, MB SIP Activity E-20-47, Rev. 0, Lawrence Livermore Laboratory, 1995

9) Gdowski, G. E. Yucca Mountain Project Activity Plan, Long Term Oxidation and Corrosion Studies under Controlled Humidity Conditions, MB SIP Activity E-20-59, Rev. 0, Lawrence Livermore Laboratory, 1997
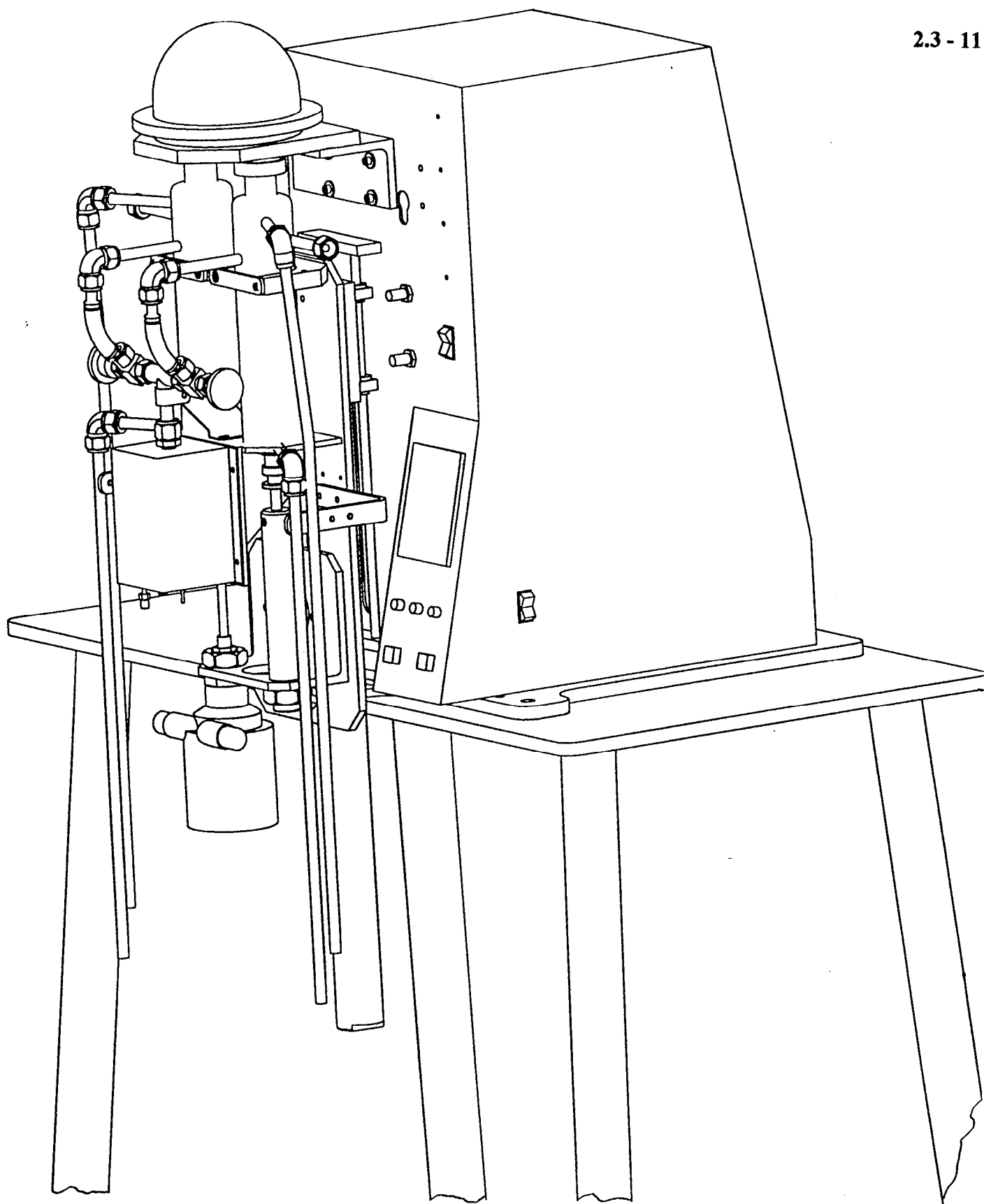
Fig.2.3 - 1a.   Schematic of thermogravimetric analyzer (TGA) apparatus; the humid air
            delivery unit is not shown.

Thermogravimetric Analyzer Apparatus

Microbalance

Silicon oil
outlet

He purge
gas inlet

Gas
Outlet

Reactant
gas Inlet

Humidity
sensor &
RTD
temperature
probe

Silicon oil
inlet
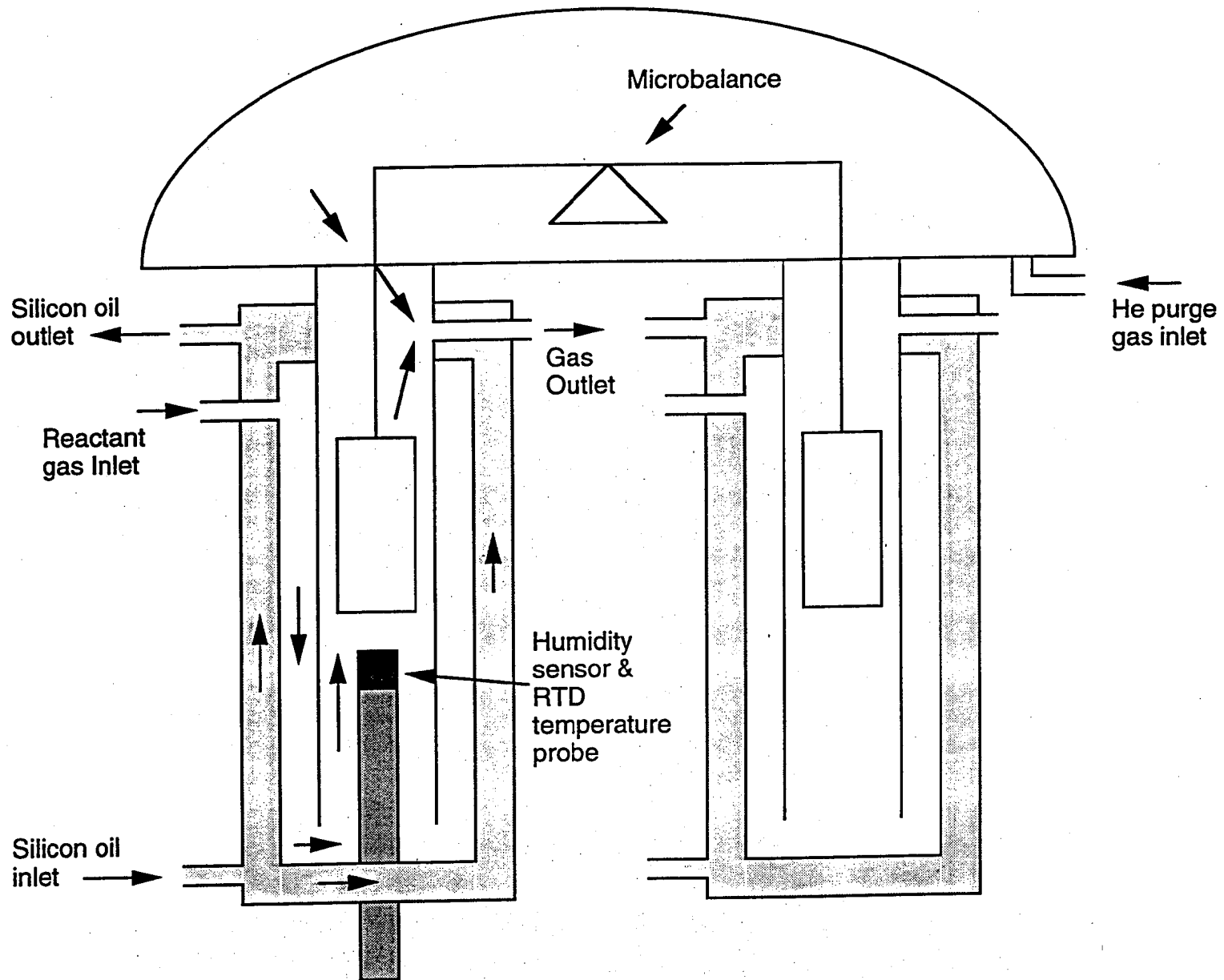
Fig. 2.3 -1b.   Simplified cartoon of the reaction chamber of the TGA apparatus.

2.3 - 12

Fig. 2.3 - 2.   Weight gain versus time at various temperatures and at high relative humidities. Specimens were clean and polished.
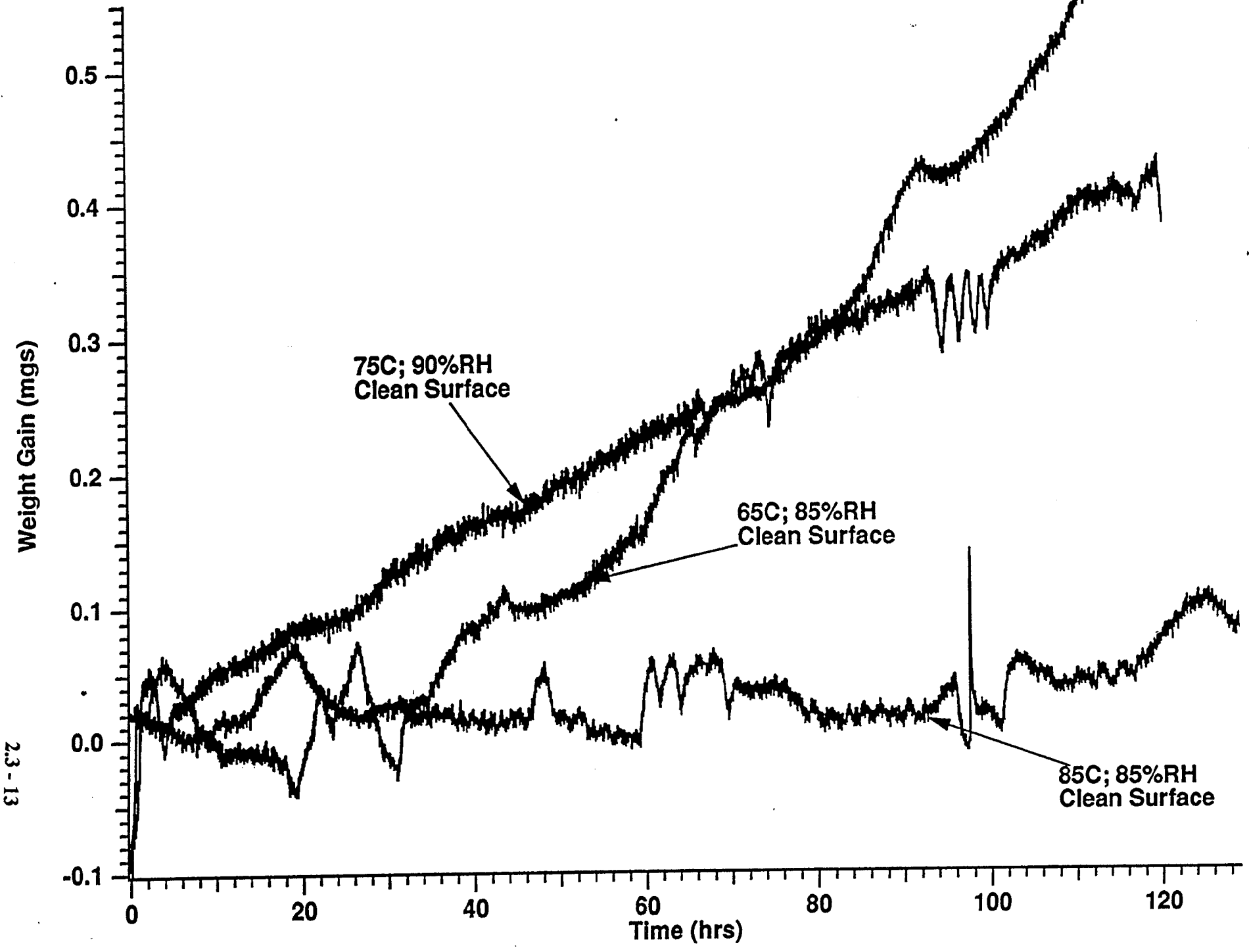
1020 Carbon Steel at 65°C
Various Relative Humidities

90%

85%

75%

65%

1%
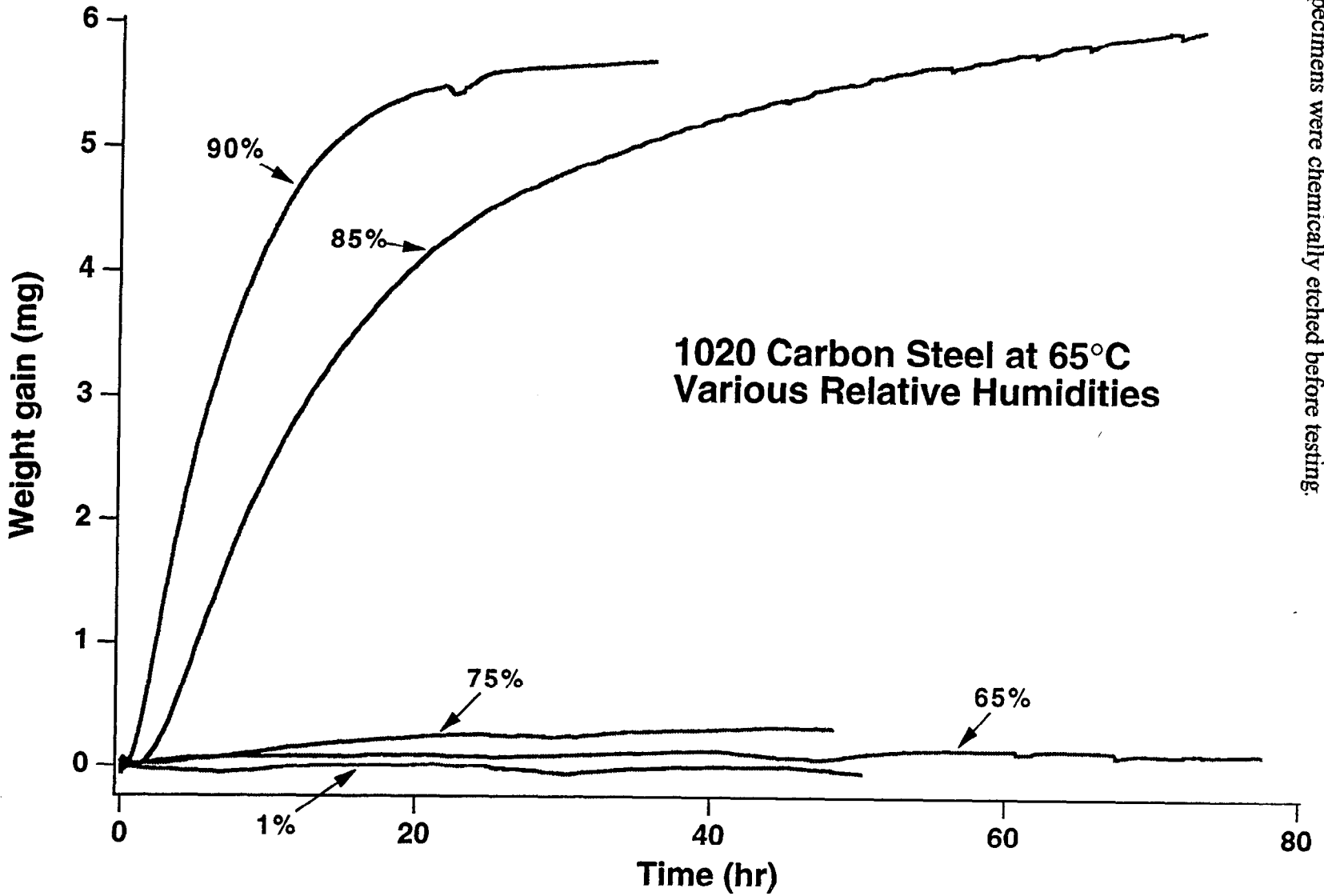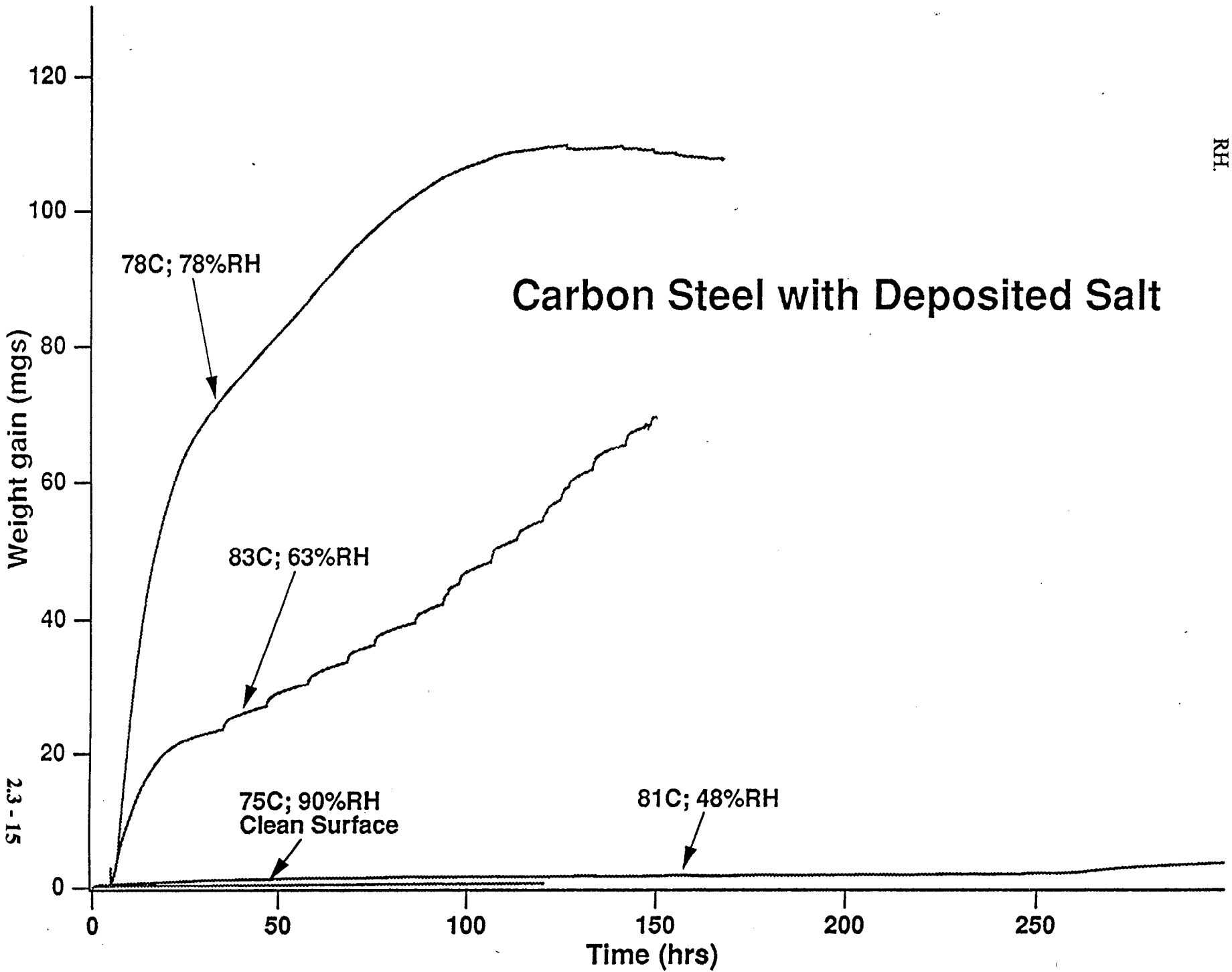
Fig. 2.3 - 4.   Weight gain versus time at various relative humidities and nominal 80°C. Specimen had adsorbed NaCl. Also shown is data for clean specimen at high RH.
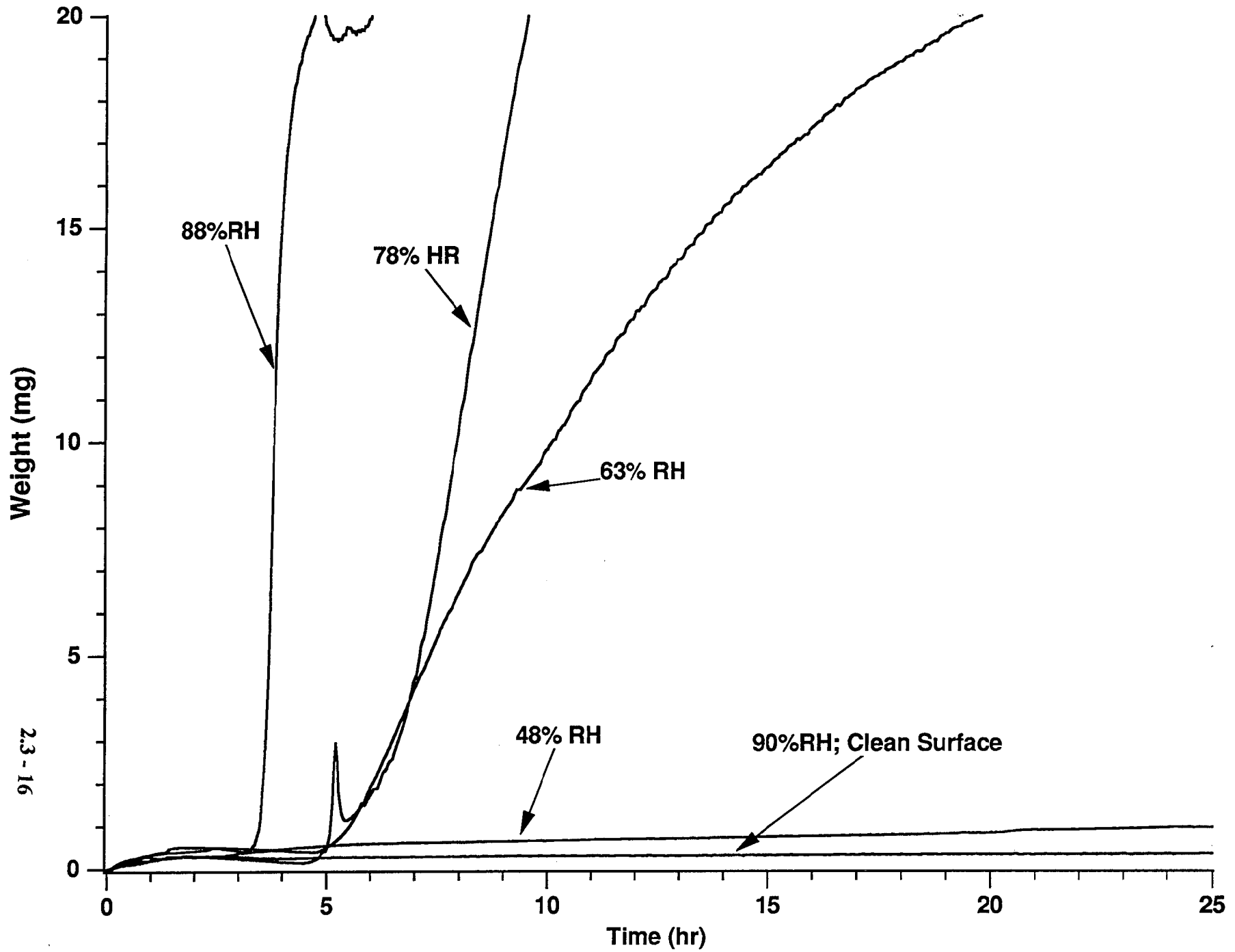
Fig. 2.3 - 5. Expanded view of Fig. 4 showing the initial weight gain versus time data.

88%RH

78% HR

63% RH

48% RH

90%RH; Clean Surface

Weight (mg)

Time (hr)

2.4 Long Term Comprehensive Corrosion Tests

A corrosion test facility is under construction in which a number of vessels will contain corrosion test specimens for long term exposure to repository relevant environments. When completed, corrosion tests will run for at least a period of five years, and some tests may continue for much longer periods of time beyond the license application period and into the repository construction period. The tests are said to be comprehensive, in the sense that many forms of corrosion can be tested: general corrosion, pitting corrosion, crevice corrosion, intergranular corrosion, stress corrosion, hydrogen embrittlement, and galvanic corrosion. Different specimen configurations allow measurements of different forms of corrosion. A planned interval test approach will be used, in which large numbers of specimens are initially exposed to the test environment and then periodic withdrawals of specimens are made and the specimens characterized. Thus, the time-dependence of the corrosion phenomena can be determined. Because the information from the long-term comprehensive corrosion test is expected to be a key piece of information for licensing, the test is planned to operate under strict quality assurance controls. The long term comprehensive corrosion test is MB SIP Activity E-20-50.

2.4.1 Test Environments

The test environments are construed to be of the "bounding" type and were selected so that there would be an expectedly large difference in behavior for the different candidate materials. Several discussions were held with several principal investigators in the geochemical and geological disciplines on which type of water would be appropriate, a groundwater composition like the J-13 well water or water simulating the "perched water" that could be extracted from the Topopah Spring member. In any case, the water composition would be simulated in the laboratory by making up the water from various ionic compounds, since it would be impractical to obtain the water from the site. Finally, at a workshop held in March 1996, it was determined that the "base composition" would be a water containing ten times the ionic composition of a water whose composition was between that of J-13 well and the perched water.

Formulas have been developed for making up these test environments. The formulas were based on previous experience at this laboratory and at Argonne National Laboratory on making up simulated J-13 well water from various ionic salts. In order to make up the more "concentrated" waters, the EQ3/6 geochemical modeling code was run to test for the interactions between ionic species since the solubility products would be exceeded for some (particularly for Ca and Mg containing compounds). Details of the formulas to be used were prepared as technical implementation plans (TIPs). The characteristics of the four bounding water environments have been estimated from the geochemical code, as follows:

(1) the "base case" water with the low concentration of ions will have a pH of 8.5 and contain 1700 ppm total dissolved solids. For the purpose of comparison, this water is estimated to contain 67 mg/liter chloride ion.

(2) the base case water concentrated 100-fold, with the high concentration of ions will have a pH of 10 and contain 146,000 ppm total dissolved solids. This water is estimated to contain 6700 ppm chloride ion. This bounding environment represents what would happen with repeated plumes of pluvial water descending toward the repository, encountering the thermal zone, evaporating and concentrating dissolved salts. Finally, after the container surface temperature reaches the water boiling point, subsequent plumes of water will dissolve the halo of salts and carry these to the container surface.

(3) the concentrated water acidified with sulfuric acid to a target pH of around 2. This water is estimated to have a total dissolved solids content of 146,000 ppm and contain 24,200 mg/liter of chloride ion. This bounding case represents the condition where microbial activity from certain species have produced acidic metabolic products. It also represents a bulk test condition simulating the case of a localized, sequestered water chemistry, such as that produced in a creviced geometry.

(4) the concentrated water alkalized with calcium hydroxide to a target pH of 12. This water is estimated to have a total dissolved solids content of 132,000 ppm and contain 20,900 mg/liter of chloride ion. This bounding case represents water conditioned by prolonged contact with cementitious materials used to line the drift wall or used in the invert material underneath the waste package emplacement.

The four proposed bounding environments provide a range of pH (acid, neutral, and alkaline) and a range of ionic strength (dilute and concentrated). Generally speaking, the pH and the E_h of the water have a profound effect on metal corrosion, so that species that affect pH and E_h usually affect corrosion. It is noted that simply the concentration of the ionic species moves the pH into the mild alkaline range, probably because of the increased bicarbonate ion concentration and its influence on the bicarbonate/carbonate equilibrium. The ionic strength affects the conductivity of the water, which in turn affects "local corrosion cell action" on the metal surface. From the point of view of metal corrosion, the species normally found in the J-13 well water and other NTS groundwaters are expected to give the following general reactions:

Anions
Chlorides and fluorides -- usually aggressive, since they tend to break down protective passive films on many metals
Sulfates -- somewhat aggressive to some metals; indifferent effects on others
Nitrates -- oxidizing, therefore aggressive to some metals; promote passivity on other metals
Bicarbonates -- tend to buffer pH, indifferent effects or even protective effects if calcium and/or magnesium are present
Silicates -- because presence of alkaline earth ions favor scale formation, often protective to metals

Cations

Sodium, potassium, calcium, and magnesium ions -- depending on which anions are also present, these ions have an indifferent to protective effect, the latter if pH is increased and/or Ca- and Mg-rich protective scales form on metal surface

"Heavy metal ions" -- largely absent from tuff repository groundwaters, but would have important effect on metal corrosion since they are oxidizing and acid hydrolyzing. The effects of ferric ions produced from corroding rock bolts, steel mesh to support the drift, conveyances to transport and support waste packages, emplacement drift rails, etc. could be significant.

The corrosion response is a composite of the separate influences of these different ions. In many cases, it is the ratios of the concentration of aggressive ionic species to those of the protective or indifferent species that determine the overall corrosivity of the water. This is why it is important that the combined effects of all the various water constituents are present in the long term corrosion test.

The test vessels are filled to approximately 60% of their volume so that when the specimen racks are inserted, half of the test specimens will be fully immersed in the aqueous phase and the remaining half exposed to the vapor phase above the water. A few specimens will be placed right at the water line. Because the vessel is closed and reasonably tight, this atmosphere will become saturated with water vapor. Atmospheric air will be passed into this vapor space to insure that the normal oxygen, carbon dioxide, and other atmospheric gas levels will be maintained in the vapor and in equilibrium with the dissolved gases in the liquid. O_2 and CO_2 are the main gases of interest because of their effect on E_h and pH, respectively.

Two test temperatures were selected for the long term tests, 60 and 90°C. These temperatures are bounding in the sense that the highest corrosion rates for the corrosion allowance materials will be found in this range and the effects of localized corrosion and stress corrosion cracking will be greatest in this temperature range for the corrosion resistant alloys. The test conditions were based on recommendations made at the YMP Materials Workshop held in May 1994 and reported in Volume 1 of the original EMCR.

2.4.2 Test Vessels

In order to contain the bounding environments, the choice of construction material is very important. The test vessels measure 1.3 m x 1.3 m x 1.3 m. Foremost, it was desirable to have as inert a material as possible (and one which would not degrade over the prolonged test periods) at the temperature, pH and water chemistry envisioned for each bounding environment. Also, it was desirable not to have too costly a material. Therefore, Teflon-type materials were out of consideration because of the cost in making vessels of the size required, although some of the individual internal components in the vessel are coated with Teflon. Discussions were held with several colleague knowledgeable about polymeric materials and their performance in various aqueous media. Additionally, potential vendors were queried. Ultimately, it was determined that a fiberglass-reinforced, vinyl ester polymer (Hetron 922) material was suitable for construction of all

the vessels except for the vessels to be used in the very alkaline environments (pH 12). This same material was used for construction of the internal specimen racks, as well. The test vessels and test racks were manufactured by Fibreglass Reps (Antioch, CA). Vessels to accommodate the very basic solutions must be constructed from a different material: Siloxirane 2131 was identified for this purpose.

Construction and installation of 12 fiberglass-reinforced, vinyl ester polymer vessels was completed in FY-96. These 12 vessels will be used for exposure of specimens to the first three test environments, the "dilute water", the "concentrated water" and the "acidified concentrated water".

At the time of this writing (January 1997), six of the twelve vessels are filled with test specimens and are operating. The remaining vessels are expected to go on-line in the next few weeks.

2.4.3 Test Specimens

Because the long-term test is also a comprehensive test for several mode of corrosion, three different specimen configurations are exposed in the test environment. A "weight loss" coupon, of approximate 5 cm x 2.5 cm x 0.3 cm thick, yields information on the rate of general corrosion. Examination of the pattern of attack reveals whether the corrosion is uniform, or shows localized attack such as pitting or intergranular. A "crevice" specimen, 5 cm x 5cm x 0.3 cm thick, arranged so that a Teflon sleeve held in place by a metallic Belleville washer will assure formation of a tight crevice. Teflon used by itself tends to creep at the test temperature so that the crevice geometry changes with time and usually becomes less tight. Third, a plastically strained U-bend specimen is used to determine stress corrosion cracking and hydrogen embrittlement susceptibility. The U-bend specimens are 0.16 cm thick and formed to be 3 cm high x 1.9 cm wide. In all cases, the test specimens are carefully isolated from mounting bolts and hardware. The specimen configurations are depicted in Figures 2.4-1 through 3. These specimen designs are based on ASTM standard configurations for corrosion testing. All test specimens were procured from Metal Samples Inc. (Munford, AL)

Some 13,000 specimens were procured in FY-96 in the three configurations. The initial materials to be tested are arranged in three categories:

Corrosion Allowance materials:
Wrought carbon steel (AISI 1018)	UNS K01800
Centrifugally cast carbon steel	UNS J02501
2.25 Cr - 1 Mo alloy steel	UNS K21590

Intermediate Corrosion Resistant Alloys:
Alloy 400 (Monel 400)	UNS N04400
70-30 Cu-Ni (CDA 715)	UNS C71500

Corrosion Resistant Alloys

Alloy 825 (Incoloy 825)	UNS N08825
Alloy G-3 (Hastelloy G-3)	UNS N06985
Alloy 625 (Inconel 625)	UNS N06625
Alloy C-22 (Hastelloy C-22, Inconel 622)	UNS N06022
Alloy C-4 (Hastelloy C-4)	UNS N06455
Titanium Grade 12	UNS R53400
Titanium Grade 16 (Ti-0.05 Pd)	none to date

For the first series of corrosion tests in the first 12 vessels (referred to as Increment 1), the test specimens are kept within their respective categories in order to avoid any cross effects between corrosion products. It was felt that the corrosion products from the highly corrosion resistant nickel-base alloys and titanium-base alloys will be so minimally produced, that these specimens can be mixed in the same vessels. In a later increment of tanks, galvanic specimens will be placed where the cross effects are definitely wanted. These will be discussed later. For Increment 1, the current plan is to install specimens of carbon and alloy steels in vessels containing the "dilute" water and the "concentrated" water environments at the two test temperatures (thus requiring four tanks), the specimens of the Ni-base and Ti-base highly corrosion resistant materials in the dilute and concentrated water environments at the two temperatures (thus requiring another four tanks). Then, specimens of these same Ni-base and Ti-base alloys, and specimens of the intermediate copper and nickel bearing alloys will be placed in the acidified concentrate environment. It is desirable to start an early exposure of these two categories of materials to the most aggressive environments. Plans are to build additional test vessels in FY-97 as Increment 2 so that additional combinations of materials and environments can be tested.

An initial design for a galvanic test specimen was completed in FY-96 (shown in Fig. 2.4 - 4), but funding did not permit acquisition of the test specimens and test vessels. The galvanically coupled specimens will be tested in the same environments as the single metal specimens, but they will be tested in separate vessels. However, the design of the galvanically coupled specimens will be revised in FY-97 in order to simulate a number of ways the two barrier may be fabricated. For instance, if the two barriers are fabricated as separate containers and then slipped one into the other, the contact between the two will be more or less casual. At the other extreme, if the two barriers are clad, the contact is everywhere intimate and complete. In between these two extremes, there are fabrication processes, such as a sort of "shrink-fit" that would assure close contact over nearly all of the surface. In the shrink fit container assembly, the outer barrier would be heated and slipped over the inner barrier while still hot. As the outer barrier cool, it contracts against the inner barrier. Also, in some of the looser-fit configurations, the annulus could be filled with metal powder or shot to provide some electrical continuity. For these reasons, a great deal of care should be exercised in the specimen design, and perhaps more than one specimen configuration will ultimately be used.

2.4.5 Test Operation

In order to heat the vessels, two 6-kW immersion heaters are placed in each vessel. Temperatures are measure by thermocouples. An Allen-Bradley Programmable Logic System (PLS) provides the feedback to the electrical system to increase or decrease the power input. The solutions are slowly stirred . The liquid level in each vessel is controlled by three sensors. If the liquid level falls (for instance, due to evaporation), the PLS signals to draw in distilled water to restore the liquid to the proper level. The test vessels were constructed to be reasonably tight to minimize water loss. If for some reason, the level rises, the operator will be called and power shut-off to prevent an overflow. The vessels are well insulated to minimize heat loss, so that in the event of a power failure, the temperature will only slowly drop. Power outages of less than 4 hours will hardly cause a noticeable temperature decrease.

Test temperature and the liquid level are the only two parameters which are controlled. Other parameters will be measured, and, in some cases, adjustments made over the duration of the test. These parameters include pH, solution chemistry, oxygen content, and microbial activity. Although it may have been desirable to try to control all of these variables, the system to do so would have been enormously complicated and costly.

Each test vessel holds six test racks. These are planned so that a rack can be withdrawn from the vessel at the scheduled time interval for inspection of the state-of-corrosion of the test specimens. Five planned intervals for inspection are after 6 months of exposure, 1 year, 2 years, 3 years, and 5 years. (The sixth rack is for additional test specimens, if needed). At each withdrawal period, the weight loss coupons will be reweighed and the corrosion rate calculated. Surfaces will be inspected for evidence of localized corrosion. The creviced regions will be the focus of investigation, as will the stressed U-bend surfaces. Some specimens contain welds, so that the weld and associated heat-affected-zone will be the object of inspection. Depending on what is initially observed, appropriate types of analyses will be pursued to fully characterize the specimens. Periodic withdrawals of water samples will provide an analysis of any water chemistry changes. These samples will also be characterized for the nature and extent of microbial activity.

Details of the test plan, including specimen dimensions, configuration of the test vessels, controls in the operation, sequence of testing, kinds of analyses planned, etc. can be found in the activity plan for this work [1]. Also, several technical implementation procedures [2-9], which support the activity plan, can be consulted for even more detail about the solutions, specimens, calibration of equipment, controls, operations., etc. An individual software plan was written for the software operating the programmable logic controller, which controls the power to maintain temperature and the liquid level in each vessel. [10]. Additional TIPs will be prepared, as needed, for specimen characterization and other subsequent activities.

2.4.6 Test Start-up and Future Work

As stated previously, six of the twelve vessels comprising Increment 1 are operational. Tests in the first vessel were initiated in September 1996, with start-up of the next five vessels occurring in the last months of 1996. Withdrawal of the first racks of test specimens from each vessel will occur six months following the test initiation date, meaning that the characterization of the first group of test specimens will begin with the others to follow sequentially.

The operational vessels (in January 1997) and their contents are as follows:

• Vessel #23, operating with the "dilute groundwater" at 60° C, containing specimens of candidate corrosion allowance materials (carbon and alloy steels). The initial pH of the solution in this vessel was measured at 9.18, corrected to room temperature.

• Vessel #22, operating with the "dilute groundwater" at 90° C, containing specimens of the candidate corrosion allowance materials (carbon and alloy steels). The initial pH of the solution in this vessel was measured at 9.61.

• Vessel #21, operating with the "concentrated groundwater" at 60° C, containing specimens of the candidate corrosion allowance materials (carbon and alloy steels). The initial pH in this vessel was 8.40.

• Vessel #20, operating with the "concentrated groundwater" at 90° C, containing specimens of the candidate corrosion allowance materials (carbon and alloy steels). The initial pH in this vessel was 8.94.

• Vessel #19, operating with the "acidified, concentrated groundwater" at 60° C, containing specimens of the "intermediate" materials (70/30 Cu/Ni and Alloy 400). The initial pH of the solution was 2.78.

• Vessel #18, operating with the "acidified, concentrated groundwater" at 90° C, containing specimens of the "intermediate" materials (70/30 Cu/Ni and Alloy 400). The initial pH of the solution was 2.68.

Vessels numbered 25 to 30 will contain the corrosion resistant Ni-base and Ti-base alloys, exposed to the three environments (dilute groundwater, concentrated groundwater, and acidified groundwater at the two temperatures). Test specimens (several thousand) are being readied, and these vessels should be brought on-line in the next few weeks.

All of the test vessels have operated without any major problems or perturbations. Early on, two of the liquid level sensors in the concentrated solution became plugged (due to salt precipitation), but power and make-up water automatically shut off to the affected vessels (as it was programmed to do) until the sensors were cleaned and re-installed. Since that time, no other malfunctions have occurred. The first rack of corrosion allowance materials will be removed from Vessel #23 (the first one to operate) in late

March 1997. These specimens will then be characterized and corrosion rates/attack patterns measured. Therefore, the first results from the long-term corrosion test facility will become available in the April-May 1997 time period.

At the beginning of the exposure period, a water sample was withdrawn for chemical analysis; additional water samples will be withdrawn to determine any variations of the water chemistry with time. Microbiological samples were also withdrawn; as expected, there is evidence that there is microbiological activity. The microbiological activity and its significance will also be tracked with time.

Depending on the level of funding, additional vessels and hardware will be acquired for completing the planned test matrix for the range of environments and candidate materials. Current plans are to add six vessels to complete the "single metal" part (Increment 2), and six vessels for the galvanically coupled specimens (Increment 3) in FY-97. These additions are planned for the summer of 1997.

Beyond FY-97, it is possible that some revision in the choice of environments will occur, since the corrosion (at least of the corrosion resistant materials) will be so greatly reduced to negligible amounts in the very high alkaline environments. Also, the susceptibility to localized corrosion for the corrosion resistant materials is very much reduced (see Section 2.5). On the other hand, testing in moderately acid environments (pH 4-5) may be very instructive in projecting the performance of these materials, since the intermediate pH condition also represents a condition caused biotically (microbial activity) or abiotically (creviced geometry), and a *condition more likely to occur*. However, no firm decision has been made on which environments to pursue and which vessels to allocate to which environments. Also, in the coming year, vessels for exposing the galvanically coupled specimens will be procured and installed, and a decision reached on which environments to use for these tests.

The long-term comprehensive corrosion test is a cornerstone for much of the testing effort. Several other activities interface with the long term test. For example, the electrochemical testing, described in Section 2.5, predicts the relative susceptibilities of the candidate materials to localized corrosion; the long term corrosion test validates whether these predictions are true for the longer term. Future electrochemical work will focus on measurements of the corrosion potential over the same range of pH and electrolyte concentrations as the long term test. These measurements are important for modeling efforts. Parts of the long term comprehensive corrosion test have counterparts in the shorter term stress corrosion tests and galvanic corrosion tests, to be discussed in Sections 2.7 and 2.8. The saturated steam condition existing in the top half of the test vessels represents a condition approaching 100% relative humidity, and thus is an extension of data points obtained at lower humidities, as described in Section 2.3. Although the long term comprehensive corrosion test was designed to be indifferent to microbial activity (in the sense that neither microbes were inoculated nor were bactericides used to prevent their development), periodic measurment and interpretation of microbial activity will correlate with work discussed in Section 2.6.

References for Section 2.4

1) Gdowski, G. E., Yucca Mountain Project Activity Plan, Long Term Corrosion Studies, Metallic Barriers SIP Activity E-20-50, rev. 3, Lawrence Livermore Laboratory, 1996

2) Gdowski, G. E., Yucca Mountain Project Technical Implementation Plan, Accounting of Test Specimens for the Long Term Corrosion Testing, TIP-CM-01, Lawrence Livermore Laboratory, 1995.

3) Gdowski, G. E. Yucca Mountain Project Technical Implementation Plan, Receiving, Handling, and Storage of Specimens for Long Term Corrosion Testing, TIP-CM-02, Lawrence Livermore Laboratory, 1995.

4) Estill, J. , Yucca Mountain Project Technical Implementation Plan, Electronic Weight and Dimensional Data Entry in a Computer Database, TIP-CM-03, rev.1, Lawrence Livermore Laboratory, 1996.

5) Estill, J. Yucca Mountain Project Technical Implementation Plan, User Calibration of Mettler AT200 Analytical Balance, Lawrence Livermore Laboratory, 1996.

6) Estill, J. Yucca Mountain Project Technical Implementation Plan, User Calibration of Fowler Ultra Cal Mark III Digital Caliper, TIP-CM-05, rev. 1, Lawrence Livermore Laboratory, 1996.

7) Gdowski, G., Yucca Mountain Project Technical Implementation Plan, Formulation and Make-up of Simulated Dilute Water, Low Ionic Content Aqueous Solution, TIP-CM-06, rev. 1, Lawrence Livermore Laboratory, 1996.

8) Gdowski, G., Yucca Mountain Project Technical Implementation Plan, Formulation and Make-up of Simulated Concentrated Water, High Ionic Content Aqueous Solution, TIP-CM-07, rev. 1, Lawrence Livermore Laboratory, 1996.

9) Gdowski, G., Yucca Mountain Project Technical Implementation Plan, Formulation and Make-up of Simulated Acidic Concentrated Water, High Ionic Content Aqueous Solution, TIP-CM-08, Lawrence Livermore Laboratory, 1996.

10) Green, R., Yucca Mountain Project Individual Software Plan, Individual Software Plan for the Programmable Logic Controller, ISP-CM-01, Lawrence Livermore Laboratory, 1996.

Weight Loss Assembly

Specimen

Teflon Spacer

Mounting Bolt

Flat Washer
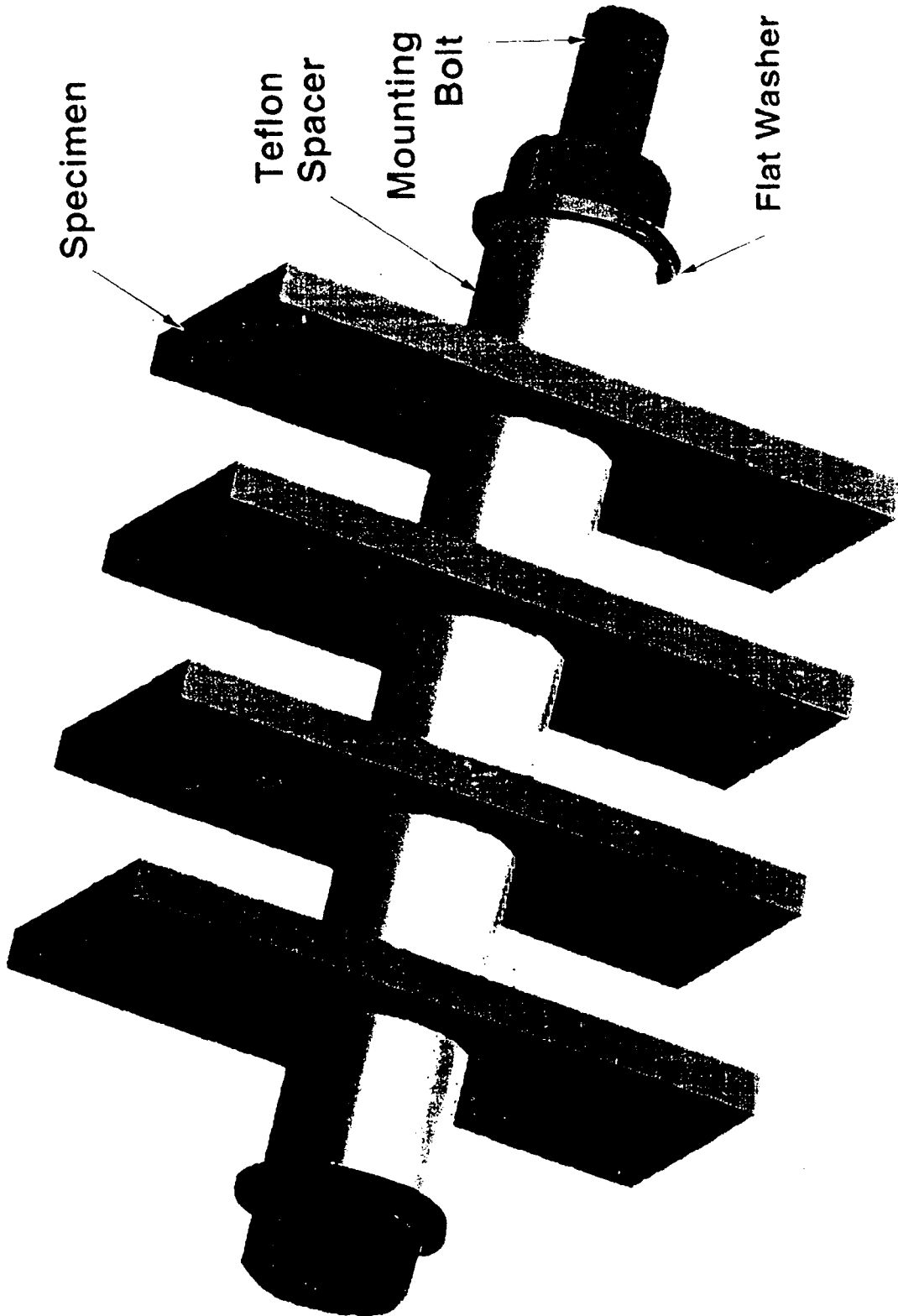
Specimen size: 2.5cm x 5cm x 0.3cm

Figure 2.4 - 1 Assembly of corrosion coupons for weight loss measurements in the long-term comprehensive corrosion test. Besides general corrosion, examination of the as-corroded surface will reveal susceptibility to pitting corrosion, crevice corrosion, selective leaching, and intergranular corrosion. The Teflon spacers maintain electrical isolation between specimens and the mounting hardware.

Crevice Corrosion Assembly

Specimen

Teflon Crevice Former

Belleville Washer

Mounting Bolt
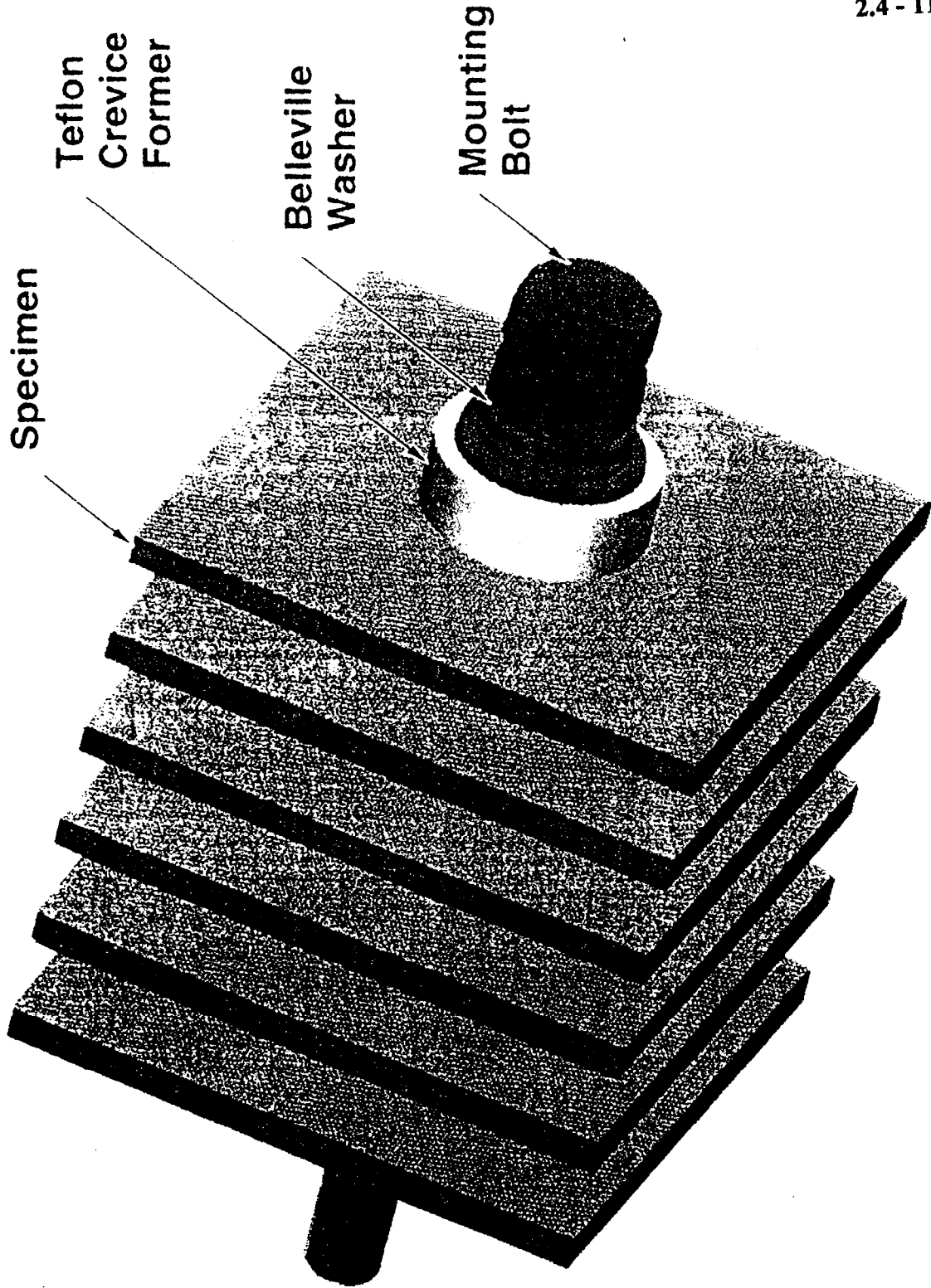
Specimen size: 5.0cm x 5.0cm x 0.3cm

Figure 2.4 - 2 Assembly of crevice corrosion specimens for the long-term comprehensive corrosion test. The Belleville washer, actually a spring made from Ni-base Alloy C-276, applies force to the Teflon to maintain tight crevice conditions. The Teflon electrically isolates the specimens from one another and from the mounting hardware and Belleville washers.

U-Bend Assembly

Specimen

Zirconia
Shoulder
Washer

Flat Washer

Mounting Bolt
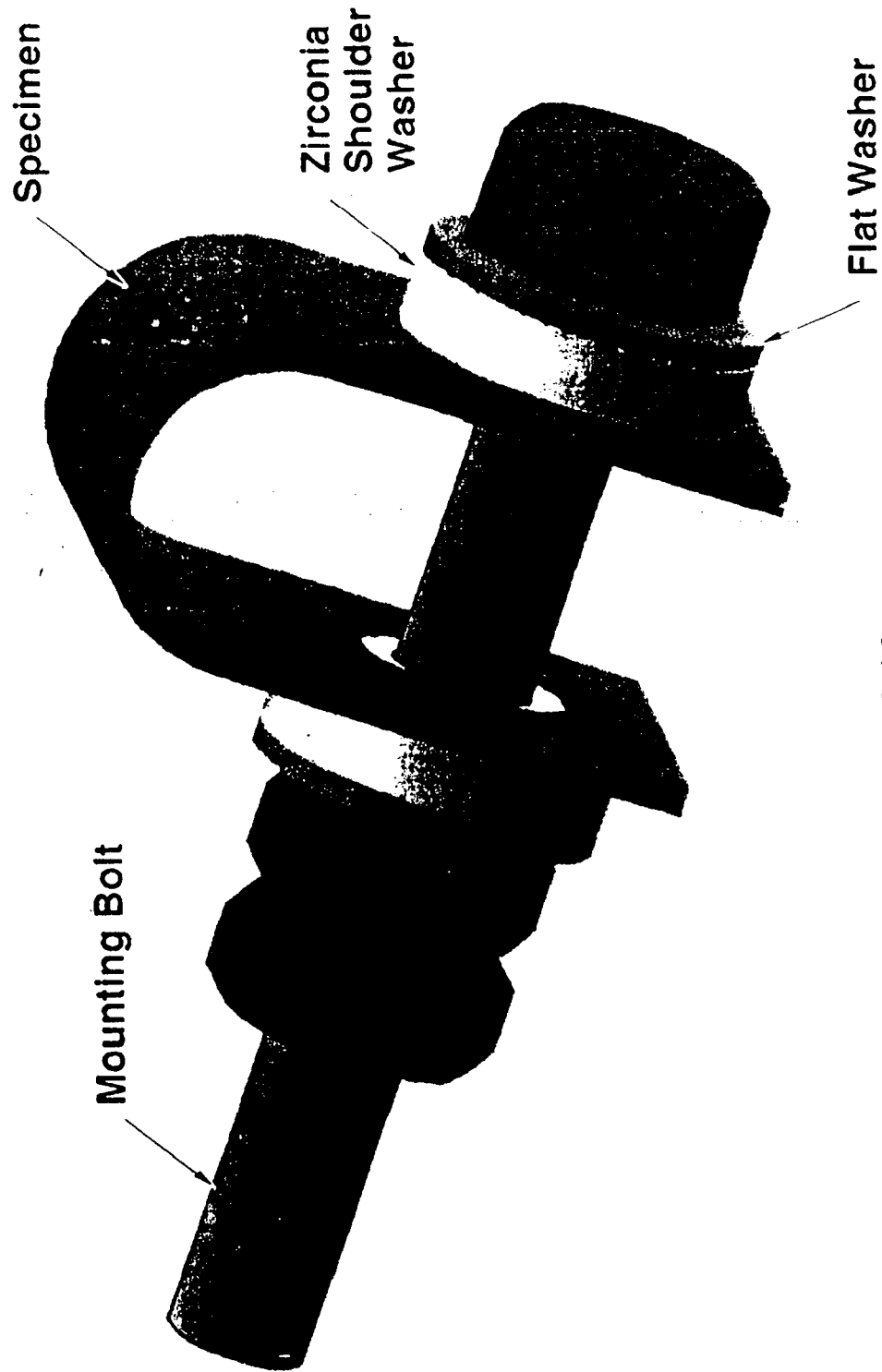
Specimen size: 3cm high x 1.9 cm x 0.16 cm

Figure 2.4 - 3 U-Bend assembly for the long-term comprehensive corrosion test.
Specimens are deformed plastically. The zirconia washer provides electrical isolation
from the mounting hardware. If the material is sensitive to stress corrosion cracking or
hydrogen embrittlement, cracks will form on the "U" and run perpendicular to the
direction of the bend.

Galvanic Specimen

Teflon
Coating

Corrosion
Allowance
or Cu-Ni

Corrosion
Resistant

Specimen size: 5cm x 5cm x 1cm
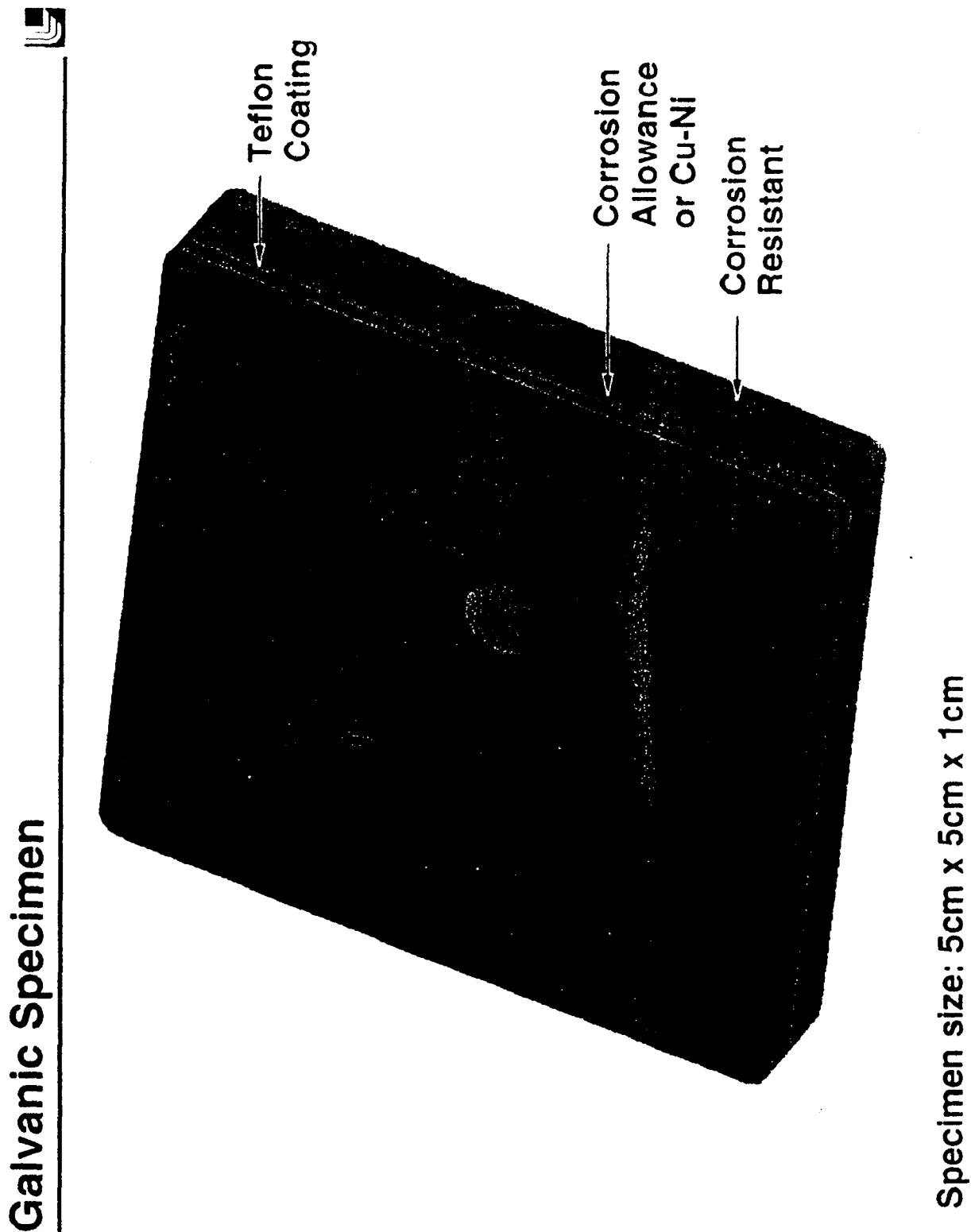
Figure 2.4 - 4 Proposed design for two-metal galvanic corrosion specimen for the long-term corrosion test. The outer corrosion allowance materials contains a bevelled hole to allow access of the test fluid to the inner corrosion resistant material. Some aspects of this specimen design may be modified.

2.5 Electrochemical Corrosion Testing

Input to this section of the report was provided by Ajit Roy.

2.5.1 Potentiodynamic and Potentiostatic Polarization

Electrochemical polarization experiments are being performed on several candidate materials for the corrosion resistant inner barrier to evaluate their susceptibility to localized corrosion, such as, pitting in deaerated acidic, neutral, and alkaline brines containing 1, 5, and 10 weight percent (wt%) NaCl at room temperature, 60°C, and 90°C. Materials tested include iron-nickel-chromium-molybdenum (Fe-Ni-Cr-Mo) Alloys 825, G-3, and G-30, nickel-base Alloys C-4 and C-22, titanium-base alloy Ti Gr-12, nickel-copper Alloy 400, and 70/30 Cupronickel. For comparative purposes, austenitic Types 304 and 316L stainless steels are also being tested. The chemical compositions of these alloys are shown in Table 2.5.1. All test solutions were prepared with distilled water and reagent-grade chemicals. While acidification was done by adding sulfuric acid to the brine, calcium hydroxide was added to prepare the alkaline salt solution. The pH of these solutions ranged between 2 and 3, 6 and 7, and 10 and 11, respectively. This work constitutes Metallic Barriers SIP Activities E-20-43 and E-20-44.

A three-electrode technique was used to conduct cyclic potentiodynamic polarization (CPP) and potentiostatic polarization experiments in Pyrex corrosion cells that contained a test specimen as a working electrode, two graphite counter electrodes, and a Luggin capillary connected to reference electrode. While, initially, a saturated calomel reference electrode was used at ambient temperature and 60°C, Ag/AgCl was later used as the reference electrode at all test temperatures. Cylindrical specimens were used in the CPP tests. Specimens used in the potentiostatic polarization experiments were disc-shaped. The test specimens were polished with 600-grit paper and cleaned with distilled water, acetone, and ethanol prior to their exposure to the test solutions.

Prior to conducting the polarization experiments, a few confirmatory tests[1] were performed on Type 430 stainless steel in deaerated 1.0 N sulfuric acid solution at 30°C to obtain the standard polarization plots, and to verify the reproducibility of the instrumentation. Electrochemical potential was applied to the test specimens using EG&G Models 273 and 283 potentiostats, controlled by an IBM-compatible PC with EG&G Model 252/352 Softcorr II software. A controlled-temperature water bath maintained the test temperature at the desired value within ± 0.1°C. For elevated temperature tests, a Pyrex condenser was fitted to one port of the cell to capture evaporated water and return it to the test cell. Dynamic potential scans were carried out in CPP experiments in the noble direction at the ASTM-specified[1] rate of 0.17 millivolt per second commencing at the stable corrosion potential (E_{corr}), and continuing to a potential sufficiently noble to cause pitting prior to reversing the scan at the same rate.

In electrochemical terms, the initiation of pitting occurs at a critical potential[2], E_{pit}, which is used as a measure of resistance to pitting corrosion. At E_{pit}, the anodic

polarization curve changes its slope abruptly, showing a dramatic increase in current density (Figure 2.5 - 1). The more noble E_{pit} is, the more resistant the material is to pitting attack. For susceptible metals and alloys, as the direction of polarization is reversed after some degree of anodic polarization above E_{pit}, a hysteresis is observed in which the return polarization curve follows an active (higher current) path, compared to the initial anodic one. The crossover at the passive current density defines a repassivation or protection potential[2], E_{prot}, below which established pits are presumed not to continue to grow. By contrast, new pits can initiate only at potentials above E_{pit}. Between E_{prot} and E_{pit}, new pits cannot initiate, but old ones can still grow.

E_{pit} values measured by CPP experiments were used in selecting the controlled potential to be applied in potentiostatic polarization tests involving a few selected susceptible materials. These tests were performed only in the acidic brine to evaluate pit growth at 90°C at applied potentials at or above the measured E_{pit} values.

The pH of the test solution was measured at room temperature both before and after each experiment. At the conclusion of each test, the specimen was cleaned with distilled water, acetone, and ethanol. The cleaned specimen was visually examined, followed by an optical microscopic evaluation to detect the presence or absence of pitting. The specimen underwent further metallographic examination if pits were detected by optical microscopy.

2.5.2 Cyclic Potentiodynamic Polarization Test Results

Results[3-5] indicate that, as expected, Types 304 and 316L stainless steels were susceptible to severe pitting corrosion in all three tested environments at 60°C and 90°C showing discernible E_{pit} values. Alloy 400 and 70/30 Cupronickel showed propensity to dissolution in all environments, both at ambient and elevated temperatures. Thick, orange-colored corrosion products were seen floating in the solutions, suggesting that elemental nickel, relatively electronegative compared to copper (i.e. -250 mV versus +337 mV, SHE), might have undergone preferential dissolution in response to the application of potential during the CPP experiments. As with austenitic stainless steels, the maximum current density attained just prior to the potential scan reversal was quite high.

With respect to the localized corrosion behavior of Fe-Ni-Cr-Mo alloys, Alloys 825, G-3, and G-30 suffered from pitting corrosion in acidic brines at all three chloride levels tested, with Alloy G-30 showing the least attack. Figure 2.5 - 2 shows a plot[6] of E_{pit} as a function of chloride concentration for all three alloys, showing a shift in E_{pit} to more negative (or active) values with increasing chloride concentration. This observation is consistent with the results obtained by other investigators[7,8]. In the presence of chloride, pitting of susceptible metals and alloys is due to the breakdown of protective oxide film. It has been suggested[7,9] that transition from passivity to pitting conditions can be explained by a competitive adsorption mechanism by which chloride ions (Cl^-) move into the double layer (oxide/liquid interface), eventually reaching a critical potential, E_{pit},

corresponding to the Cl⁻ required to displace the adsorbed oxygen species. The relationship between E_{pit} and pH for these three susceptible materials in solutions containing 10 wt% NaCl is illustrated in Figure 2.5 - 3[6]. It is obvious that for all three alloys, E_{pit} was shifted significantly to more noble values with a change in pH from acidic to neutral, as expected. The more active E_{pit} value in acidic solution is the result of acceleration of the cathodic reaction due to the high concentration of H^+ ions. At alkaline pH, Alloys G-3 and G-30 showed slightly lower E_{pit} values compared to those in neutral solution. However, E_{pit} for Alloy 825 was shifted to a more noble value at alkaline pH. The fact that E_{pit} was shifted to more positive values in alkaline brines (compared to that in acidic solutions) is in line with the well-established pitting inhibition effect of hydroxyl ions[10]. No explanation can, however, be provided as to the cause of lower E_{pit} value for Alloy 825 at the neutral pH. As to the effect of Cl⁻ concentration and pH on E_{prot}, no consistent pattern was observed.

The overall results from the CPP tests indicate that of all the materials tested, Alloys C-4 and C-22, and Ti Gr-12 exhibited the maximum corrosion resistance, showing no pitting or general corrosion in any environments tested. These three highly corrosion-resistant materials maintained their shiny surface appearances even after exposure to the test solutions and at very oxidizing potentials (~ 1 volt, SCE).

An effort was also made to correlate E_{corr} to the test temperature and the solution pH. However, no consistent pattern was observed[3]. At least in the case of variations in temperature, the lack of a consistent pattern is to be expected based on similar studies conducted by other investigators.

A comparison of the material responses to electrochemical polarization to high anodic potentials is illustrated in Figure 2.5 - 4. Cylindrical specimens were exposed to acidc brine at 90° C and polarized from E_{corr} to potentials well into the transpassive region. The surfaces indicate the relative susceptibilities of the candidate materials to these aggressive conditions. The two stainless steels showed extensive pit formation, while the higher Ni alloys, G-3 and 825, showed fewer pits. Alloy G-30 showed some very light pits, while Alloys C-4 and C-22, as well as Titanium Grade 12, were free of pits despite the harsh conditions. The Cu/Ni alloys, Monel 400 and 70/30 copper nickel, underwent enhanced general corrosion at these high anodic potentials.

A limited number of longer-term (2-8 hours) potentiostatic polarization tests were performed[5] using Alloys 825 and G-3 in the acidic brine at 90°C to characterize the numbers, sizes (depth and diameter) and shapes of pits formed. In contrast to fairly deep round pits observed with Alloy 825, pits observed in Alloy G-3 specimens were elongated and deeper. These data are expected to be used in developing and verifying stochastic pitting models. The data obtained on Alloy 825 and used in the stochastic pitting model are further described in Section 2.11 of this report.

More recently, some polarization tests were performed on specimens of Alloy 625. As expected, the behavior of this material is intermediate between that of the lower Mo

content alloys (Alloys 825 and G-3) and that of the high Mo alloys (Alloys C-4 and C-22). In the acidic chloride solutions, Alloy 625 showed some pitting as a result of the potential excursion to high anodic potentials. These tests are continuing. To date, none of the cyclic polarization tests on Alloy C-22 have shown any pitting or crevice attack, even when tested in the same aggressive acid chloride solutions. This evaluation is also continuing.

2.5.3 Electrochemical Testing Future Work

CPP experiments are ongoing to evaluate the effects of Cl⁻ concentration, pH, temperature, and potential scan rate on E_{pit} and E_{prot} for materials susceptible to pitting corrosion. Determination of the potential scan rate effect forms and extrapolating the scan rate to zero provides the linkage between the potentiodynamic and potentiostatic methods. The effect of ferric ion will then be investigated, since ferric ion will be produced by the corroding steel outer barrier material. Ferric ion, particularly in acidic solutions, is well known as favoring pitting corrosion on some of the nickel-base alloys that are candidate materials for the inner barrier. A series of tests was recently begun, using the same test solutions as those in the Long Term Corrosion Test (See Section 2.4). As expected, the individual polarization curves show a more complex shape than those determined in simple chloride solutions. This effect is probably due to the combined effects of the various ionic species -- some tending to promote passivity, while others favor breakdown of the passive film. These tests are continuing in order to consider the full test matrix with different intermediate pH values. Discussion of the test matrix, as well as additional test technique details, can be found in the activity plan for this work [11].

Susceptibility to stress corrosion cracking (SCC) is also dependent on electrochemical potential, and there is a "critical potential" for the onset of these phenomena. Work is proposed to determine these critical potentials using strained electrodes to determine the potential at which the current rises appreciably due to film breakdown and rapid dissolution. This is the work described in Metal Barrier Activity E-20-45. Efforts are also being made to initiate galvanic corrosion studies of candidate waste package container materials using both electrochemical and immersion techniques. (MB Activity E-20-46). Finally, in conjunction with the environments used for long term comprehensive corrosion test, determination of the corrosion potentials of the candidate materials in these environments, and possible changes in the corrosion potential with exposure time, will be performed as MB Activity E-20-51.

References for Section 2.5

1.ASTM Designation: G 5-94, "Standard Reference Test Method for Making Potentiostatic and Potentiodynamic Anodic Polarization Measurements," American Society for Testing and Materials 1995 Book of Standards, Volume 3.01, pp. 48-58, ASTM, Philadelphia (1995).

2.R. Baboian and G. S. Haynes, "Cyclic Polarization Measurements - Experimental Procedure and Evaluation of Test Data," Electrochemical Corrosion Testing, ASTM STP 727, F. Mansfeld and U. Bertocci, Eds., American Society for Testing and Materials, pp. 274-282 (1981).

3.A. K. Roy et al., "Electrochemical Corrosion Studies of Container Materials in Repository-Relevant Environments," LLNL UCRL-ID-122860, December 1995.

4.A. K. Roy and R. D. McCright, "Pitting Corrosion of Container Materials in Anticipated Repository Environments," LLNL UCRL-JC-122572, November 1995, presented at the 1996 International High Level Radioactive Waste Management Conference, Las Vegas, NV, April 29-May 3, 1996.

5.A. K. Roy et al., "Localized Corrosion of Container Materials in Anticipated Repository Environments," LLNL UCRL-JC-122861, May 1996, presented at the 189th Meeting of The Electrochemical Society, Inc., Los Angeles, CA, May 5-10, 1996.

6. A. K. Roy et al., "Effect of Chloride Concentration and pH on Pitting Corrosion of Waste Package Container Materials," LLNL UCRL-JC-123891, presented at the 190th Meeting of The Electrochemical Society, Inc., San Antonio, TX, October 6-11, 1996.

7.H. P. Leckie and H. H. Uhlig, "Environmental Factors Affecting the Critical Potential for Pitting in 18-8 Stainless Steel," J. Electrochem. Soc. Vol. 113, p. 1262 (1967).

8. N. Sridhar and G. A. Cragnolino, "Applicability of Repassivation Potential for Long-Term Prediction of Localized Corrosion of Alloy 825 and Type 316L Stainless Steel," Corrosion Vol. 49, No. 11, pp. 885-894 November 1993.

9 .J. Horvath and H. H. Uhlig, "Critical Potentials for Pitting of Ni, Cu-Ni, Cr-Fe, and Related Stainless Steels," J. Electrochem. Soc. Vol. 115, p. 791 (1968).

10. .Z. Szklarska-Smialowska, Pitting Corrosion of Metals, NACE, Houston, TX, p. 147 (1986).

11. Yucca Mountain Project Activity Plan, Critical Pitting Potential Measurements (43); Critical Crevice Potential Measurements, Using Electrochemical Potentiodynamic Polarization Techniques, Metallic Barrier SIP Activitie E-20-43/44, Lawrence Livermore Laboratory, 1996

Table 2.5.1

Chemical Composition of Materials Tested (Weight Percent)

Material	Heat No.	C	Mn	P	S	Si	Ni	Cr	Mo	Fe	Ti	Al	Cu	Others
Type 304 SS	K299	0.07	1.55	0.031	0.009	0.48	10.18	19.90	0.10	Bal	-	-	0.10	N-0.05
Type 316L SS*	16650	0.03 (max)	2.00 (max)	0.03 (max)	0.03 (max)	0.75 (max)	10.00 - 14.00	16.00 - 18.00	2.00 - 3.00	Bal	-	-	-	N-0.10 (max)
Alloy 825	HH3884FG	0.03	-	-	0.001	0.33	39.84	22.11	3.40	Bal	0.88	0.70	1.80	-
Alloy G-3	1298558857	0.004	0.80	0.009	0.003	0.36	Bal	22.26	6.88	19.29	-	-	1.90	(Nb+Ta)-0.30 W-0.85;Co-1.01
Alloy G-30	1810397529	0.01	1.10	0.013	0.002	0.30	Bal	29.30	5.10	15.00	-	-	1.90	(Nb+Ta)-0.83 W-3.20;Co-3.80
Alloy C-4	1245550905	0.004	0.16	0.006	0.006	0.02	Bal	15.66	15.49	0.25	0.21	-	-	Co-0.10
Alloy C-22	1227793285	0.004	0.26	0.008	0.002	-	Bal	21.80	13.60	4.70	-	-	-	W-3.20;V-0.14 Co-1.65
Ti Grade-12	G9557	0.0075	-	-	-	-	0.75	-	0.30	0.13	Bal	-	-	O-0.14;N-0.0065 Y-<0.005;H-0.0016
Alloy 400	D068	0.050	1.01	-	0.007	0.050	66.46	-	-	0.93	-	0.002	31.49	-
70/30 Cupronickel[+]	NA	-	1.00 (max)	-	-	-	29.00 - 33.00	-	-	0.40 - 1.00	-	-	Bal	Pb-0.05 (max) Zn-1.00 (max)

*Nominal composition per ASME Specification: SA-240, 1990. Actual composition was not analyzed.
[+]Nominal composition per ASTM Designation: B 171 / B 171M-91a. Actual composition was not analyzed.
NA: Not available
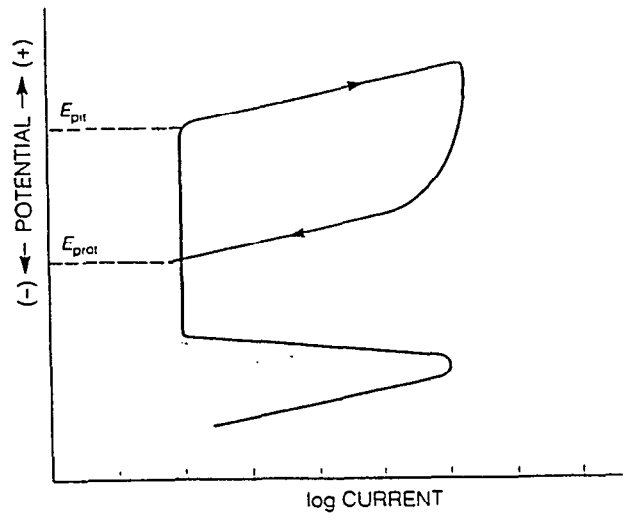
Figure 2.5-1   A Schematic View of a CPP Diagram Showing E_{pit} and E_{prot}
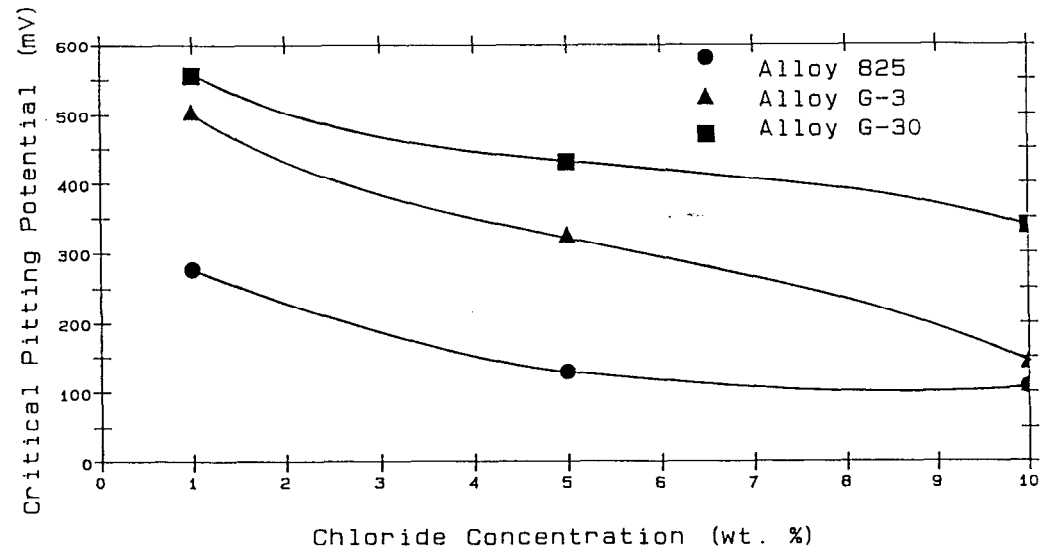

Figure 2.5-2 E_{pit} (Ag/AgCl) vs Chloride Concentration in Acidic
Solutions (pH~2.36 to 2.85) at 90°C
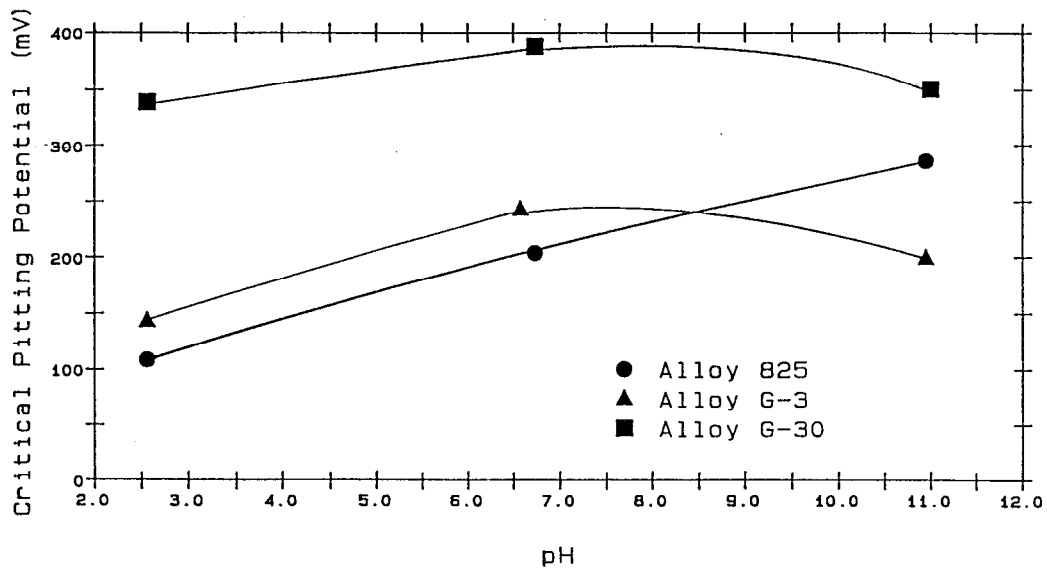
**Figure 2.5-3** E_{pit} (Ag/AgCl) vs pH in Solutions Containing
10 wt% NaCl at 90°C
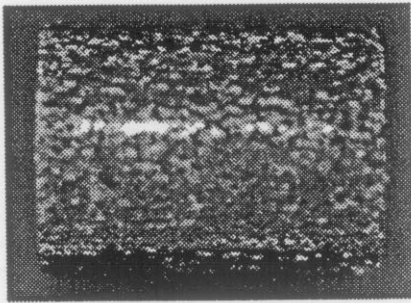
Type 304 SS
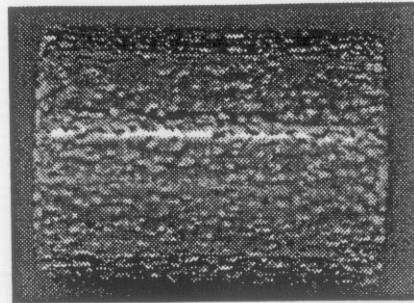
Type 316L SS
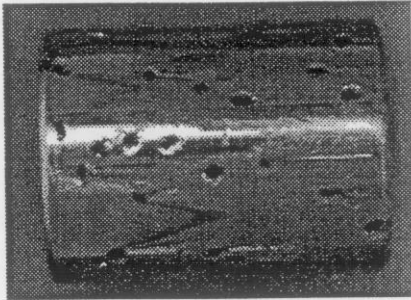
Alloy 825
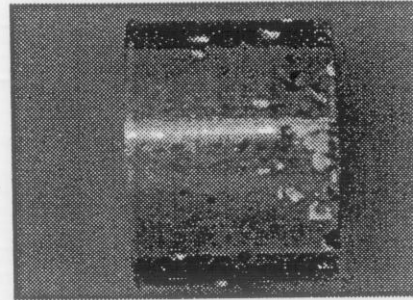
Alloy G-3
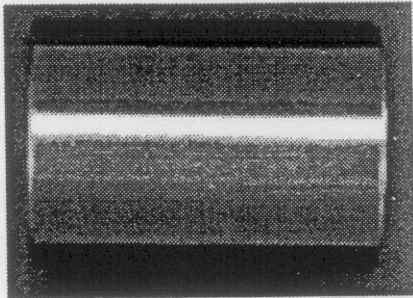
Alloy G-30
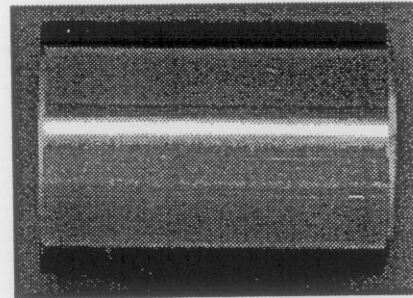
Alloy C-4
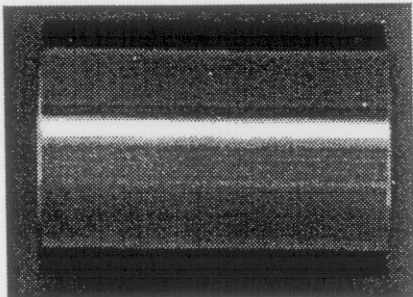
Alloy C-22
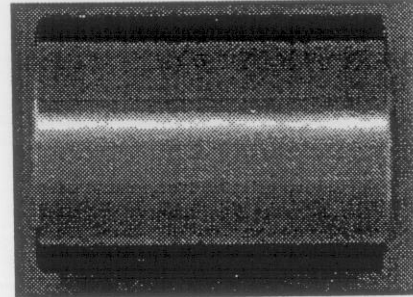
Ti Gr-12
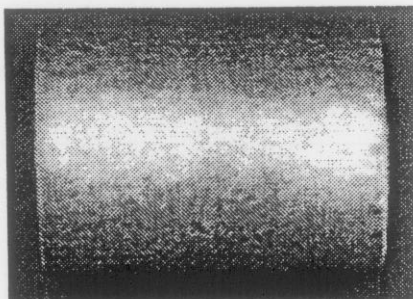
Alloy 400
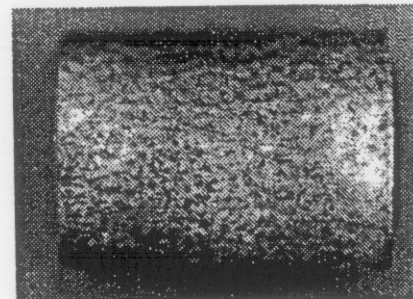
70/30 Cupronickel

Figure 2.5-4 Comparison of specimen surface appearance
of all materials tested in acidic brine at 90°c

2.6 Microbiologically Influenced Corrosion (MIC)Testing

(input to this section of the report was provided by Joanne Horn and Denny Jones)

Native micro-organisms reside within the potential repository environment. Microbial communities have been characterized from a variety of deep sub-surface environments, and previous work has already identified some of the native microbiota in the Yucca Mountain region [1]. Microbes vary widely in their types of metabolic activities, and the consequent alterations to the surrounding environment that they can facilitate [2]. Presumably, native microbes that are currently present have or have had adequate nutrient resources for their existence. The establishment of bacteria introduced through drift construction will likewise be dependent on adequate nutrient supplies and their rates of adaptation to the repository environment.

Conditions anticipated upon waste emplacement in the Yucca Mountain repository will include extreme heat, desiccation, and *possibly* high levels of ionizing radiation. The initial presence of extreme conditions within the repository may not completely preclude microbial activity; even if general conditions extend beyond those able to support microbial activity, there may be micro-environments in which environmental extremes are mitigated. In any case, eventual repopulation of the near-field environment through re-entry of water carrying both nutrients and microbes is anticipated as overall repository conditions become less extreme. Organisms that thrive at high temperatures or which form spores under adverse conditions will be extant within the native or introduced microbial communities at Yucca Mountain. These species will regain activity as conditions become favorable. Microbial populations may acidify and otherwise alter the water chemistry of the near-field repository environment, as well as directly affect the corrosion of waste packages. The degradation of materials and the consequent alteration of the aqueous chemical environment will depend on the presence of adequate nutrients and water to maintain at least a minimum of activity.

Work in the microbiologically-influenced corrosion (MIC) activity seeks to establish the range of probability, rate, and required conditions for MIC of candidate metal barrier materials in the potential Yucca Mountain (YM) Repository. Specifically, the work described here is designed to at least initiate the determination of: 1) whether microorganisms contained within the post-construction YM environment possess activities that have been associated with metal corrosion, 2) define boundary conditions for these activities and characterize their rates under varying conditions, and 3) the rate of microbially-influenced corrosion of candidate metal barrier materials under accelerated testing conditions. Screening and quantification of microbiological activities will establish the likelihood and conditions under which bacterially-facilitated metal corrosion may occur, and may thus impinge on the design of various repository elements. Accelerated testing will provide the degree of resistance of various candidate alloys to microbial corrosion, and thereby contribute information germane to the final choice of waste package materials. A survey of MIC effects on both the outer barrier candidate materials and the inner barrier corrosion resistant material is underway as Metallic Barrier

SIP Activity E-20-60. Much of the work to date has been focused on isolating and culturing the various strains of bacteria known to influence the corrosion of candidate materials for the waste package container.

2.6.1 Microbiological Mechanisms of Metal Corrosion

Currently, it is recognized that MIC is a complex group of interacting processes, carried out by a number of classes of bacteria (as reviewed by Borenstein [3], illustrated in Fig 2.6 -1). Not all of these microbial processes occur in every instance of MIC. Rather, the different classes of microbes, each contributing, their own corrosive properties, occur in various permutations, depending on the metal surface and surrounding environmental conditions.

Many micro-organisms secrete organic and inorganic acid metabolites into the surrounding environment. Clearly, the production of oxidizing acids (including sulfur oxidizers that cause the formation of H_2SO_4) are directly corrosive, and contribute to hydrogen generation for consumption by sulfate reducers.

Iron oxidizing bacteria use ferrous ions as an electron source, generating ferric ion which precipitates as an oxide. The resulting tubercles also act to create anoxic cells beneath colonies of these organisms. Additionally, ferric cations attract and combine with free chloride anions, producing ferric chloride, which is very aggressive toward many metals.

Bacteria which secrete exopolysaccharides form slime capsules that obstruct the free diffusion of oxygen to the metal surface; this is exacerbated by aerobic slime producers embedded within the slime layer that consume available oxygen. The anoxic environment within the slime creates an electrochemical potential change beneath the film which degrades the protective metal oxide film and causes pitting. The creation of anoxic cells also facilitates the growth of sulfate reducers.

2.6.2 Prior Studies Performed in the Near Field Environment Task

Growth of Whole YM Communities

As part of the Near Field Environment Task (WBS 1.2.3.12), samples of Topopah Springs tuff were initially aseptically collected from a mined Fran Ridge outcrop (the Large Block Test Site, LB), and rock excavated during construction of the Exploratory Studies Facility (ESF, Yucca Mountain, NV). The aim was to collect rock samples which had been exposed to construction activities and were representative of the post-construction repository environment. Bacteria which had been introduced by construction machinery, introduced materials, and human intervention could thus be included in subsequent isolations and testing.

Growth rates of YM-derived microbial communities were determined by adding 10g of crushed rock samples (1.68-2.36 mm grain size) to 50ml of R2 broth, a low nutrient

formulation [4]. Samples were incubated aerobically by shaking in covered flasks at ambient temperature, $30^{\circ}C$, and $50^{\circ}C$. Sterile controls were prepared by repeated cycles of autoclaving ($120^{\circ}C$) and incubation. Growth was monitored by periodic live plating of appropriate dilutions on R2 agar (Difco). Growth rates of whole communities of YM-derived microorganisms in low nutrient R2 broth varied somewhat, depending on the temperature of incubation. While communities grown at room temperature or $30^{\circ}C$. showed altered doubling times with respect to those grown at $50^{\circ}C$., all cultures, demonstrated significant increases in cell numbers, ranging to over 20,000 cells/ml of media, at the conclusion of the 10 h. growth period (Fig. 2.6-2). Additionally, it was found that some bacterial isolates, most likely spore-forming species, survived repeated exposure to $120^{\circ}C$.

These results reveal that even a modest nutrient source supports significant logarithmic growth of native and introduced YM bacteria, and total microbial cell densities reach similar levels regardless of the temperature of incubation (Figure 2.6-2). Probable spore-forming microbial species were able to survive repeated autoclaving ($120^{\circ}C$), demonstrating that even at the highly elevated temperatures expected to occur after waste emplacement in the repository, some of the endogenous microbiota may be able to survive through these extended periods of intense heat.

Isolation of Individual YM Bacterial Strains

Microorganisms were isolated both aerobically and anaerobically from whole and aseptically-crushed (1.7-2.4mm) rock samples at room temperature by plating directly, or washing rock samples with Artificial J-13 Pore Water (APW) [5], and plating onto low nutrient R2 agar. Organisms that survive in nutrient-depleted environments and at elevated temperature were isolated from crushed samples (1.0g) after extended growth (aerobic incubation, 72 h.; anaerobic incubation, 17 days) in R2 broth at room temperatures and $50^{\circ}C$. After extended cultivation, samples were incubated on R2 agar at the temperature of previous growth.

Plating of whole and crushed rock/washes at room temperature on R2 agar showed higher species diversity contained in LB samples than those obtained from ESF samples. Also, crushed rock/washes displayed generally lower species diversity and cell numbers than those arising from whole rock (e.g., Fig.2.6 -3). Finally, greater diversity and cell numbers were obtained after growth under aerobic conditions than under anaerobic culture conditions. Extended growth at room temperature and $50^{\circ}C$ showed generally a low diversity of microbial forms (one to three cell types). However, high cell numbers were reached after extended growth under aerobic conditions (2×10^8-10^9 cells/ml), while anaerobic conditions produced low cell densities (e.g., 140 cells/ml), and no growth was evident after extended anaerobic incubation at $50^{\circ}C$.

Since manipulation of rock samples has been reported to alter the kinds and numbers of organisms recovered [6] , our results regarding the number and types of organisms from whole versus crushed rock, are consistent with past findings.

YM tuff was collected and crushed while exposed to the ambient air, also initial transfers of organisms cultivated on oxygen-depleted agar plates and broth were briefly exposed to air. Therefore, it must be assumed that those organisms cultivated under reduced conditions are either somewhat aero-tolerant (i.e., oxygen is not completely toxic to them, for at least brief periods), or they are capable of both oxic and anoxic growth (so-called "facultative anaerobes"). This became more evident in the results of subsequent experiments (below).

It may also be expected that both higher temperatures and anoxic conditions could result in lower cell numbers and diversity of those microbes obtained under these culture conditions. Topopah Springs tuff and its associated pore water has been characterized as generally containing a significant amount of oxygen [7], such that strictly anaerobic, or even facultatively anaerobic organisms, might be expected in lower abundance relative to strict aerobes. Since elevated temperatures are not the norm in the subsurface, those organisms adapted to growth at $50^{\circ}C$. may not likewise be immediately expected to be present in high abundance. However again, the demonstration that at least some organisms at the YM site are capable of growth at higher temperatures and under lower oxygen tensions shows that a subset of the extant YM microbial community harbor the potential to grow and survive at elevated temperatures and under reducing conditions .

LB samples, originating from a Fran Ridge outcrop that more closely resembles the geological characteristics of the repository unit, display greater microbial diversity (on R2 agar) that those from the ESF-excavated rock, which had not yet reached the repository horizon. Thus, greater microbial diversity might be extant in the repository horizon than in overlying geological units.

The paucity of microbial forms after extended growth is expected. It is accepted that under stressed conditions, such as those created by the depletion of nutrients, that only a few members of the community are equally well-adapted to exploit the minimal resources available; these will outgrow those species less able to compete.

While any given growth media (e.g., R2) permits only the growth of a small fraction of a microbial community [8, 9] , a multiplicity of microbial types were still detected from whole and crushed YM rock on R2 media; henceforth these were treated as a sample of the total microbial community present at this site. A representative group of distinct individual isolates were purified by repeated streaking of single colonies, many of these were identified by fatty acid analysis [10] (Welch, 1991; Analytical Services, Inc., VT), but some remain unidentified. All purified isolates (ca. 60) were preserved for use in further experiments.

Identified and preserved YM bacterial isolates included representatives of the following genera: *Bacillus, Arthrobacter, Cellulomonas, Corynebacterium, Pseudomonas, Staphylococcus, Xanthomonas,* and *Flavobacterium.* These bacterial classes collectively contain members that are capable of forming spores, producing acids, degrading a wide variety of organic compounds, and remaining active under both oxic and anoxic conditions.

2.6.3 Enrichment of Corrosion-Specific Bacteria from YM Tuff

The oxidation of $Fe(II)$ to $Fe(III)$ and the reduction of sulfate to sulfide are elements of different microbial metabolic pathways that have been linked to metal corrosion processes [3, 11]. Therefore, efforts were made to culture organisms that carry out these transformations from YM geologic samples. Iron oxidizers, such as species of bacteria of the genus *Thiobacillus*, utilize $Fe(II)$ as an energy (electron) source with the concomitant production of $Fe(III)$, and they obtain carbon for cellular growth by fixing carbon dioxide from the surrounding environment. The ferric iron produced by these bacteria can react with iron sulfide (pyrite) spontaneously to form more ferrous ions and sulfuric acid. As a result iron oxidizing bacteria have evolved to function under very acidic conditions.

Iron oxidizing microorganisms were cultured from YM tuff by inoculating 5g samples of crushed tuff into media previously reported to support the growth of these organisms (i.e., ATCC Media #64, containing $Fe(III)$, no exogenous carbon source, and at pH 2.8; [12]. As a control for suitable growth conditions, three known and characterized iron-oxidizing microbial strains were grown in parallel with those enriched from YM tuff (*Thiobacillus ferrooxidans* ATCC#21834, #14119, #33020).

Sulfate reducing bacteria use sulfate as a terminal electron sink, thereby transforming it to sulfide. These organisms typically are grown with lactate as a carbon and electron source. Thus, to encourage the growth of these organisms from YM geologic media, 5g samples of aseptically ground tuff were similarly inoculated into two types of media containing sulfate and lactate (Baar's media and sulfate-reducing media; shown in the Atlas of Microbiological Media)[12]. The suitability of growth conditions was judged by the growth of a known sulfate-reducer, *Desulfovibrio vulgaris* ATCC#29579, grown in parallel with test samples.

All cultures were incubated at room temperature and periodically 5-10% of the culture was transferred to fresh media; a total of four transfers were made over several months of incubation. In this fashion, if iron-oxidizing or sulfate-reducing organisms were extant within the samples, their growth would be encouraged due to hospitable culture conditions, over other members of the microbial community.

All control strains grew well under the conditions provided, showing that the media and conditions used did allow growth of these types of organisms. The iron-oxidizing enrichments from both LB and ESF geologic samples, likewise produced iron-oxidizing cultures (as adjudged by later plating on solid ISP media; Fig. 2.6.4) [13]. However,

sulfate reducing bacteria were not recovered from either ESF or LB tuff, despite repeated attempts using two types of sulfate reducing media and the growth of the control strain under the same conditions. Sulfate reducing bacteria were recovered using the same enrichment techniques from some select sites within the ESF, demonstrating that the presence of sulfate reducing bacteria, key players in the corrosion process, are clearly not ubiquitous.

Enrichment cultures may or may not be a single bacterial species or strain, and thus it must be assumed in the absence of further characterization, to be a consortium of bacteria all having either sulfate-reducing or iron- oxidizing metabolic modes. Iron-oxidizing enrichment cultures were frozen for preservation and use in further experiments, as were the sulfate reducers that were obtained outside the immediate YM site.

Iron reducing strains, which use Fe(III) as a terminal electron acceptor producing Fe(II), may effect corrosion directly by anodic depolarization [14], and affect the availability and source of Fe(II) for subsequent microbial iron oxidation. As an initial attempt to enrich these organisms from YM rock, 5g of crushed ESF and LB material was inoculated into a media formulation that provided lactate as a carbon and energy source and nitrate as an electron acceptor [15]. This type of media has been shown to support the growth of iron reducing strains under aerobic growth conditions, however it should be noted that it will also support the growth of other types of organisms as well. A characterized iron reducer, *Shewanella putrifaciens* ATCC#8071 [12], was grown in parallel as a control. Growth was observed of both the control strain and arising from crushed YM rock samples, and periodic transfer of the cultures were carried out (as above). Finally, after four transfers, the enrichment culture was frozen for future analysis.

Colorimetric assays for determining the concentrations of Fe(II) and Fe(III) using ferrozine reagent [16, 17] were tested using water as a solvent. Linear standard curves were obtained [with a dynamic range extending 5-100ppm Fe(II)] under these conditions. Iron oxidizing and possible iron-reducing consortia will be analyzed to quantify their rates of iron reduction/oxidation using these assay techniques.

2.6.4 Screening for Acid- and Sulfide-Producing Bacteria
Screening for Acid-Producers

The production of organic acids as products of microbial central metabolism is well-documented [2]. The generation of acids has been both directly and indirectly linked to metal corrosion. Microbially-generated acids have been shown to directly dissolve the protective calcareous film on stainless steel [18]. Coupling of protons with electrons results in electron removal from the cathode [3], and forms hydrogen which is a substrate for microbial sulfate reduction (Fig; 2.6 -1) [19]. Therefore, the library of YM isolates that were recovered from LB and ESF geologic samples (above) were screened for those that demonstrated a decrease in pH during active growth.

As an initial screen to identify acid-producing strains among the preserved YM microbial isolates, all isolated strains were grown separately in R2B media (with or without amendment of 0.5% glucose), using the pH indicators bromocresol purple ($pK_{indicator}$=5.3) or methyl red ($pK_{indicator}$=4.1). Under these conditions, a change in the color of the culture indicates the production of acid, thereby providing a rapid means of assessing acid production by the 46 strains tested. Anaerobically-grown strains were incubated under anaerobic conditions, while aerobically-isolated strains were cultivated with aeration, and all strains were incubated at either room temperature or 50°C., depending on their temperature of isolation. Sterile, uninoculated controls were included in all experiments. The pH endpoint was determined using a standard pH meter for at least one trial.

Results revealed that both growth and acid production were more rapid when the media was amended with glucose. This is not surprising given that acid production is largely a result of carbon utilization; addition of glucose provides at once more carbon and energy for growth, together with a greater potential rate of acid generation. When 46 bacterial isolates were tested with glucose amendment, 10 (21.7%) of these displayed a decrease in pH (from about pH 7.0) to pH 5.3 or less after a period of growth lasting from 3 to 16 days. When glucose was not added to the media, only 5 strains tested showed similar extents of acid production. Sterile control cultures maintained the initial pH of the media. While there was some interference of the pH indicator with measurement of the pH endpoint (probably due to titration of protons by the indicator) and even growth in some instances, the lowest pH attained was 4.46 after a 76 hour incubation by a *Pseudomonas stutzeri* LB isolate in media with added glucose and the methyl red indicator.

These results indicated that microbially-induced metal corrosion will be accelerated with inclusion of a readily metabolizable carbon source which promotes both growth and acid production. Thus, materials testing should include added glucose in the media, as glucose will contribute towards accelerated testing conditions. Compilation of the screening results revealed eleven strains that produce acid under the described conditions of growth, which included members of the genera *Cellulomonas, Pseudomonas, Flavobacterium, Bacillus,* and *Arachnia*. (Table 2.6 -1), five strains were further analyzed to determine their rates and extents of acid generation, and to further determine conditions under which acid is produced; these strains would be considered for specific inclusion in accelerated materials testing (below): LB-71h-RT-13 (*Pseudomonas stutzeri*); ESF-71h-RT-4 (*Flavobacterium esteroaromaticum*); LBan-U7 (uncharacterized); LB-71h-50-3 (*Bacillus pumilus* GC subgroup B); LBan-C1 (poorly matched to *Propionibacterium*).

<u>Screening for Sulfide Producers</u>

Microbially-produced sulfide may be corrosive to metals, as are the ferrous sulfides that form when produced sulfide reacts with solubilized ferrous ions. Most often these activities are associated with sulfate reducing bacteria, which directly promote corrosion by depolarizing the cathode through consumption of available hydrogen from the metal surface [3] . Attempts to isolate sulfate reducers from the immediate YM environs failed. However, microbes can also produce sulfide by the decomposition of proteins, a process

known as "putrefaction" or "desulfurylation", in which the sulfur-containing amino acids methionine and cysteine are broken down, releasing sulfide in the process.

While the evidence that sulfide and ferrous sulfide *directly* contribute to metal corrosion is not entirely conclusive [20] , a screening technique was devised to detect desulfurylating microbes among the preserved isolates contained in the YM library. These efforts were aimed at determining whether YM microorganisms harbor desulfurylation capabilities, assessing the potential contribution of desulfurylation to metal corrosion (i.e., the direct effects of sulfide and ferrous sulfide), and to ascertaining those alloys that may be more resistant to these microbial products.

All preserved isolates were screened in test tubes containing R2 agar supplemented with 0.75% proteose peptone #3 (Difco), to provide an excess supply of amino acids for desulfurylation reactions (R2 normally contains only 0.05% of peptone;[4] . Additionally, the media contained 0.05% lead acetate, which precipitates as lead sulfide when sulfide is produced as result of microbially-driven peptone decomposition; the lead sulfide is detected by blackening of the agar medium.

The library of YM bacteria were each individually inoculated into R2+peptone+lead agar acetate media contained in screw-top test tubes, by streaking on top of the agar surface (exposed to the air in the headspace of the tube) and stabbing into the agar within the tube (under which conditions growth is anoxic or micro-aerobic). Sterile, uninoculated control tubes were monitored in parallel with inoculated ones. All samples were incubated at room temperature or 50° C., depending on the temperature of strain isolation. Growth and (lead) sulfide generation was monitored over a 34 day period.

21 of the 45 aerobic strains tested (46.7%) demonstrated sulfide production in the oxic area of the culture (none of these were strains that were isolated and incubated at 50° C.), whereas only three of the aerobically-isolated strains (all 50° C. isolates) showed sulfide production in the anoxic area of the culture. Three of the 17 (17.6%) anaerobically-isolated bacteria tested showed sulfide production in the anoxic butt of the tube, one of these had significant sulfide production under aerobic conditions as well. A total of 7 of the 17 (41.2%) anaerobic isolates displayed some detectable sulfide production under aerobic conditions. No sulfide production was detected in any of the sterile controls.

These results demonstrate that a significant proportion of YM bacterial isolates are capable of producing sulfide *via* putrefaction under both oxic and anoxic conditions, at least when provided with excess protein substrate. Isolates of *Pseudomonas*, *Flavobacterium*, *Bacillus*, *Arachnia*, and *Cellulomonas* were all found to produce sulfide; four of these isolates were found to produce both acid and sulfide using these screening techniques (Table 2.6 -1). The use of these putrefying bacteria in accelerated corrosion tests should allow a more precise determination of whether hydrogen sulfide and associated metal sulfides are directly capable of causing corrosion to waste package alloys. Since these microbes generate sulfides in the absence of sulfate reduction (and

hydrogen utilization), the effects of *only* sulfides on corrosion can be assessed absent cathodic depolarization effects.

All strains were incubated under aerobic conditions, by streaking on top of the agar, as well as under [somewhat] reducing conditions by stabbing into the semi-solid agar surface. Many of the aerobic strains were capable of growth within the agar (all of the 50° C.-incubated cultures grew well under these anoxic conditions), and some of the anaerobes were also capable of growth under aerobic conditions. This may have been expected since the selection and transfer protocols used (above) precluded the isolation of "strict" anaerobes (i.e., those to which oxygen is toxic). Employed methods resulted in isolation of organisms that were at least tolerant to limited exposure to oxygen or are so-called "facultative anaerobes", which are capable of both oxic and anoxic metabolism. Likewise, some of the "aerobes" can be facultatively capable of anoxic growth.

Several of the identified sulfide producers were further quantitatively analyzed for their rates and extents of sulfide production (below).

2.6.5 Screening for Slime under Varying Culture Conditions

The production and export of polysaccharides (long chain sugars) to the exterior of cells is characteristic of many bacterial species. Exopolysaccharide production results in the build-up of a slime layer which protects, embeds, and allows anchorage of cells to solid surfaces. The microenvironments contained within slime layers (or "biofilms") can be drastically altered from the general conditions in the exterior meileu, and from other areas within the biofilm. Generally, it can be expected that differential nutrient concentrations, relative humidity, and oxygen tensions exist throughout the film [21]. Consortia composed of different microbial species can become embedded by polysaccharide produced by one or more consortial members and these slime capsules provide a three dimensional spatial configuration and permit concentration gradients that facilitate intermicrobial interactions. Slime producing organisms probably indirectly contribute to corrosion by permitting adherence and facilitating interactions among the different types of organisms that cause corrosion. Direct effects of slime on corrosion include the creation of differential aeration cells and localized elevations in ion gradients, which in turn form crevices under which corrosion is accelerated [3, 22].

Since slime production is an integral element of microbially-induced corrosion, the library of YM bacterial isolates was screened for slime production first on R2 agar and then R2 + 0.5% glucose agar, R2 + 0.75% peptone agar, and R2 + 0.5% glucose + 0.75% peptone agar. All isolates were incubated anaerobically or aerobically at room temperature or 50° C., depending on their mode of isolation. Slime production was assessed by observation of gross colony morphology: the appearance and quantity of a viscous slime layer was noted and scored (e.g., Fig 2.6 -5).

Prodigious amounts of polysaccharide were produced by two *Bacillus* isolates and two as yet unidentified isolates with very similar colony morphologies. All of these strains were

identified as sulfide producers in former screening analyses, however none of these were identified acid-producers (above, Table 2.6 -1). Moderate quantities of slime were generated by five other YM strains that included representatives of the genera *Arthrobacter* and *Pseudomonas*. Retesting of six of these slime generators on R2 agar supplemented with peptone and glucose revealed that slime production varied with media type. The greatest degree of slime production occurred on media containing glucose for two of the strains tested. This observation is in agreement with the fact that the synthesis of polysaccharides requires sugar precursors; amended glucose provides a source of building blocks to support slime synthesis. The other isolates showed little difference in the quantity of polysaccharide produced between media types, and one strain showed no growth at all on R2 + peptone. A single anaerobic isolate demonstrated copious slime generation on R2 agar.

These results demonstrate that YM isolates are capable of slime production under low nutrient conditions, and could therefore play a role in corrosion of waste package materials. Generally it appears that the availability of carbohydrates could increase slime production, and possibly accelerate corrosive microbial activities.

2.6.6 Rates of Acid Production Under Varying Growth Conditions

Five strains identified in preliminary screening for the production of acids were further analyzed for their rates and extents of acid generation in R2 media containing additional peptone and glucose. Each strain was separately inoculated into R2, R2+0.5% glucose, R2+0.75% peptone, and R2+peptone+glucose. Cultures were incubated either anaerobically in serum bottles with pre-reduced media, or aerobically in shake flasks at either 30° C. or 50°C., depending upon the mode of isolation. The pH was monitored in withdrawn samples periodically over a three to five day period (Fig 2.6 -6).

The two anaerobic strains showed a negligible effect of added glucose and peptone, and the pH did not fall below pH5.2 in either of these cultures. The aerobically-incubated strains, however, showed greater dependence of the composition of the growth media on the production of acids. The *Pseudomonas stutzeri* isolate, LB-71h-RT-13 only generated acid when glucose was added to the R2 media, displaying a decrease to pH4.2. The pH probably did not decrease coordinately after growth of the *P. stutzeri* in R2+glucose+peptone media due to deamination of amino acids contained in the added peptone, which releases alkaline amines, counteracting the effects of acid production. This counter-effect of added peptone was not as evident in the *Pseudomonas pseudoflava* isolate, LB-71h-RT-4, which showed decreases in pH after growth in both R2+glucose and R2+glucose+peptone, as did a 50° C.-isolated strain, LB-71h-50-3 (most probably a *Bacillus*).

In summary, the effect of available nutrients on the production acids by YM isolates varies by strain. Some isolates are only capable of acid production when supplied with an added carbon source, others are less affected by this requirement and are capable of acid generation even when available carbohydrate concentrations are minimal. Also, the presence of other metabolizable nutrient sources can affect overall pH; if end products include alkaline compounds (such as

amines produced by deamination of amino acids), then acid production can be mitigated. The rates of acid production, in view of the long time spans that must be considered to evaluate the integrity of the YM repository, are significant. Rates of acid production over a three to seven day period are measurable and result in orders of magnitude differences in proton concentrations.

2.6.7 Rates of Sulfide Production by YM Isolates

Seven YM isolates identified as sulfide producers (*via* desulfurylation) were analyzed for their rates of sulfide production under aerobic and anaerobic conditions, because it had already been shown that many isolates are capable of growth at high or low oxygen tensions (above). All strains were inoculated into R2 media amended with 0.75% peptone. Both anaerobic (contained in serum bottles with pre-reduced media, cysteine as a reducing agent and rezasurin as a redox indicator) and aerobic (contained in flasks) were incubated at 30°C. or 50°C. unshaken to minimize air stripping of the produced hydrogen sulfide. Uninoculated media was also incubated to detect spontaneous abiotic sulfide production. Periodically, samples were withdrawn, cells removed by filtration, and the supernatants analyzed using a modification of the methylene blue assay, which relies on the reaction of sulfide, ferric chloride and dimethyl-*p*-phenylenediamine to produce methylene blue (measured spectrophotometrically, 664nm [17]). Standard curves were prepared using sodium sulfide diluted in the appropriate media, and sample sulfide concentrations were calculated by interpolation of the standard curve.

Preliminary results (depicted in Fig 2.6-7.) showed that sulfide production *via* desulfurylation increased for all tested strains within a two day incubation period, even in anaerobic cultures which metabolize and grow more slowly than do aerobic cultures. Sulfide concentrations increased to about 500ppb for all strains grown under anaerobic conditions and to approximately 150 ppb for the same isolates incubated aerobically. Sulfide concentrations continued to increase in aerobically grown cultures, reaching a maximum of approximately 330 ppb over a 7 day period, although extents of maximal sulfide concentrations varied between the strains tested. Thereafter, aerobic sulfide production, in general, decreased until 22 days after initiation of growth, when there was again a trend towards increasing sulfide found in the media.

These aerobic incubation results could be explained with reference to volatilization of hydrogen sulfide from the culture, combined with an initial growth phase, followed by cell death. In "batch" cultures such as those tested (which are not continually fed), growth of aerated cultures continues for a relatively short time, probably at the most for a week, after which nutrients are exhausted. While efforts were made to minimize the loss of sulfide through volatilization, it is estimated that sulfide losses resulted from inadvertent air-stripping in the death phase of the cultures where little or no new sulfide production could replace that which had been lost. The final increase at day 22 may be due to the growth of surviving cells on those that had died, with concomitant sulfide production resulting from metabolism of the amino acid content of dead cells.

Anaerobically-grown cultures also displayed a decrease in sulfide concentrations, starting after two days of incubation. In most cases, these decreased to zero over a 17 day period of incubation. These cultures were contained in sealed vials, and maintained under reducing

conditions. Thus, loss of hydrogen sulfide from the media through volatilization is unlikely. Rather, since the employed assay only detects the presence of soluble sulfides, it is likely that sulfide may have precipitated by interacting with other media components.

While these preliminary analyses are not entirely conclusive, it is important to note that microbially induced sulfide production increased significantly above background levels, was detected among a wide variety of YM isolates under both aerobic and anaerobic conditions, at least when strains were provided with an excess sulfur source (in the form of added peptone). These preliminary results additionally aid in determining conditions under which to conduct accelerated testing of alloy candidates, and which strains to include in accelerated corrosion tests.

2.6.8 Preliminary Corrosion Testing of Carbon or Mild Steel

An electrochemically-based system for monitoring of microbial corrosion rates was devised (schematic of the system depicted in Fig. 2.6 -8) that employs test cells assembled from 4cm diameter, 13cm long glass flat-bottom test tubes containing R2 media prepared using APW to simulate the electrolyte present at the YM site. A low concentration (0.5%) agar was added to the media such that its final consistency is a semi-solid which somewhat impedes the diffusion of air into the system. Working and counter electrodes were sealed into the cell through a soft rubber stopper. The 1020 carbon steel working or specimen electrode in each cell was a sheet ribbon approximately 5-mm wide, 1-mm thick, immersed to a length of about 10 cm, giving an exposed surface area of 9.7 cm^2. The 0.5-mm Pt-wire counter electrode was coiled around the working electrode while avoiding contact between them. The saturated calomel (SCE) reference electrode was immersed in a second identical test tube containing aqueous 1% KCl connected to the test cell through an agar-KCl salt bridge of 1.5-mm polyethylene tubing. This work is being performed under a sub-contract to the University of Nevada, Las Vegas with Prof. Penny Amy as the lead Principal Investigator.

Slime-producing strains isolated from the YM microbial community, and sulfate reducing, and iron oxidizing bacterial consortia were enriched from Yucca Mountain using techniques similar to those described (above). Each consortia was grown separately in their respective media to a standard cell density. Triplicate sterile test cells were inoculated as follows: each of the three consortia individually, pairwise combinations, and all three consortia inoculated together. Abiotic, sterilized, control cells were also prepared in triplicate to evaluate abiotic corrosion effects. The inoculated and abiotic cells were finally sealed around the rubber stoppers with paraffin tape to prevent biological contamination during subsequent long-term exposures. Polarization resistance (PR) measurements [23] were conducted at regular intervals on each cell by conventional potential-scan methods using a potentiometer and accompanying software (Gamry Instruments, Inc., PA). During polarization resistance measurements, potential was scanned from -10 mV to +10 mV at a maximum rate of 0.05 mV/sec, above which the polarization resistance curves became scan-rate dependent and did not represent necessary steady-state conditions [24]. The software automatically calculated the polarization resistance, R_p, from the slope at the origin of the PR curve; and calculated the corrosion rate (current density), i_{corr} according to the method of Stern [23] :

$$R_p = \beta_a \beta_c / 2.3\, i_{corr}\, (\beta_a + \beta_c)$$

Finally, the corrosion rate was calculated from i_{corr} using Faraday's Law. The β_a and β_c are terms expressing the Tafel slope for the respective anodic and cathodic polarizations from the corrosion potential. They are treated as constants and included in the calculational software.

Corrosion rates generated from collected data varied considerably between replicates (e.g., Fig 2.6 -9), however averages of the data points between replicates appear to be representative of observed trends and the variation decreased after approximately 50 days of incubation. Also variation was considerably less in abiotic control cells. Pairs of consortial types may have somewhat higher early corrosion rates, but with time decrease to near the same levels as the single consortial tests. Still, the combination of all three types of consortia shows significantly higher corrosion rates than any of the rest, especially up to about 20 days, where they reach a maximum, and then drop to lower values approaching corrosion rates for sulfate reducing bacteria alone (Fig 2.6 -9). Data, at this time, are only available up to only about 65 days for tests employing combinations of bacterial types.

While it took several weeks to sufficiently establish conditions to measure significant corrosion rate changes using this described system, it appears that the iron oxidizers had the least effect on enhancing the corrosion of carbon steel, followed by slime-producing bacteria. The sulfate reducers appear to have the greatest ability to corrode carbon steel. Clearly, from these results it is evident that given a complete microbial community including all three of these classes of organisms, corrosion could proceed up to five times the rate as that observed in their absence, given the required conditions for microbial growth and activity. The system, as employed, does have some limitations: the observed decrease in corrosion rates probably results due to the depletion of oxygen within the system, which may not be representative of *in situ* repository conditions. Within the window of time between establishment of conditions and the observed decrease in corrosion rates, however, the system appears useful to determine corrosion rates of candidate barrier materials.

Corrosion rates were increased from approximately 1 mpy [25 μm/yr] (abiotic control) to 1.5 mpy [38 μm/yr], 2 mpy [51 μm/yr], and 3 mpy [76 μm/yr] in cell environments containing iron-oxidizers, slime producers, and sulfate reducers alone, respectively; to somewhat higher levels when paired together in various combinations. In a mixture of all three bacterial classes, corrosion rates reached a maximum at 5 mpy and decreased thereafter, probably due to oxygen depletion in the sealed electrochemical measurement cells.

These results support a microbial corrosion mechanism in which anaerobic sulfate reducers grow most efficiently and corrosion is exacerbated under exopolymer films and insoluble $Fe(OH)_3$ deposits, with reduction of dissolved oxygen required on surrounding oxide and sulfide surfaces.

2.6.9 Optimization of the Corrosion Testing System and Future Plans

Corrosion rate determinations will be carried out on mild steel coupons as described above at temperatures elevated to 50°C. In addition, individual YM strains culled from various screening and assay results (Table 2.6 -1) will be used in a similar fashion, in various combinations, to assess the resistance of more corrosion-resistant alloys (e.g. nickel containing alloys, such as Monel 400 and Incoloy 825), the results will be compared to corrosion tests run under sterile conditions and those employing whole YM-derived microbial communities. The work on the corrosion resistant alloys is being performed at the LLNL site. An activity plan has recently been completed; this plan outlines the work on MIC for the corrosion resistant materials.[25]

Testing of the more corrosion-resistant metal alloys, such as nickel-base and titanium-base alloys, necessitate a more sensitive detection of corrosion rates (since corrosion is anticipated to progress at a slower rate). Thus, improved inoculation protocols are devised, whereby bacteria are directly inoculated onto alloy coupons prior to insertion in the test cell, to decrease observed variations between otherwise like replicates, and improve the signal to noise ratio of compiled data. Also, various concentrations of APW have been tested with different amendments to the basic R2 media (i.e., added glucose and peptone), to improve the conductance of the media and accelerate rates of different corrosive microbial activities. Initial corrosion monitoring of stainless steel alloys will be undertaken at room temperature, and subsequent tests will be conducted at elevated temperatures. Finally, corrosion activities will be screened and assayed under differing environmental conditions to continue to assess bounding conditions for microbially-induced corrosion and aid in determining the rates of these activities under simulated repository conditions.

Periodic samples are also planned to be taken from the test solution in the long-term comprehensive corrosion test (discussed in Section 2.4) and will be analyzed for microbial activity.

References for Section 2.6

[1] W. C. O'Neal, et al, Preclosure Analysis of Conceptual Waste package Designs for a Nuclear Waste package in Tuff, LLNL report, UCRL-53595 , 1984

[2] Horn, J. and A. Meike. Microbial Activity at Yucca Mountain. Dept. of Energy, Lawrence Livermore Natl. Laboratory Report #UCRL-ID-122256, September 25, 1995.

[3] Borenstein, S.W. 1994. Microbially Influenced Corrosion Handbook. New York, NY, Industrial Press Inc.

[4] Reasoner, D.J. and E.E. Geldreich 1985. A new medium for the enumeration and subculture of bacteria from potable water. Appl. Environ. Microbiol. 49:1-7.

[5] Amy, P.S., D.L Haldeman, . Ringelberg, D.H. Hall, and C. Russell. 1992. Comparison of identification systems for classification of bacteria isolated from water and endolithic habitats within the deep subsurface. Appl. Environ. Microbiol. 58:3367-3373.

[6] Haldeman, D.L., P.S. Amy, D.C. White, and D. Ringelberg. 1994. Changes in bacteria recoverable from subsurface volcanic rock samples during storage at 4°C. Appl. Environ. Microbiol. **60:2697-2703**.

[7] Buscheck, T.A. and J.J. Nitao. The impact of buoyant gas-phase flow and heterogeneity on thermo-hydrological behavior at Yucca Mountain. Proceedings of the International High Level Radioactive Waste Management Conference, 22-26 May, 1994, Las Vegas, NV and Dept. of Energy, Lawrence Livermore Natl. Laboratory Report #UCRL-JC-115351.

[8] Atlas, R.M. 1982. Enumeration and estimation of biomass of microbial components in the biosphere. Experimental Microbial Ecology eds. R.G. Burns and J.H. Slater. Oxford, England, Blackwell Scientific Publishers. pp.84-102.

[9] Roznak, D.B. and R.R. Colwell. 1987. Survival strategies of bacteria in the natural environment. Microbiol. Rev. **51:365-379**.

[10] Welch, D.F. 1991. Applications of cellular fatty acid analysis. Clin. Microbiol. Rev. **4:422-438**.

[11] Lee, W., A. Lewandowski, P. H. Nielsen and W. A. Hamilton. 1995. "Role of sulfate-reducing bacteria in corrosion of mild steel: a review." Biofouling **8:165-194**.

[12] Gherna, R., P. Pienta, and R. Cote., eds. 1989. Catalogue of Bacteria and Bacteriophages. 17th edition. Rockville, MD, American Type Culture Collection.

[13] Manning, H.L. 1975. New medium for isolating iron-oxidizing and heterotrophic acidophilic bacteria from acid mine drainage. Appl. Microbiol. **30:1010-1016**.

[14] Westlake, D.W.S., K.M. Semple, and C.O. Obuekwe. Corrosion by ferric iron-reducing bacteria isolated from oil production systems. Proceedings of the International Conference on Biologically Induced Corrosion, June 10-12, 1985, Gaithersburg, MD.

[15] Meyers, C.R. and K.H. Nealson. 1990. Respiration-lined proton translocation coupled to anaerobic reduction of Manganese (IV) and Iron (III) in *Shewanella putrefaciens* MR-1. Appl. Environ. Microbiol. **172:6232-6238**.

[16] Lovley, D.R. and E.J.P. Phillips. 1987. Rapid asay for microbially reducible ferric iron in aquatic sediments. Appl. Environ. Microbiol. **53:1536-1540**.

[17] Greenberg, A.E., R.R. Trussell, L.S. Clesceri, and M.A.H. Franson, eds. 1985. Standard Methods for the Examination of Water and Wastewater. 16th edition. Washington, D.C., American Public Health Association.

[18] Little, B.J., P.A. Wagner, and D. Duquette. 1987. Microbially induced cathodic depolarization. Corrosion/87, National Association of Corrosion Engineers, Houston, TX.

[19] Pope, D. H., S. Lockwood, A. Lee, R. Skultety, and K. Keas. 1994. Mitigation of microbiologically influenced corrosion in natural gas storage facilities. Corrosion/94 National Association of Corrosion Engineers, Houston, TX.

[20] Licina, G.J. 1988. Sourcebook for Microbiologically Influenced Corrosion in Nuclear Power Plants. EPRI NP-5580, Electric Power Reasearch Institute, Palo Alto, CA.

[21] Costerton, J.W. and G.G. Geesey. The microbial ecology of surface colonization and of consequent corrosion. Proceedings of the International Conference on Biologically Induced Corrosion, June 10-12, 1985, Gaithersburg, MD.

[22] Costerton, J.W. and J. Boivin. 1991 The role of biolfilms in microbial corrosion *in* Microbially Influenced Corrosion and Biodeterioration, N.J.E. Dowling, M.W. Mittleman, and J.S. Danko, eds. National Association of Corrosion Engineers, Houston, TX.

[23] Stern, M. 1958. Corrosion **14:**440-

[24] Jones, D.A. 1996. Principles and Prevention of Corrosion, 2nd edition, Prentice Hall, Upper Saddle River, NJ.

[25] Horn, J and Jones, D., Yucca Mountain Project Activity Plan, Microbiologically Influenced Corrosion, Metallic Barriers SIP Activity E-20-60, Lawrence Livermore Laboratory, 1997.

Table 1. Yucca Mountain Bacterial Isolates Displaying Corrosion-Related Activities

26-

Strain#[a]	Species Identification[b]	Acid Production[c]	Sulfide Production[d]	Slime Production[e]
ESF-C1	*Cellulomonas flavigena*	X	X (oxic)	
LB-71h-RT-13	*Pseudomonas stutzeri*	X		
ESF-71h-RT-4	*Flavobacterium esteroaromaticum*	X	X (oxic)	
LBan-U7	uncharacterized	X		
LBan-UW2	*Cellulomonas turbata*	X		
LB-71h-50-3	probably *Bacillus sp.*	X		
ESFan-U4	*Bacillus circulans*	X		
LBan-C1	*Arachnia propionica* (poor match)	X	X (oxic/anoxic)	
LBan-UW2	*Cellulomonas turbata*	X		
LBan-U1	*Cellulomonas galida*	X		
LBan-U2	*Bacillus pabuli*	X	X (anoxic)	
LBan-U3	*Bacillus pantothenticus*		X (anoxic)	X
LB-71h-50-2	*Bacillus pumilus* subgroup B		X (anoxic)	
LB-71h-50-4	*Bacillus subtilus*		X (anoxic)	X
LB-71h-50-6	probably *Bacillus sp.*		X (anoxic)	X
ESF-71h-RT-1	*Flavobacterium esteroaromaticum*		X (oxic)	
LB-C1	uncharacterized		X (oxic)	X
LB-C2	uncharacterized		X (oxic)	
LB-C7	*Pseudomonas stutzeri*		X (oxic)	
LB-71h-RT-15	*Pseudomonas pseudoflava*			X
LB-71h-RT-4	*Pseudomonas pseudoflava*			X
LB-CW-6	*Arthrobacter oxydans*			X

[a]ESF=Exploratory Study Facility; LB=Large Block; an=isolated under anaerobic conditions; C=crushed rock isolate; U=uncrushed rock isolate; W=isolated from after washing rock; 71h=isolated after 71 hours of growth; RT=room temperature isolate; 50=50°C. isolate
[b]Determined by fatty acid analysis using the MIDI/Hewlett Packard microbial identification system (MIS; Analytical Services, Inc., VT); identification of given isolates may be tentative due to a lesser degree of similarity with type organisms contained in the MIS database
[c]Determined after growth in R2 media (Reasoner and Geldreich, 1985) with or without 0.5% glucose and pH indicators bromocresol purple and methyl red.
[d]Determined after growth in R2 agar media (Difco) containing 0.75% proteose peptone #3 (Difco) and lead acetate
[e]Determined after growth on R2 agar (Difco).
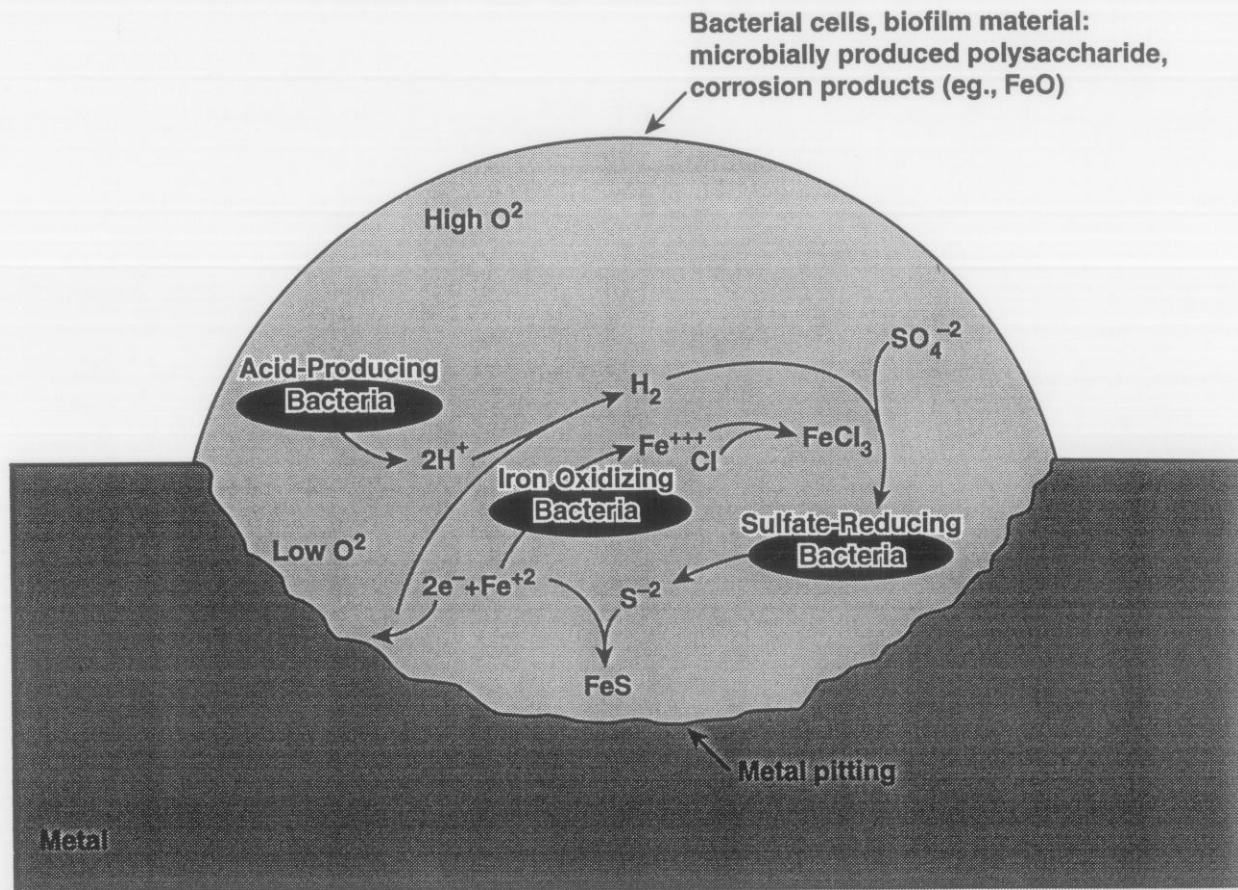
Fig.2.6-1 Microbial contributions to metal corrosion. Acid-producing bacteria generate protons that contribute to metal dissolution and form hydrogen when coupled with corrosion-generated electrons. The resulting hydrogen, together with sulfate, is consumed by sulfate-reducing bacteria, resulting in sulfide production. Consumption of hydrogen by sulfate reducers drives corrosion by eliminating the layer of hydrogen that would otherwise occlude the metal surface, a process termed "cathodic depolarization." Sulfide couples with dissolved ferrous ions to form ferrous sulfide. Ferric ions generated by iron oxidizing bacteria bind chloride ions, generating iron chlorides which contribute to pitting.
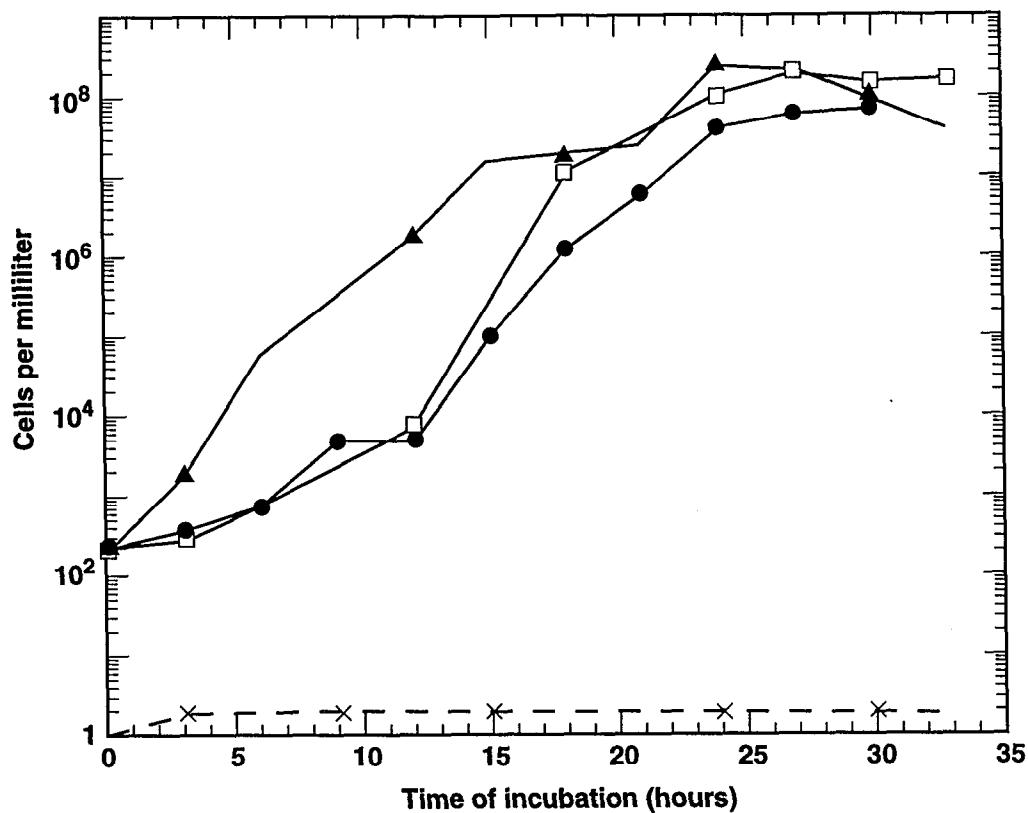
Fig.2.6-2 Effect of temperature on the growth rates of whole YM microbial communities in K2 media. Crushed YM tuff was inoculated in media and incubated aerobically at 20°C (●), 30°C (□), or 50°C (▲). Periodically samples were withdrawn and cell count was determined by live planting (×), sterile uninoculated media incubated at 20°C.
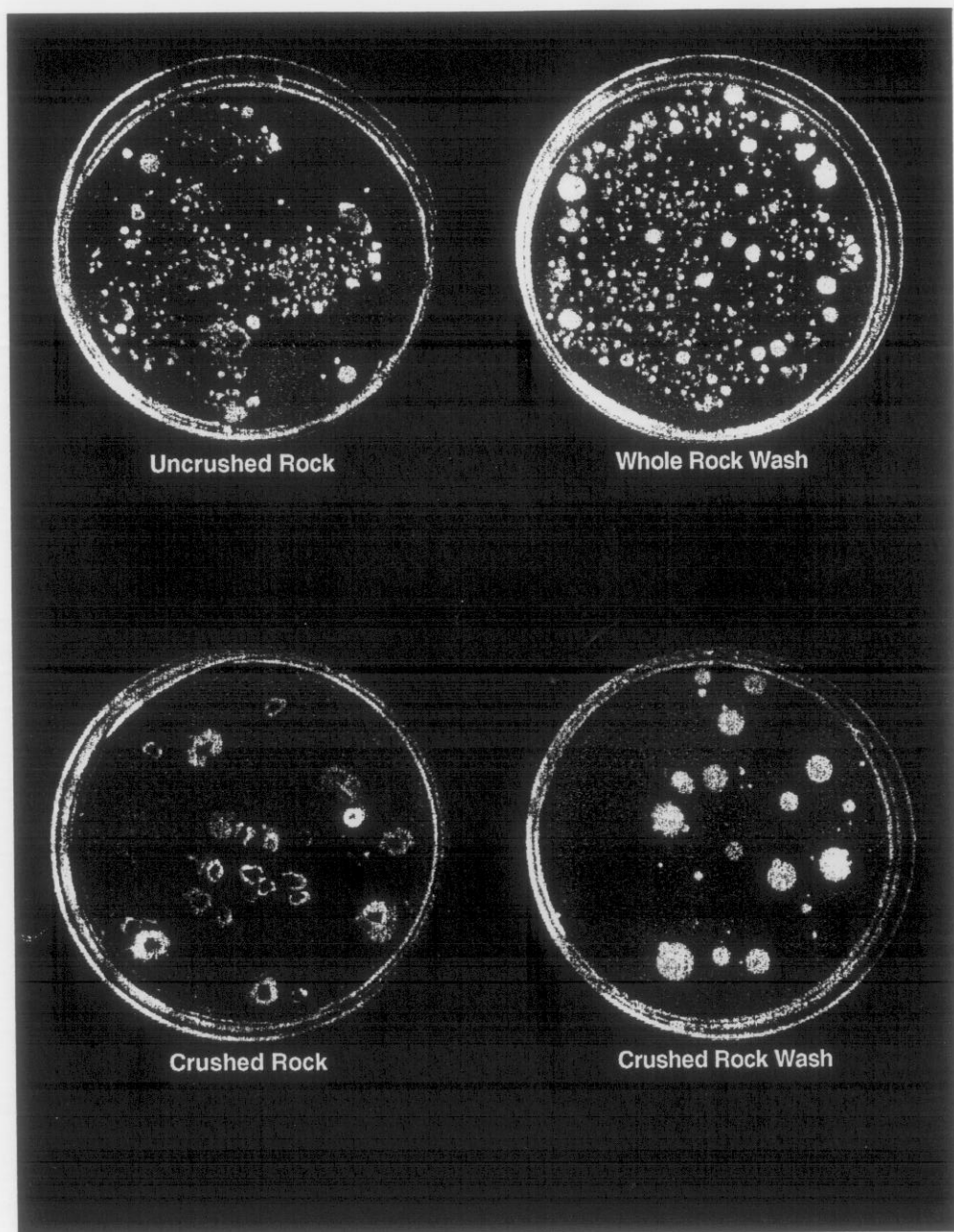
Fig.2.6-3 Bacterial growth arising from Large Block tuff (Fran Ridge, NV). Whole and crushed tuff, and artificial well J13 water (Amy *et al.*, 1992) which had been used to wash tuff samples were plated on R2 agar media (Difco) under aerobic conditions and incubated at room temperature. Each of the spots on the agar surface is a bacterial colony originating from a single cell.

ESH enrichment   *Thiobacillus ferrooxidans*
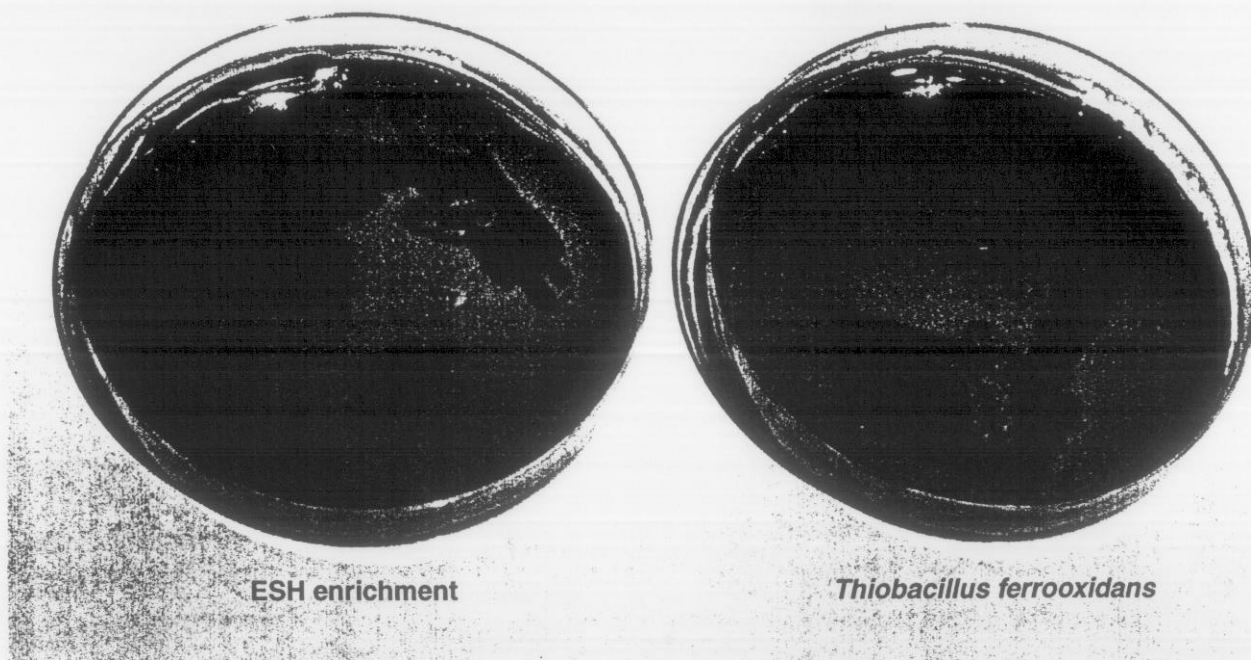
**Fig.2.6-4** Enrichment of iron oxidizing organisms from ESF tuff. Tuff samples were incubated in ATCC Media #64 (Gherna *et al.*, 1989), as was *Thiobacillus ferrooxidans*, a characterized iron-oxidizer, which was grown separately. After periodic transfer of the cultures, both were plated out on ISP agar media (Manning, 1975). Colony morphology indicated iron scavenging from the media (i.e., note clearing of the media in areas of high growth) and deposition of ferric iron oxides (i.e., rust color), both characteristics of iron oxidation, in both the known *Thiobacillus* culture and the enrichment from ESF tuff.

R2 agar   R2 + 0.5% glucose   R2 + 0.75% peptone   R2 + glucose + peptone
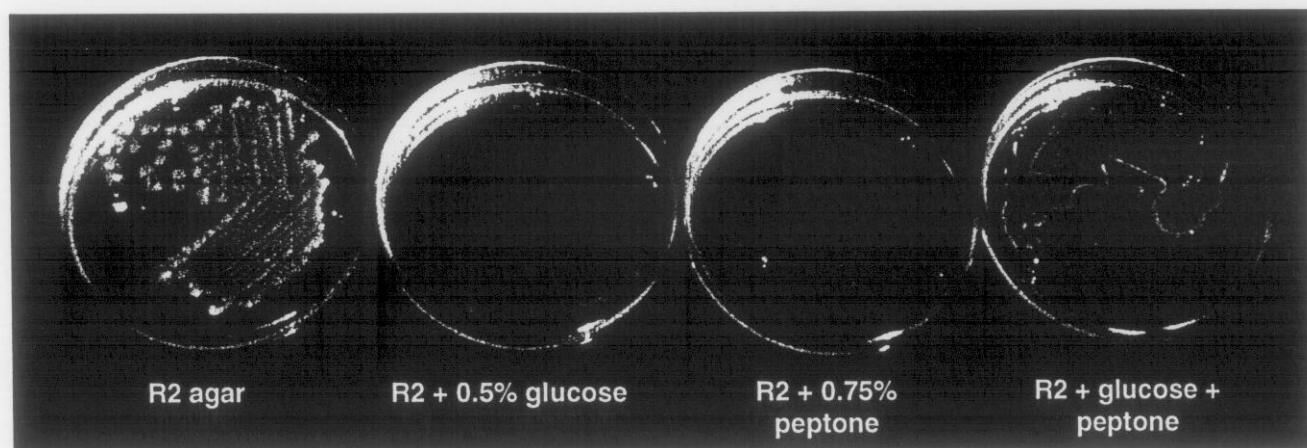
Fig.2.6-5 Exopolysaccharide slime synthesis by a Pseudomonas Large Block (Fran Ridge, NV) isolate, as a function of available nutrients. The bacterial isolate was plated onto R2 agar media (Difco), with the indicated amendments and incubated at room temperature. No growth at all occurred on R2 containing 0.75% peptone, however when both 0.5% glucose and peptone were incorporated into the media a good deal of viscous slime production was observed. While R2 agar alone produced some slime, growth was light on R2 containing 0.5% glucose.

2.6 - 21
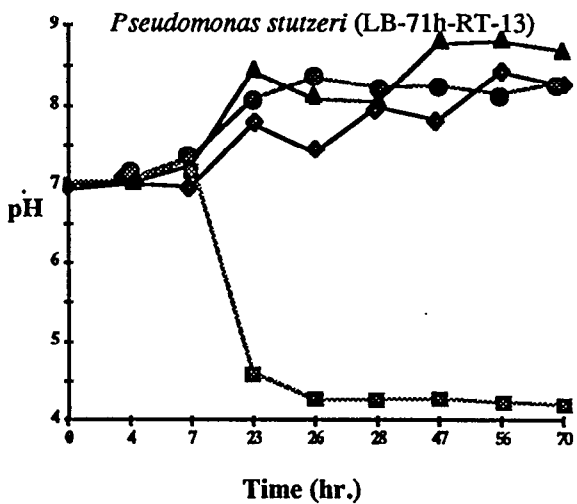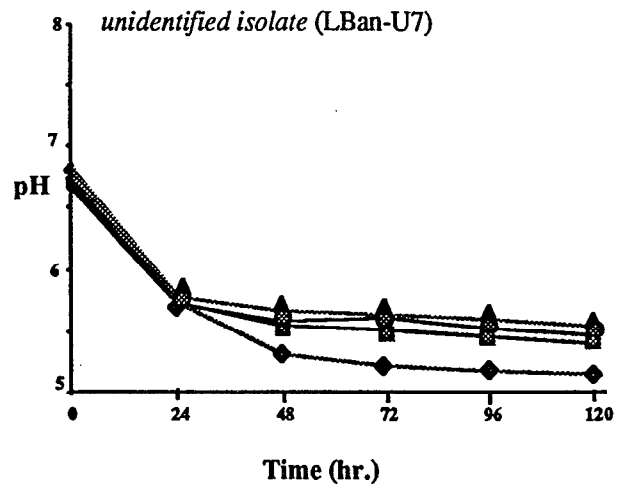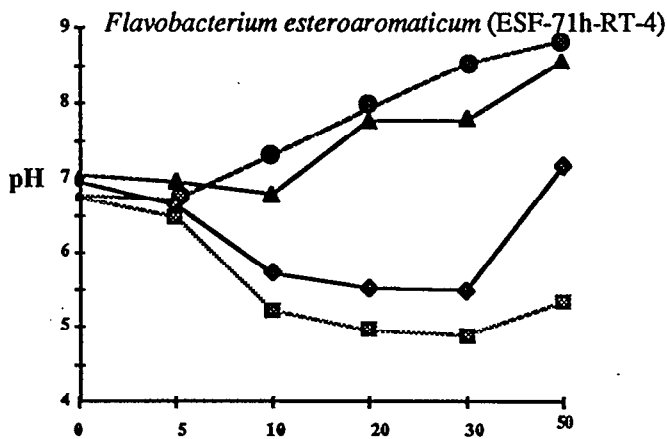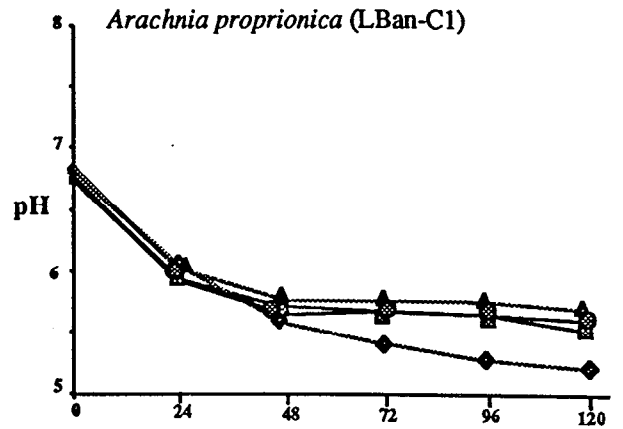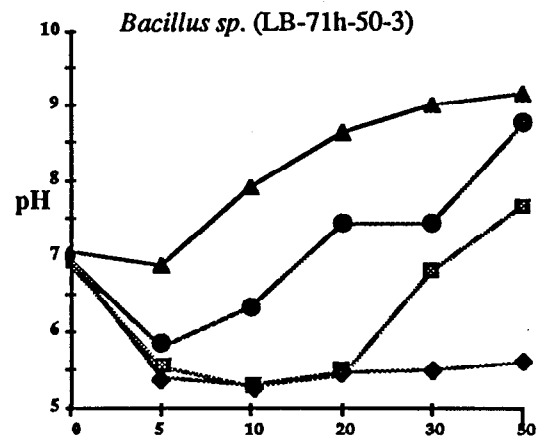
Fig.2.6-6 Effect of nutrients and growth on acid production in individual YM isolates. Each indicated isolate was inoculated into R2 media (●), R2 + 0.5% glucose (▣), R2 + 0.75% proteose peptone #3 (▲), and R2 + glucose and peptone (◆). Periodically, through subsequent growth the pH of the media was determined.
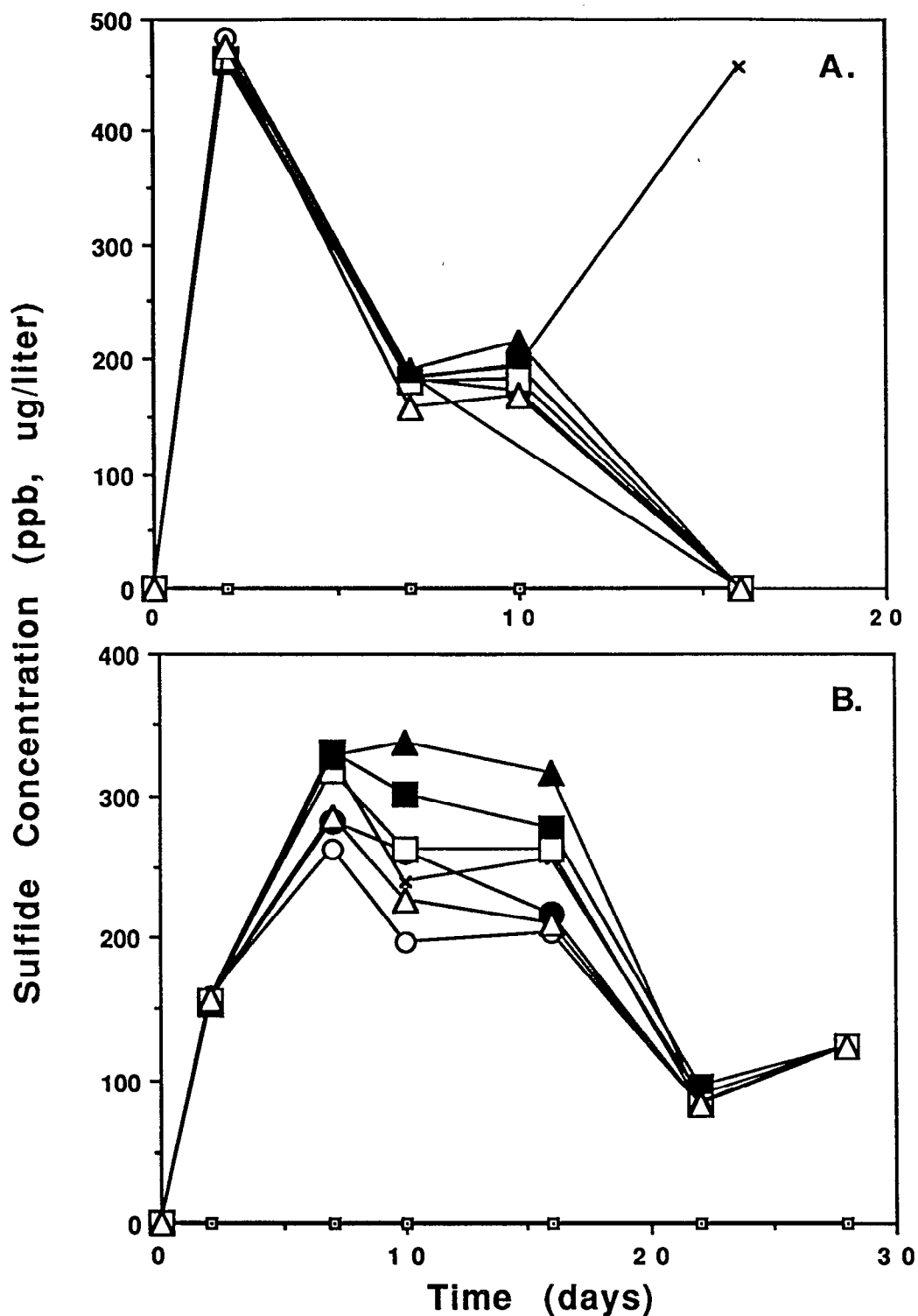
Fig.2.6-7 Sulfide production by individual YM isolates grown in R2 media amended with 0.75% proteose peptone #3 (Difco) under anaerobic (Panel A) and aerobic (Panel B) conditions. Samples were taken periodically following inoculation into fresh media and assayed for soluble sulfide concentrations as described in the text. ⊡, uninoculated control; ○, *Bacillus subtilus* (LB-71h-50-4); △, *Flavobacterium esteroaromaticum* (ESF-71h-RT-1); ✗, *Cellulomonas flavigena* (ESF-C1); ●, *Bacillus sp.* (LB-71h-50-6); ■, *Arachnia propionoica* (LBan-C1); □, *Pseudomonas stutzeri* (LB-C7); ▲, *Bacillus pabuli* (LBan-U2).
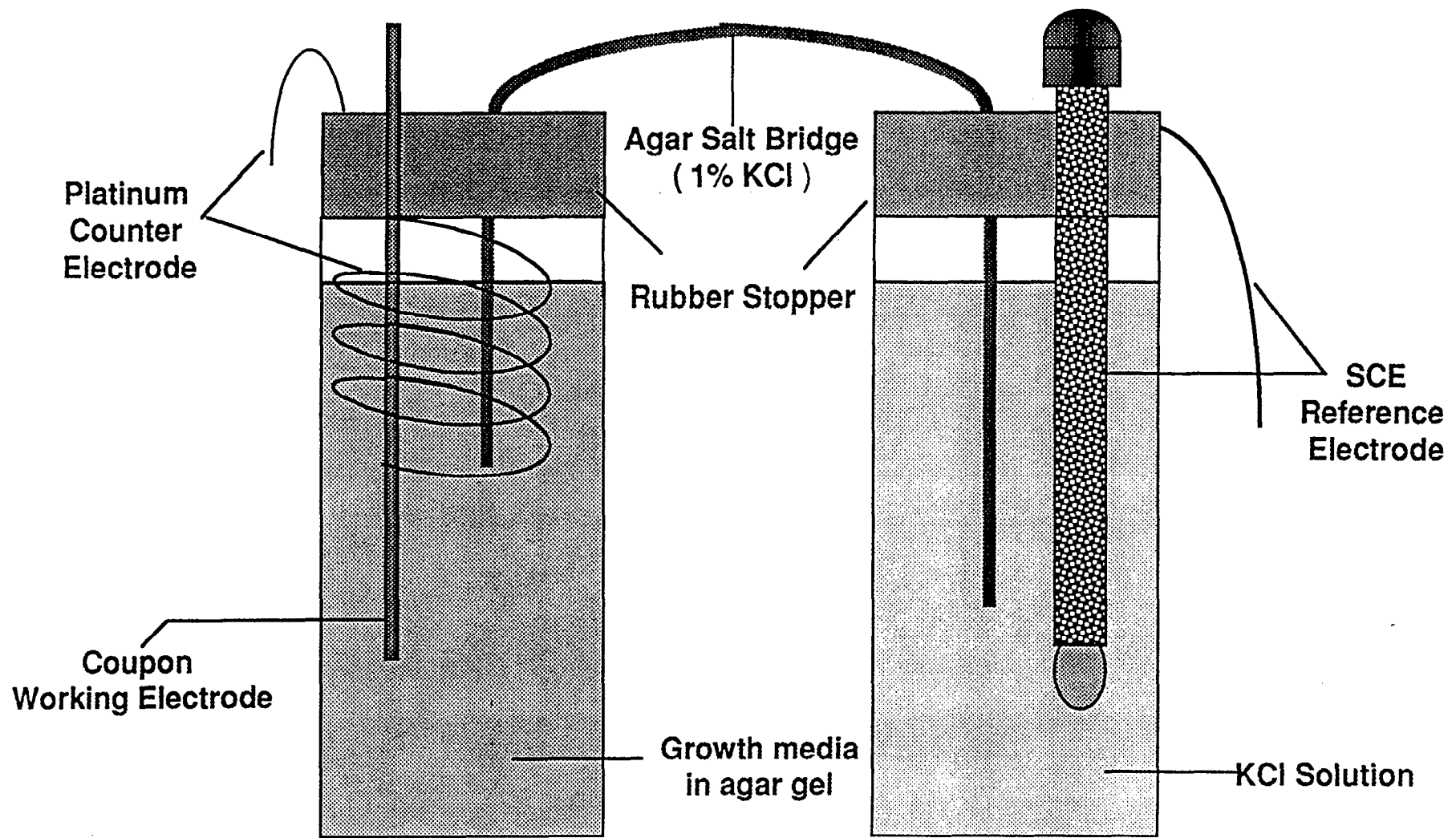
Fig.2.6-8   Electrochemical cell for monitoring microbially-induced corrosion rates.   Current is applied through the platinum electrode, and potential differences are measured with respect to the reference electrode.
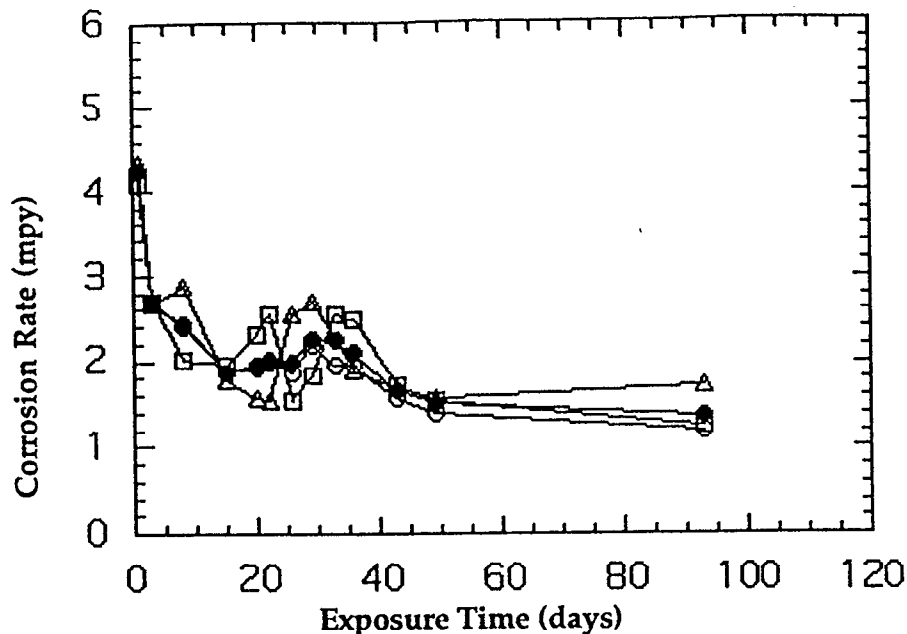
Fig.2.6-9 Variation of corrosion rates among replicates inoculated with iron-oxidizing bacteria. Triplicate mild steel coupons were inoculated at time 0 with the same enrichment culture of iron oxidizers. The corresponding corrosion rate of each inoculated coupon was monitored as described in the text (open symbols). The calculated average corrosion rate (closed symbol) of all three inoculated coupons at each time point is shown.
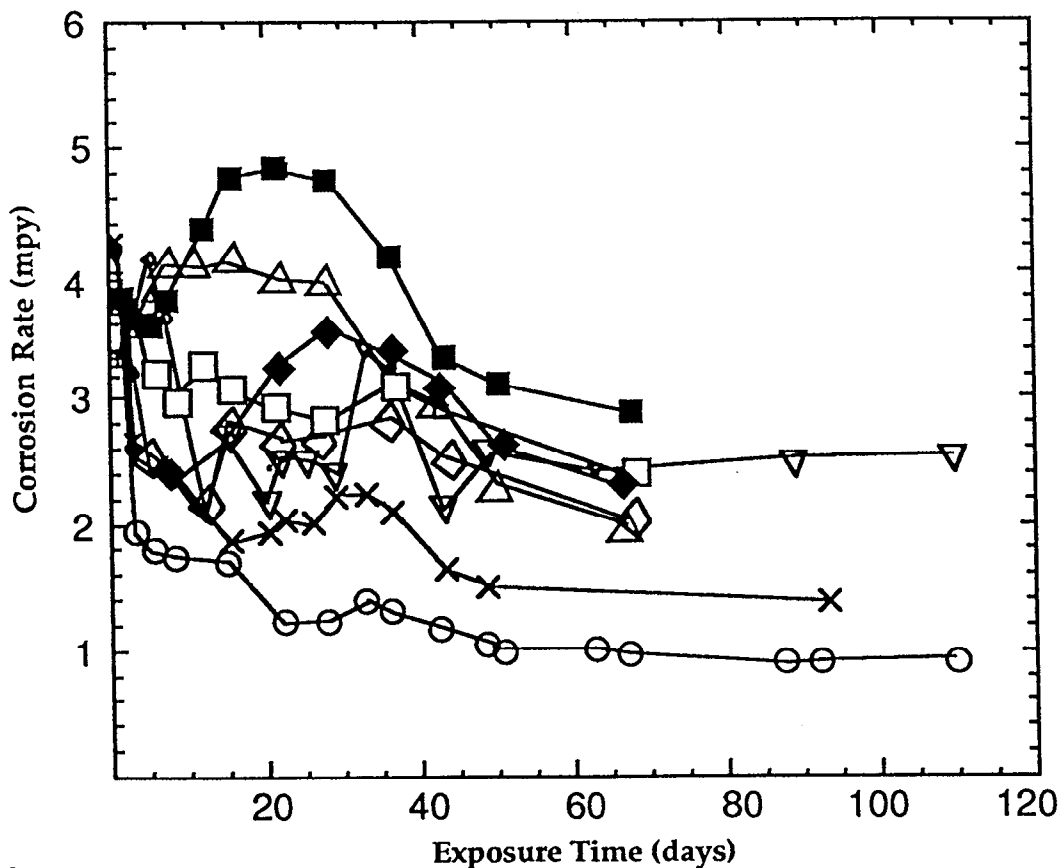
Fig.2.6-10 Comparison of corrosion rates of mild steel after inoculation with various types of microorganisms. Corrosion rates were monitored as described in the text after coupons were left uninoculated (O), or were inoculated with iron-oxidizing bacteria (x), sulfate reducing bacteria (∇), exopolysaccharide slime producing organisms (◊); mixtures of iron oxidizers and sulfate reducers (△), slime producers and sulfate reducers (◆), slime producers and iron oxidizers (□), and slime producers and iron oxidizers and sulfate reducers (■).

2.7 Stress Corrosion Cracking (SCC) Testing

Activities are proposed for determining the stress corrosion cracking (SCC) susceptibility of candidate materials, both those for the inner barrier and the outer barrier. Often, the stress corrosion cracking concerns center around the welded area because unrelieved residual stress is most often found here, a result from the welding operation. Stresses near the yield stress of the metal are introduced in the welded area; this level of stress is usually sufficient to cause SCC in susceptible materials. Also, the rapid cool down and non-equilibrium conditions after the welding operation can favor microstructures more prone to SCC. Strain energy in the welded regions can also provoke phase transformations. Although the so-called "assembly welds" used to form the empty container can be stressed relieved, post-weld heat treatments of the final closure weld are much more limited or practically impossible. Much of the same concerns are also present for hydrogen embrittlement (HE), the major difference being that SCC is associate with the anodic process of intense but very localized dissolution to initiate the fracture while HE is associated with the cathodic process of hydrogen discharge on the metal surface and subsequent entry of hydrogen into the metal and its residence in a susceptible microstructural feature. Exposure of the stressed U-bend shaped specimens in the long term comprehensive corrosion test is a qualitative evaluation of the susceptibility of candidate materials to SCC and HE. Additional work is aimed at determining more quantitative aspects of these phenomena.

There are a number of ways to perform SCC (and HE) tests. Two approaches discussed in the Metal Barriers SIP are self-loaded tests and externally loaded tests. As contrasted with the U-bend specimens which are smooth (uncracked) and plastically stressed (but the stress not measured), these two approaches use fracture mechanics techniques for very accurate calculation of the stress (or more accurately the stress intensity). Both approaches use pre-cracked specimens so that the emphasis is on measuring the propagation of the crack.

2.7.1 Self Loaded Stress Corrosion Tests

In self-loaded tests a wedge is inserted into the crack to maintain a high stress intensity at the tip of a crack (generally, cracks have been previously initiated by fatiguing in another apparatus) while exposed to the test solution. The advantage of self-loaded specimens (as contrasted to externally loaded specimens) is that many specimens can be simultaneously emplaced in the same test solution so that different alloys, different microstructures, and replicate specimens can be tested together. Specimens are removed periodically to check visually and microscopically for crack elongation in SCC susceptible materials. Often, the specimens are intentionally broken open so that the stress corrosion crack length can be measured (it will be a different color). There are a number of specimen geometries and loading arrangements that have been developed by the ASTM and other organizations over many years. One such geometry is the "double cantilever beam (DCB)". Knowing the specimen dimensions, the equilibrium wedge load, and the crack length, the stress intensity can be calculated from a fracture mechanics formula. By measuring the crack

length at different exposure times to determine the crack velocity, the crack velocity is plotted against the changing stress intensity. When the crack velocity approaches zero, the stress intensity is said to be the critical stress intensity for SCC (K_{Iscc}). The value of the critical stress intensity is important to waste package design because it indicates the combination of maximum stress and surface flaw size that can be tolerated. Generally, one designs for the operating stresses to be much lower than the critical stress.

In FY-96 DCB specimens of the corrosion resistant candidate materials were procured. These include Ni-base Alloys 825, 625, G-30, C-4, C-22, as well as Titanium Grade 12. Several test cells were acquired, but funding and other priorities curtailed initiation of these tests. These tests started in early FY-97 with initial exposures of the corrosion resistant materials in chloride solutions acidified (5% Cl⁻) to the pH 2-3 range and at temperatures in the 70 - 90° C range. The wedges used to sustain the crack opening were made from the same material as the test specimen to avoid undesirable galvanic effects. Various heat treatments will be performed on some of the specimens, since several of these alloys are more prone to SCC and HE in particular microstructures. An Activity Plan (E-20-56) has been prepared and gives greater details on the test method and proposed test matrix. [1] .

In December 1996, some DCB specimens of Alloy 825 were initiated in an acid chloride solution maintained at 90° C. The stress intensities maintained at the crack tip were high, 40 to 50 ksi$\sqrt{}$ in. After one month of testing, the specimens were removed and crack propagation and branching were observed. The cracks appeared to follow an intergranular pattern. Additional SCC tests are continuing for this material and environment but for longer exposure times. Also, SCC testing on some of the other candidate alloys has begun or will soon begin.

In the future, specimens of the corrosion allowance materials will be acquired and tested in somewhat different aqueous environments. Carbon steels are susceptible to SCC in relatively high pH environments in which they begin to passivate. This susceptibly also depends on microstructure. A further advantage to using the self-loaded types of specimens is that they are amenable to electrochemical control, meaning that potentials can be applied to the specimen to accelerate the cracking. Eventually, some SCC and HE testing will be performed with applied potentials.

2.7.2 Externally Loaded SCC Tests

The other generic type of SCC/HE test involves application of the load from outside the test cell so that the specimen is simultaneously stressed and exposed to the aqueous environment. The apparatus for applying the load can be very simple to rather complex. Techniques for measuring crack formation and growth range from the very simple to the more sophisticated. One type of testing that has been used in the nuclear energy industry for estimating crack propagation in light water reactor components is the reversing DC technique, in which the crack elongation is measured as the small change in electrical resistance as the crack grows. The sensitivity of this technique is very high so that crack

growth rates on the order of 10^{-10} meters/sec can be measured. Pre-cracked compact tension fracture mechanics specimens are used. The stress on the specimen can be applied as a constant load or cyclically. Generally, cyclic tensile loads (as opposed to tension-compression loads) are more damaging to metals (and therefore advantageous for an accelerated test) because broken passive films on the metal do not have the opportunity to "heal" between tension cycles.

A series of reversing DC SCC tests were operated under contract to Argonne National Laboratory (J. Y. Park and D. R. Diercks, PIs) for several years. Specimens of the corrosion resistant alloys (Alloys 825, C-22, and Ti-Grade 12) were exposed to artificial J-13 well water at 93 °C. Different stress intensity values and different load ratios (also called R values and defined as the ratio of the minimum stress to the maximum stress) were used. As might be expected, these alloys did not show any SCC or HE susceptibility in the conditions tested. Because of funding limitations and the fact that these are costly tests because they tie up pieces of expensive equipment for long periods of time (and thus limit the numbers of environments that can be tested), they were discontinued in 1995 in favor of self-loaded SCC tests. The purpose of the self-loaded SCC test is to screen alloy/environments so that eventually the more definitive reversing DC tests can be run at a later time when the choice of materials is more narrowed. The reversing DC test is superb for determining K_{Iscc} in a quantitative way. (MB Activity E-20-55). This work was governed by another activity plan. [2]

References for Section 2.7

1) A. Roy, Yucca Mountain Project Activity Plan, Stress Corrosion Cracking Tests Using Double Cantilever Beam Specimen, Metallic Barriers SIP Activity E-20-56, Lawrence Livermore Laboratory, 1996.

2) E. Dalder and D. McCright, Yucca Mountain Project Activity Plan, Fracture Mechanics Stress Corrosion Crack Growth Tests of Candidate Waste Container Materials, Metallic Barriers SIP Activity E-20-56, rev.2, Lawrence Livermore Laboratory, 1995.

2.8 Galvanic Corrosion

As explained previously in Sections 1.0 and in 2.2, galvanic corrosion will occur because of the electrochemically dissimilarity between the metals proposed for the outer barrier and those proposed for the inner barrier. However, the galvanic effect can be used favorably in the sense that the material comprising the outer barrier will corrode sacrificially and thereby protect the inner barrier. Proposed testing work to determine the galvanic effects between candidate materials for the outer and inner barrier has been discussed in Section 2.4 on the long-term corrosion test. Additional work to determine some of the electrochemical parameters that govern galvanic corrosion is described as Metal Barrier SIP Activity E-20-46.

2.8.1 Factors Influencing Galvanic Corrosion

Any factor that affects corrosion of a single metal may also control galvanic corrosion involving two or more dissimilar conducting materials. Besides flow rate and pH, these factors include temperature, electrolytic composition, surface condition of the metals, thermomechanical history of the surfaces, and many more factors too numerous to mention. Factors such as the anode/cathode area ratio, distance between electrically connected materials, and geometric shapes are unique to galvanic corrosion behavior of many different metals and alloys. Area effects involve the ratio of the surface area of the more noble to the more active member. An unfavorable area ratio exists when the surface area of the cathodic member is larger compared to that of the anodic one. Under this condition, the anodic current density on the more active material will be extremely large, thus leading to more pronounced galvanic attack. On the other hand, large anodic surface area and smaller surface area of the noble member produces only slightly accelerated galvanic effects because of enhanced polarization of the cathodic member. In the case of a thick barrier of carbon steel coupled to a Ni-base or Ti-base inner barrier, the exposed area of the carbon steel will, for the most part, be much greater than that of the inner barrier. Only in the final stages of consumption of the outer barrier will the area ratios change substantially and favor more rapid corrosion of the remaining carbon steel. Thus, the area ratio effect is considered to be favorable. The same argument would hold for a Cu-Ni alloy as an outer barrier corroding sacrificially to protect a more corrosion resistant inner barrier material, made of a Ni-Cr-Mo alloy or a Ti-base alloy.

As to the effect of distance between metals in the galvanic couple, dissimilar materials usually suffer greater from galvanic corrosion than those separated by larger gaps. Conversely, the galvanic or cathodic protection offered by the sacrificial material is not as effective when the gaps are large and the contact is not continuous. The distance effect is also dependent on the solution conductivity since the path of current flow is the primary consideration. Sometimes, the solution conductivity and geometric factors are referred to as the "throwing power" of the current in much the same way the term is used in electroplating and battery operations. Although a continuous, complete bond between the two metals is desirable to assure full cathodic protection, some discontinuity can be tolerated particularly if the electrolyte is sufficiently conducting. Also, cathodic

protection works in degrees, meaning that if the contact is less than ideal, the corrosion on the more noble metal, while not entirely eliminated is nevertheless decreased from what it would have been if the metals were disjoined. The processes used for fabricating the individual barriers and configuring the waste package has an obvious effect on the efficacy of the cathodic protection. Tightly bonded processes such as cladding one metal onto another assure everywhere intimate contact. On the other extreme, fabricating the two barriers as separate shells and slipping one over the other is bound to create some points of contact, but result in many gaps between contact points. Not only does this result in less efficient cathodic protection, but the gapped regions may act as crevices and may be beyond the "throwing power" of the electrolyte. Recently, the design group has proposed a "shrink fit" approach to assure a reasonable degree of contact between the two metals.

2.8.2 Measurement of Galvanic Effects

Work began in FY-96 to build an electrochemical test cell in which the common potential of the couple and the current (magnitude and direction) between members of the couple are measured. The test cell can accommodate different size specimens to simulate different area ratios between cathode and anode, as well as testing at different temperatures and in different electrolytes. For the coupled test specimens, the change of the potential with time and the current with time are measured. These test use the Potentiostat/Galvanostat (described in Section 2.5) as a zero resistance ammeter for accurate measurement of the galvanic current. These electrochemical test methods are quantitative and very useful for interpretation of results from the long term galvanic corrosion tests. Because of funding and personnel limitations, experimental work has just begun for this activity. An activity plan governing this work has been prepared and issued. [1]

Although the galvanic effects appear to be mostly positive in protecting the inner barrier, there are two potentially damaging "side effects". First, corrosion products from the sacrificial material, e.g. ferric ion (but also cupric ion if one of the Cu-Ni alloys were used as the outer barrier) in conjunction with chloride may create an aggressive local environment. Second, hydrogen evolution and subsequent entry into the cathodic member can be damaging to titanium and some microstructural conditions in the nickel-base alloys. Both of these phenomena will be investigated.

In addition to the long-term galvanic tests planned for FY-97 (Section 2.4) , weld-clad specimens made by the Waste Package Design group will be tested. These were made by repeatedly and separately depositing weld wire corresponding to Alloy 825 and to Alloy 625 onto carbon steel plate to build up a layer of the more corrosion resistant metal. Specimens will be cut from this plate and exposed to the test environments of the long term, comprehensive corrosion test as a proof of principle.

Reference for Section 2.8

(1) A. Roy, Yucca Mountain Project Activity Plan, Galvanic Corrosion Testing Using Electrochemical and Immersion Techniques, Metallic Barriers SIP Activity E-20-46, Lawrence Livermore Laboratory, 1996.

2.9 Corrosion Modeling

2.9.1 Types of Corrosion Models

Modeling work proposed for the waste package container is organized according to degradation mode and described in the Metallic Barriers SIP. All of the degradation modes will have a deterministic model, in which the rate of attack is described in terms of important parameters, that are physical (for example, temperature), chemical (for example, pH and chloride ion concentration), metallurgical (for example, alloy composition and alloy microstructure) and mechanical (for example, stress). Not every degradation mode will have a parameter from each of the four categories. However, some parameters, such as temperature and alloy composition, affect just about every degradation mode.

In addition to the deterministic component, some degradation modes have a probabilistic component in their models, as indicated in Table 2.9 - 1. These modes include most of the localized corrosion and forms of environmentally accelerated cracking. While advances in corrosion science have fostered a better understanding of how and why metals corrode and, therefore, have improved our capability of predicting corrosion behavior, there are some aspects of corrosion phenomena that are still only explainable statistically. Local perturbations in the structure and compositions of usually protective, passive films on metals plus local perturbations in electrolyte composition give rise to variations in electrochemical potential on a micro-scale (on the order of a few 100 Å) with the result that localized corrosion (such as pitting) is favored by these variations in conditions over small regions. Similarly, the distribution of mechanical strain is subject to local perturbations in a real metal because of structural inhomogeneities from one location to another (on a similar scale to the electrochemical potential variations). Thus, stress corrosion cracking often shows a probablistic component because of a non-uniform electrochemical potential distribution *and* a non-uniform strain distribution.

Microbiologically influenced corrosion (MIC) is an even more complex case. Because the attack resulting from MIC is often of a localized nature, it is expected that electrochemical perturbations will also introduce a probabilistic term in the MIC model. Additionally, the biochemical variations surrounding microbial activity is expected to introduce a further probablistic consideration.

TABLE 2.9 -1   Types of Models for Metallic Barrier Degradation Modes

DEGRADATION MODE	TYPES OF MODELS
Low Temperature Oxidation	Deterministic
General Corrosion	Deterministic
Intergranular Corrosion	Deterministic
De-alloying or Selective Leaching	Deterministic
Galvanic Effects	Deterministic
Pitting Corrosion	Deterministic and Probabilistic
Crevice Corrosion	Deterministic and Probabilistic
Stress Corrosion Cracking	Deterministic and Probabilistic
Hydriding and Hydrogen Embrittlement	Deterministic and Probabilistic
Microbiologically Influenced Corrosion	Deterministic and Probabilistic
Phase Instability and Embrittlement	Deterministic and Probabilistic(?)

Notes and Commentary on Table 2.9 -1:

1. Electrochemical perturbations give rise to probabilistic terms in modeling pitting, crevice, stress corrosion, hydrogen embrittlement, and microbiological forms of corrosion. Additionally stress/strain perturbations result in probabilistic terms for stress corrosion and hydrogen embrittlement.

2.. Because rates of phase transformations are governed by temperature, chemical gradients, and strain, there is the possibility that some of the strain effects can be treated as probabilistic. At this stage, we are unsure whether a probabilistic term will be needed for the model of this degradation mode.

2.9.2 Candidate Materials and Modeling Needs

Several candidate materials are under consideration for the multi-barriered container. Each barrier has a somewhat different function, and this has been described in detail in the Metallic Barriers SIP. Candidate materials fall into two major categories: corrosion resistant materials and corrosion allowance materials, with a third category of "intermediate" materials whose performance has features of both categories. Functionally, the inner barrier will be fabricated from a corrosion resistant material while the outer barrier will be made from a corrosion allowance material or an intermediate material. For the purposes of modeling activities, this intermediate category has performance modeling needs somewhat between the other two categories, but is probably closer to the corrosion allowance category.

The candidate corrosion resistant materials consist of three groups: (A) Ni-Cr-Fe-Mo alloys with the nickel content running 40-50%. Specific candidates are Alloy 825 and Alloy G-3. (B) Ni-Cr-Mo alloys with the nickel content running around 60%. Specific candidates are Alloy C-22 and Alloy C-4. (C) "Lean" titanium-base alloys (containing less than 2% alloying elements). Specific candidates are Ti Grade 12 and Ti Grade 16. The candidate corrosion allowance materials are carbon steel (carbon content 0.20 to 0.25%) in cast form and in wrought form, and a low chromium-molybdenum alloy steel. The "intermediate" candidate materials are Alloy 400 (a Ni-Cu alloy) and 70/30 copper-nickel.

The *emphasis* of modeling activities over the next several years will vary from one category of materials to another. This is natural, since the primary reason for considering materials from different categories is their expected differences in performance. The following list, in Table 2.9.3, gives the modeling needs by degradation mode for the three categories of materials. The degradation modes are arranged in the same order as in Table 2.9.1; this listing does not follow any particular order of priority (see Table 4 for that). Testing and other experimental work may reveal additional degradation modes that need to be addressed.

TABLE 2.9.-2 Expected Models to be Developed for Different Categories of Container Materials

Corrosion Resistance Materials (e.g. Ni-Cr-Mo-Fe, Ni-Cr-Mo, and Ti Alloys)

Intergranular Corrosion
Pitting Corrosion
Crevice Corrosion
Stress Corrosion Cracking
Hydriding and Hydrogen Embritllement
Galvanic Effects
Microbially Influenced Corrosion
Phase Instability and Embrittlement

"Intermediate" Materials (e.g. Cu/Ni and Ni/Cu Alloys)

Low Temperature Oxidation
General Aqueous Corrosion
Intergranular Corrosion
Pitting Corrosion
De-alloying
Galvanic Effects
Microbially Influenced Corrosion

Corrosion Allowance Materials (e.g. Carbon and Alloy Steels)

Low Temperature Oxidation
General Aqueous Corrosion
Stress Corrosion Cracking
Hydriding and Hydrogen Embrittlement
Galvanic Effects
Microbially Influenced Corrosion

2.9.3 Key Parameters

Table 2.9 -3 gives an estimate of the key parameters for the individual degradation mode models. These are arranged according to whether they are expected to play a major role or a minor role in the model, in the sense that a "major" parameter will affect the rate significantly, while a "minor" parameter will affect the rate only moderately (if at all). This is, of course, an arbitrary call. Furthermore, the parameters are given in *very roughly* the order they are expected to influence the corrosion rate in the respective models. Whether or not this is the case will have to be verified by testing. Note that the alloy composition is almost always the first listed parameter, because with such a diverse range of candidate materials we are considering, this is the primary variable. It is expected that models for carbon steel will be quite different from those for 70/30 copper-nickel , which will be quite different from those for Alloy C-22. Alloy microstructure, which can be thought of as the alloy composition at a very local level, figures as an important parameter in many degradation modes. Since the alloy microstructure is most likely to vary in and around the welds, this is one way to account for differences in behavior for welded materials.

Other important variables come from the composition of the water that will contact the metal container. The compositional parameters are the chemical species present in groundwaters associated with the Topopah Spring tuff member, such as water from the J-13 well, are representative of water that will contact the container. For the most part, it is the anionic species, such as chloride, sulfate, nitrate, that most influence corrosion behavior; cationic species mostly influence the pH, which of course, influences corrosion so that the effect of cations is most appropriately handled by the pH term. In some cases where the effects of individual ions are not known, these are lumped these together as "electrolyte species'. Because silicate chemistry is complex, silicate is indicated simply as SiO_2.

It is always well to remember the interrelationship of various parameters, especially the chemical parameters. Changing the composition of one electrolytic species generally changes other compositional terms. The solution pH and electrochemical potential, E , are the manifestations of combined effects of a number of individual chemical species, and are, therefore, important indicators for characterizing the environment.

For the oxidation mode, the environmental parameters are expressed in terms of chemical species present in the vapor phase. These are combined together under atmospheric contaminants, such as SO_2, H_2S, NO_2, and various entrained ionic salts.

TABLE 2.9. - 3   Key Parameters for Individual Degradation Mode Deterministic Models

DEGRADATION MODE	ROLE	PARAMETERS
Low Temperature Oxidation	Major	alloy comp., T, humidity, O_2 atmospheric contaminants
	Minor	CO_2
General Corrosion	Major	alloy comp., pH, T, O_2, NO_3^-, radiolysis products
	Minor	alloy micro., Cl^-, SO_4^{-2}, F^-, HCO_3^-, SiO_2
Intergranular Corrosion	Major	alloy comp., alloy micro., O_2, NO_3^-, pH, T, radiolysis
	Minor	other electrolyte species
De-alloying or Selective Leaching	Major	alloy comp, alloy micro., pH, O_2
	Minor	other electrolyte species
Galvanic Effects	Major	alloy comp. of both metals, area ratio between metals, T, O_2, some electrolyte species, alloy micro., corrosion products from sacrificial metal (e.g., Fe^{+3}, Cu^{+2}), pH
	Minor	other electrolyte species
Pitting Corrosion	Major	alloy comp., Cl^-, pH, T, E, O_2, NO_3-, alloy micro., $SO_4^=$, F^-
	Minor	other electrolyte species
Crevice Corrosion	Major	alloy comp., crevice size, Cl^-, pH, T, E, O_2, NO_3^-
	Minor	$SO_4^=$, F^-, alloy micro., HCO_3^-, SiO_2
Stress Corrosion Cracking	Major	alloy comp., σ, alloy micro., T, pH, E, Cl^- alloy micro.,O_2
	Minor	other electrolyte species
Hydriding and Hydrogen Embrittlement	Major	alloy comp., σ, pH, E, alloy micro., T, O_2
	Minor	Cl^-, $SO_4^=$, other electrolyte species
Microbiologically Influenced Corrosion	Major	alloy comp., pH, T, O_2, $SO_4^=$, HCO_3^-, alloy micro.
	Minor	other electrolyte species
Phase Instability and Embrittlement	Major	alloy comp., alloy micro., σ, prior metallurgical history, T
	Minor	

Notes and commentary on Table 3:

1. Symbols: T = temperature; E = electrochemical potential, σ = stress (applied because of the loads supported by the container or residual because of stressed imparted during container fabrication and welding).. Other symbols and abbreviations should be self-evident.

2. Galvanic Effects are a special case. Galvanic effects can be a degradation mode if one metal accelerates corrosion on another, but the effects can be beneficial if corrosion of one metal protects the other metal from corrosion. Several different galvanic couples are under consideration. It is difficult to condense the interactions into this short table, but suffice it to say that many of the effects of particular electrolytic species will depend on the particular galvanic couples under consideration. Corrosion products, especially those from the more sacrificial metal (a corrosion allowance or intermediate material) will also alter the local chemistry and may influence subsequent corrosion activity on the more corrosion resistant material.

3. Phase Stability and Embrittlement is the only purely "metallurgical" model in the list, because this degradation mode docs not depend on chemical parameters in the environment. It does depend on temperature in the environment (T), however. It is also sensitive to the "prior metallurgical history", meaning details of the fabrication and welding used to make the container, particularly the times at the various process temperatures.

2.9.4 Effect of Time

Time has not been considered directly as a parameter, although time impacts the effect of the various physical, chemical, metallurgical, and mechanical parameters listed in Table 3. These parameters will surely change with time, especially over long periods of time. Most modeling activities are planned to produce a degradation mode rate for a given set of physical, chemical, metallurgical, and mechanical parameters. Ultimately, in order to estimate penetration damage to the container, the rate must be multiplied by the time interval over which the given set of conditions applies. This is where scenario development and analysis comes into play, and mandates close collaboration between the performance assessment and materials modeling (and testing) efforts.

In models for some of the degradation modes, there is expected to be a change in the rate with time even though conditions (physical, chemical, metallurgical, and mechanical) remain unchanged (at least on a macroscopic scale). An example is general aqueous corrosion on many materials. The rate is initially high, but decreases steadily as protective films form on the metal to slow down the corrosion rate. In this case, the time factor can be directly incorporated into the model. A different kind of example occurs in localized corrosion (such as pitting or crevice attack) where initially the rate is imperceptible until the correct combination of conditions develop on a microscopic level, initiating a critical size embryo that then begins to propagate at a measurable rate. This time effect is also considered in the model for these kinds of corrosion. In this case, the time factor is important in developing the probabilistic aspect of the model.

2.9.5 Status of Modeling Effort

The modeling effort to date has been limited to development of a model for low temperature oxidation (Metallic Barriers SIP Activity E-20-75) and one for pitting corrosion (Activity E-20-80). These are described in the sections to follow. The model on low temperature oxidation of iron and steel is a deterministic model, while the model on pitting corrosion of highly corrosion resistant material is an example of a probabilistic model. Many more modeling efforts are planned, particularly as results from the various testing activities become available.

2.10 Modeling of Low Temperature Oxidation of Carbon Steel
(input to this section of the report was provided by Greg Henshall)

Wrought and cast low-carbon steel are candidate materials for the thick (e.g. 10 cm) outer barrier of waste packages being considered for use in the potential geological repository at Yucca Mountain. Dry oxidation is one potential degradation mode for these materials at the moderately elevated container surface temperatures expected, e.g. 323 – 533 K (50 – 260 °C). Due to the long times for which this barrier must remain intact, mathematical models are required to extrapolate the available short-time experimental data. The approach taken in this study was based on the theory of oxidation for iron and low-carbon steel, and employed a numerical integration technique to solve the resulting differential equation for arbitrary thermal histories. A simple method for estimating the effects of spalling of the oxide was also included.

2.10.1 Development of the Model

A variety of physical theories exist to describe the oxidation of metals at constant temperature [1]. In iron, a logarithmic relationship exists between oxide thickness and exposure time at low temperatures (i.e. near room temperature) and for oxide films less than about 0.1 μm thick [2]. For oxide thicknesses of practical importance to WP degradation, however, both theoretical treatments and the available experimental data show that the oxidation of iron and low-carbon steels at moderately elevated temperatures (293 < T < 843 K) is diffusion controlled and therefore obeys a parabolic rate law if the temperature is constant.

In general, the parabolic oxidation of iron and low-carbon steel produces multi-layered scales due to the variable oxidation state of iron. In order of proximity to the metal surface these are: FeO (wüstite), Fe_3O_4 (magnetite), and Fe_2O_3 (hæmatite). However, at temperatures below 843 K (570 °C), FeO is thermodynamically unstable, so only Fe_3O_4 and Fe_2O_3 form [1]. At these moderately elevated temperatures, the Fe_3O_4 layer is found to be much thicker than the Fe_2O_3 layer, at least for scales up to about 20 μm thick [3]. Therefore, it was assumed in this study that the oxide scale consists of only Fe_3O_4 at the temperatures of interest. This assumption significantly simplifies the model while providing predictions that are reasonably accurate, as shown in the next section.

In addition to the assumptions of parabolic oxide growth (for constant temperature) and the presence of only magnetite in the scale, several other assumptions were made in developing the model. First, the Fe_3O_4 oxide was assumed to be 100% dense, consistent with observations [2-4] for layers up to about 20 μm thick. Second, Arrhenius behavior with a constant activation energy over the relevant temperature range was assumed. As discussed below, this appears to be a reasonable approximation of the oxidation behavior for iron in the 323 – 533 K regime. Finally, the oxide was assumed to be free of cracks and adherent to the metal surface; a specific exception to this assumption is described later.

Mathematically, the parabolic growth rate of a single-species oxide can be expressed [1]:

$$\mathrm{d}x/\mathrm{d}t = k'_p/x \tag{1}$$

where x is the oxide thickness, t is exposure time, and k'_p is the parabolic rate constant. The temperature dependence of the oxidation rate is governed by the Arrhenius behavior of k'_p:

$$k'_p = k_p \exp(-Q/RT) \tag{2}$$

where k_p is a constant, Q is the activation energy for the oxidation process, R is the gas constant and T is absolute temperature. Literature values of k_p and Q for iron and low-carbon steel are given in Table 2.9.3.1. In the parabolic regime and at temperatures below 723 K (450 °C), Q appears to be constant at about 104 kJ/mol (25 kcal/mol). The values of k_p given in Table 2.10 - 1 vary considerably, possibly because the measurements were made using a variety of materials and environments.

Table 2.10 -1. Oxidation of Iron and Carbon Steel at Moderately Elevated Temperatures.

$k_p{}^a$ (cm^2/s x 10^5)	Q (kJ/mol)	T (K)	$x_{max}{}^b$ (µm)	Regime^c	Alloy	Ref.
——	25.1	473 - 623	0.05	L	.2-.8% C	2
——	30.5	473 - 623	0.1	L	.2-.8% C	2
0.7 - 1.7^d	104	523 - 623	1.4	P	.2-.8% C	2
0.02^e	104	541 - 736	0.4	P	.04% C	6
0.03^e	102	541 - 666	2	P	.04% C	6
2.5^f	34 / 106^g	673 - 923	22	P	.02% C	3
0.02^h	72.4	673 - 823	10.5	P	Pure Fe	7,8
4.3	——	773	15	P	0 - .99% C	4

Notes:

^{a} Representative or maximum values were selected from the data provided.

^{b} Based on a fully dense layer of Fe$_3$O$_4$

^{c} L = logarithmic, P = parabolic

^{d} Measured at 573 K

^{e} Measured at 569 K

^{f} Measured at 723 K

^{g} Q=106 kJ/mol for 670 ² T ² 723 K; Q=34 kJ/mol for 723 ² T ² 853 _C

^{h} Measured at 673 K

Equations (1) and (2) can be easily integrated analytically for simple (e.g. constant) temperature histories. However, to perform the integration for arbitrary, complex temperature histories, such as those expected in the repository, a numerical approach employing the Forward Euler method [5] was implemented. Combining Eqs. (1) and (2) and writing the result as a difference equation gives:

$$\Delta x = \{(^1/_x)\,[k_p\,\exp(-Q/RT)]\}\,\Delta t \tag{3}$$

where Δx is the increase in oxide thickness over the time step Δt. Writing Δx as

$$\Delta x = x_i - x_{i-1}, \tag{4}$$

where the subscript "i" denotes the current time step, equation (3) can be written

$$x_i - x_{i-1} - \{(^1/_{x_i})\,[k_p\,\exp(-Q/RT_i)]\}\,\Delta t = 0. \tag{5}$$

This non-linear equation in the single unknown, x_i, can be solved using any standard method for solving non-linear equations in one variable. A bisection technique [5] was chosen because it is simple and robust. Also note that Eqs. (3) – (5) represent an implicit scheme for solving the differential equation (1). Therefore, while this method is unconditionally stable, the computed oxide thickness will depend on the time-step size. Therefore, convergence of the solution was confirmed by decreasing Δt until the final x values varied by less than a specified tolerance, typically 0.1%.

For predicting the degradation of WPs it is the metal penetration, p, caused by oxidation, not the oxide thickness, that needs to be calculated. Again assuming a fully dense Fe_3O_4 oxide forming on pure iron, p can be computed from the oxide thickness using:

$$p = \left[(^{\rho_o}/_{M_o})(^{M_M}/_{\rho_M})N_M\right] x \tag{6}$$

where ρ_0 and ρ_M are the density of the oxide and the metal, M_0 and M_M are the molecular or atomic weight of the oxide and the metal, and N_M is the number of moles of metal atoms per mole of oxide (3 for Fe_3O_4). For simplicity, the densities were assumed to equal their room temperature values.

It is unrealistic to assume that a 10-cm thick metal barrier will completely oxidize without cracking or spalling of the oxide scale. Such defects in the oxide decrease its protectiveness and increase the oxidation rate because fresh metal is exposed and/or a fast diffusion path for oxygen is created. Therefore, a conservative approach was taken to estimate the effects of mechanical defects in the scale. It was assumed that, due to the buildup of mechanical stresses in the oxide as its thickness increases, a critical thickness exists at which these stresses exceed the fracture strength of the oxide. Once this critical thickness, x_c, is reached the oxide is assume to completely spall away, exposing the bare metal surface. At this point, the parabolic oxidation process begins as if no oxide had

ever been present; i.e. $x = 0$. Of course, the metal penetration does not return to zero when $x = 0$, but continues to accumulate. In this case, the accumulated penetration, P, is computed from Eq. (7):

$$P = \sum_{J=1}^{n} Pj \qquad (7)$$

where n is the number of spall events or "cycles" and p_j is computed from Eq. (6). While such a model is certainly over simplified, it provides a conservative way in which to treat defects in the scale. The use of such a conservative approach is justified later.

2.10.3 Numerical Results

The accuracy of the assumptions used in developing the model, other than those associated with spalling, were tested by simulating literature data for the oxidation of iron and low-carbon steel at constant temperature. Figure 2.10 -1 presents such data for both pure iron and for a low-carbon steel. In both cases, the increase in oxide thickness with increasing exposure time is nearly parabolic over the range studied. These results confirm the hypothesis that the dry oxidation of these metals is diffusion controlled and can be modeled using Eq. (1). As shown in Fig. 2.10 -1(a), the simulated oxidation rate is consistent with the data of Caplan and Cohen [3] for iron up to an oxide thickness of 6 μm. The data of Boggs and Kachik [4] for 0.99% C steel are simulated with nearly the same accuracy up to $x = 16$ μm, as shown in Fig.2.10 -1(b). The accuracy of the simulations shown in this figure suggests that the assumptions used to develop the model are reasonable for oxide thicknesses up to at least about 20 μm.
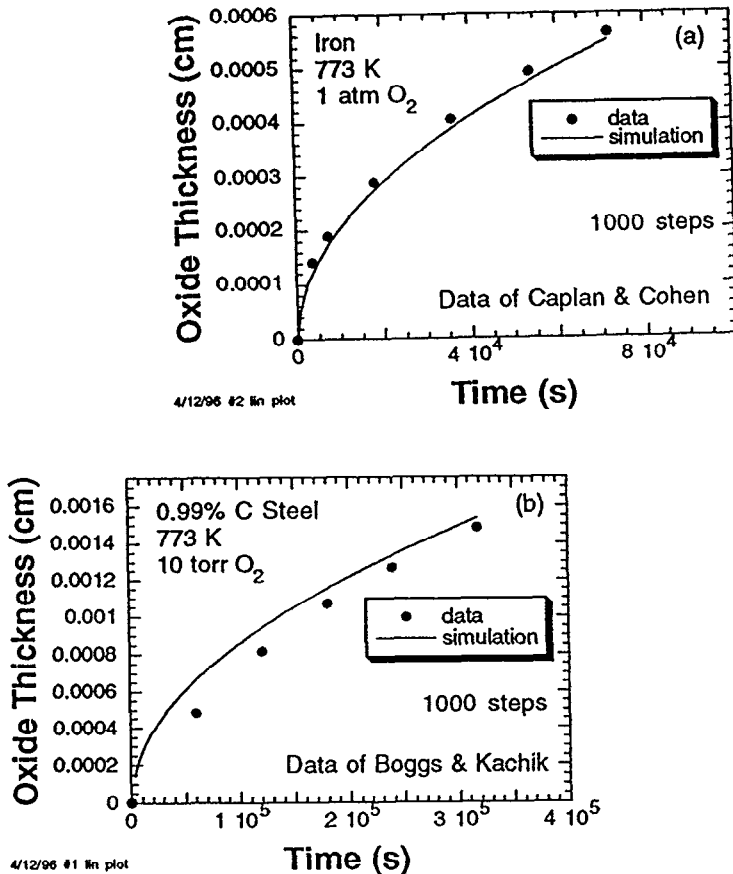
Fig. 2.10 -.1.   Model simulations of oxide growth are compared with data for (a) iron oxidized at

773 K in a 1 atm. O_2 environment [3] and (b) 0.99% C steel oxidized at 773 K in a 10 torr

O_2 atmosphere [4].

With the accuracy of the model confirmed for simple, constant-temperature conditions, predictions of oxidation were then made for complex, repository-relevant temperature histories. First, calculations were made using the WP surface temperatures calculated by Buscheck et al. [9] Then, to increase the conservatism of the predictions, the temperatures calculated by Buscheck et al. were increased by 100 K for all exposure times. Figure 2(a) compares this "extreme" temperature history with a polynomial approximation used for the oxidation calculations. Based on the experimental data given in Table 1, values of k_p = 4.3 x 10^{-5} cm^2/s and Q = 104.6 kJ/mol were used in these calculations. The use of k_p = 4.3 x 10^{-5} cm^2/s is conservative since this was the largest value indicated by the literature data. Figure 2(b) shows the resulting oxide thickness and metal penetration predictions. Note that the oxidation rate is not parabolic because the temperature is not constant. The metal penetration following 5000 years of exposure to this severe temperature history is predicted to be only about 0.127 mm, less than 0.13% of the expected container thickness of 10 cm. Using a phenomenological approach, Stahl and McCoy [10] also predicted that

little metal penetration of carbon steel would occur due to continuous dry oxidation under repository-relevant conditions.
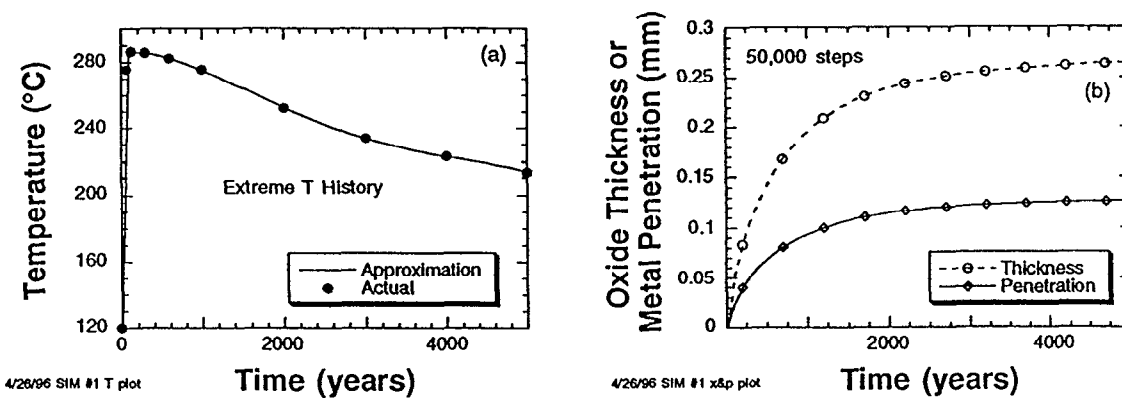

Fig. 2.10 -.2 (a) The "extreme" temperature history (solid circles) is compared with a polynomial approximation. (b) Corresponding model predictions of the oxide layer thickness and metal surface penetration histories assuming continuous oxide growth.

Defects in the oxide, such as cracking or spalling, would increase the metal penetration rate above that computed assuming a defect-free, adherent oxide layer. Using the approach described previously to account for such defects and the temperature history shown in Fig. 2.10 - 2 (a), predictions of the surface penetration into iron or low-carbon steel were made. Values of the critical oxide thickness for spalling, x_c, were chosen to be either $x_c = 0.02$ mm or $x_c = 0.1$ mm. The former roughly corresponds to the maximum oxide thickness cited in literature studies of continuous oxide growth on iron and steel at the relevant temperatures (see Table 2.10-1). Since spalling was never observed in these studies, this value provides a reasonable lower limit on x_c. The second value, $x_c = 0.1$ mm, was chosen arbitrarily to assess the influence of this parameter on the predictions. The values of $k_p = 4.3 \times 10^{-5}$ cm²/s and $Q = 104.6$ kJ/mol again were used in these calculations.

As shown in Fig. 2.10 -3, final metal penetration depths are larger than if oxide growth is continuous, Fig. 2.10 -3 (b), but are still small. Therefore, the very conservative method used to treat defects in the oxide still results in the prediction that dry oxidation damage is minimal. For $x_c = 0.02$ mm, Fig. 2.10 - 3(a) shows that the value of P following 5000 years of simulated exposure to the extreme temperature history is predicted to be approximately 1.7 mm, or about 1.7% of the expected container thickness. Increasing x_c to 0.1 mm decreases the predicted value of P to approximately 0.35 mm. In this case, the discontinuous rate of metal penetration caused by discrete spall events is clearly apparent.
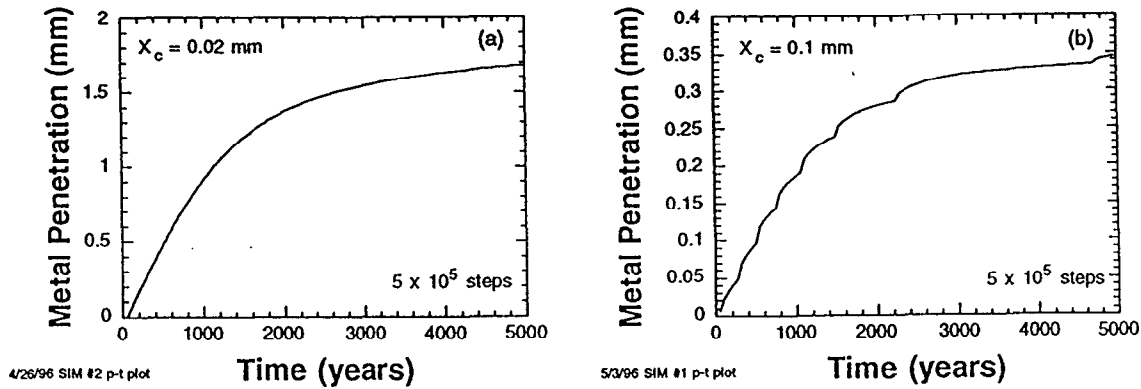
Fig. 2.10 -3. Predictions of the time-dependent penetration of an iron or low-carbon steel surface subjected to the extreme temperature history shown in Fig. 2.10 -2 (a) for: (a) $x_c = 0.02$ mm and (b) $x_c = 0.1$ mm.

2.10.4 Tentative Conclusions and Future Work

Based on the physically-based model calculations presented here, dry oxidation is not expected to significantly degrade the performance of thick, corrosion allowance barriers constructed of low-carbon steel even for very long time periods (hundreds to thousands of years). Further studies are in progress to consider internal oxidation and the effects of water vapor in the atmosphere. The transition from dry oxidation to wet corrosion, which is the focus of the experimental work, discussed in Section 2.3, is an important boundary for this model. Once aqueous conditions are established on the carbon steel surface, the degradation rate becomes higher and the pH and several other chemical parameters become influential in determining the degradation rate. A deterministic model is planned on general aqueous corrosion.

A model for microbiologically influence corrosion will follow from that of general aqueous corrosion (which represents a purely abiotic case), since the effect of microbial activity is to cause changes in the pH and other chemical parameters, whose effects are already incorporated in the general aqueous corrosion model. As the onset of aqueous corrosion depends on exceeding a critical humidity to establish an electrolytic film, microbial activity requires a sufficiently high humidity to establish a biofilm. The critical humidity level to initiate the abiotic corrosion and that to initiate the biotic corrosion may be different. Another important aspect that will need to be addressed in the MIC case is the localization of the microbial activity (to answer such questions as: Is the attack uniform or localized? Is the attack favored near a weld? Is the attack favored along grain boundaries? Is the attack favored along inclusion stringers?). Thus, additional empirical factors, dependent on test results and interpretations, will be required. This subject was

discussed at a waste package degradation model abstraction workshop held in January 1997 in preparation for the total system performance assessment (TSPA) models being developed for the viability assessment (VA) in 1998. As a result of that workshop, some restructuring and combination of the corrosion models originally proposed in the Metal Barrier SIP was suggested, and future work will be pursued to develop integrated corrosion process models, as well as the development of individual models.

References for Section 2.10

1. N. Birks and G. H. Meier, *Introduction to High Temperature Oxidation of Metals*, Edward Arnold, London (1983).
2. R. B. Runk and H. J. Kim, *Oxidation of Metals* **2**, 285 (1970).
3. D. Caplan and M. Cohen, *Corr. Sci.* **6**, 321 (1966).
4. W. E. Boggs and R. H. Kachik, *J. Electrochem. Soc.* **116**, 424 (1969).
5. G. E. Forsythe, M. A. Malcolm and C. B. Moler, *Computer Methods for Mathematical Computations*, Prentice-Hall, Englewood Cliffs, New Jersey (1977).
6. E. J. Caule, K. H. Buob, and M. Cohen, *J. Electrochem. Soc.* **108**, 829 (1961).
7. O. Kubaschewski and B. E. Hopkins, *Oxidation of Metals and Alloys*, Academic Press, London, p. 108-110 (1962).
8. M. H. Davies, M. T. Simnad and C. E. Birchenall, *J. Metals* **3**, 889 (1951).
9. T. A. Buscheck, J. J. Natao and S. F. Saterlie, in *High Level Radioactive Waste Management: Proceedings of the Fifth International Conference*, ANS, La Grange Park, IL and ASCE, New York, pp. 592-610 (1994).
10. D. Stahl and J. K. McCoy, "Impact of Thermal Loading on Waste Package Material Performance," in *Scientific Basis for Nuclear Waste Management XVIII*, Materials Research Society, Pittsburgh, PA, pp. 671-678 (1995).

2.11 Modeling Pitting Corrosion of Corrosion Resistant Alloys

Input to this section of the report was provided by Greg Henshall.

2.11.1 Introduction

Current waste package designs consider using a highly corrosion resistant material, such as a Ni- or Ti-base alloy for the inner barrier. Normally, such alloys are protected by a passive oxide film, but if they become wet and Cl^- or other aggressive species are present the passive film can break down locally, causing localized corrosion. Of the three forms of localized corrosion[1], *i.e.* pitting, crevice corrosion, and stress-corrosion cracking, that are likely to occur on container surfaces exposed to repository environments, pitting corrosion was chosen for detailed modeling. Pitting corrosion was selected because it bears many similarities with crevice corrosion. Therefore, many aspects of the pitting model are expected to be directly applicable to the crevice corrosion model. It was decided to defer development of a validated model of stress-corrosion cracking until additional experimental information on the stress-corrosion behavior of candidate container materials under repository relevant conditions become available.

Factors driving the development and experimental validation of a pitting corrosion model are centered around the need to understand the behavior of candidate waste container materials that may undergo localized corrosion in repository-relevant environments. The availability of such a model would minimize the risk of missing some critical interaction of material and environment that would result in premature failure of the container. The specific factors include:

1. A total lack of operational information on long-term storage of high-level nuclear waste;
2. Uncertainty and variability in the environmental conditions, and possible changes in these conditions;
3. The need to make technically defensible extrapolations to very long times based on experimental data bases developed over very short times (with respect to repository lifetimes); and
4. The need to make technically defensible extrapolations to very large exposed surface areas based on experimental data bases developed over much smaller areas.

In contrast to uniform corrosion where mechanistic modeling has been successful, a statistical approach to characterizing and modeling localized corrosion appears to be necessary, even though the data requirements are large[2] One advantage of a statistical, or stochastic, model is that the evolution of the pit depth *distribution*, not just the time required for initial penetration of the containers, can be computed. From this information the area available for release of radionuclides through the containers can be estimated as a function of time[3] This section describes a phenomenological approach for computing

the time evolution of these distributions that is largely stochastic in nature but combines some elements of the deterministic aspects of pit growth.

The pit depth distribution, or pitting corrosion damage function, is illustrated schematically in Fig.2.11 -1. It is simply a plot of the number (or frequency) of pits at a particular depth *vs* depth. The damage function may be represented by smooth curves, as in Fig. 1, or as a series of histograms, as shown later in this report. From a modeling standpoint, the damage function is computed for various exposure times assuming that the metal being pitted is infinitely thick. These curves then can be compared with the actual wall thickness of the waste package container, as shown in Fig.2.11 -1. The predicted time required for the first pit to penetrate the container wall is that at which the computed damage function first intersects the line corresponding to the wall thickness (t_2 in Fig. 2.11 -1). At longer times, the *number* of pits penetrating the container wall is proportional to the area under the damage function curve for pit depths greater than the wall thickness (the shaded area under the t_3 curve). The calculated *depths* of through-wall pits have no physical significance, since a pit cannot have a depth greater than the wall thickness.
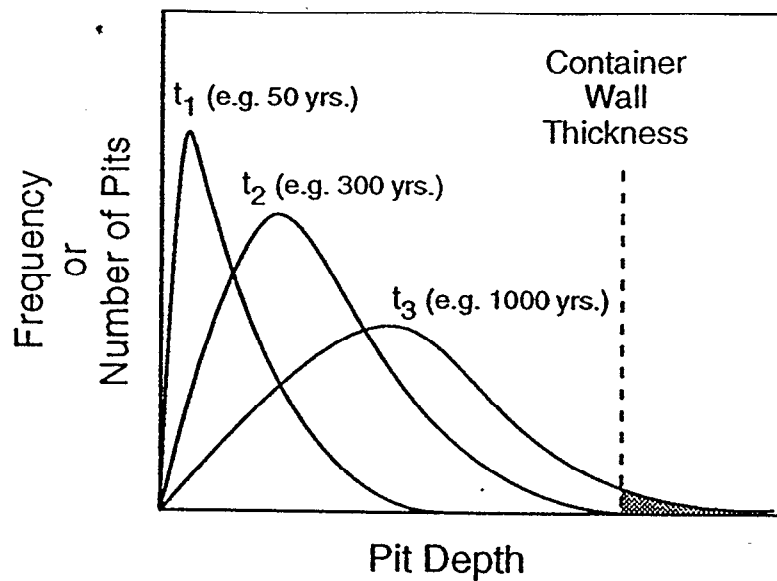

Figure 2.11 -.1. Schematic illustration of the pitting corrosion damage function.

Total specimens: 72
7 specimens did not pit

304 SS (6/0 polish)
3.5% NaCl, 35 °C
E_{app} = 350 mV SCE

Number of Specimens

25
20
15
10
5
0

20   40   60   80   100
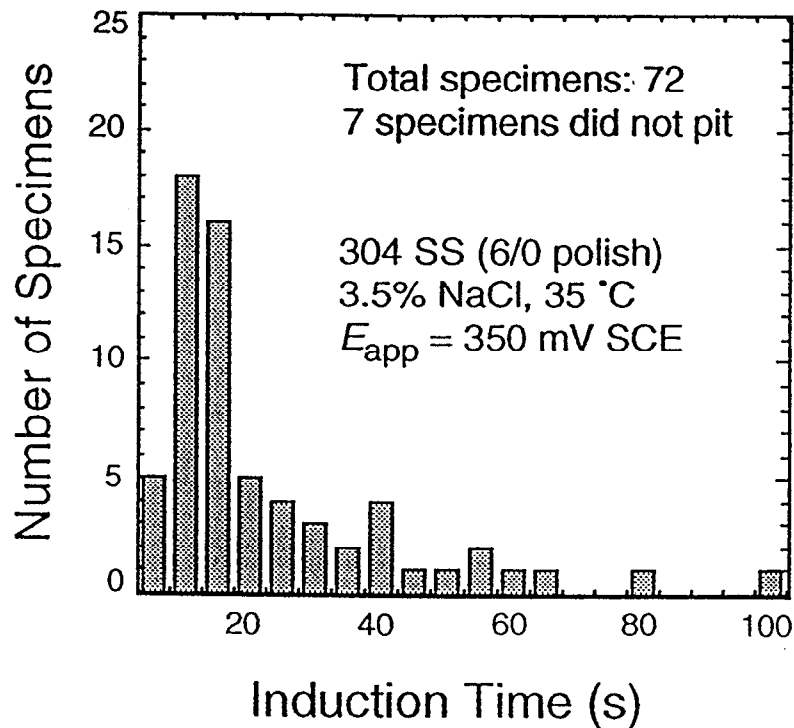
Induction Time (s)

Figure 2.11 -.2. The induction time distribution for 72 identical Type 304 stainless steel specimens immersed in NaCl solution. Data of Shibata and Takeyama[4].

2.11.2 The stochastic nature of pitting corrosion

Experimental studies have shown that the initiation of corrosion pits is a stochastic process. Shibata and Takeyama[4] were the first to show that the critical potential necessary to induce pitting and the "induction" time elapsed before pits become observable are both statistically distributed quantities. For example, Fig. 2.11 -2 presents their data showing the distribution of induction times for 72 identical Type 304 stainless steel specimens subjected to identical conditions. The data exhibit a wide distribution of induction times, suggesting that pit initiation occurs stochastically.

There is also evidence that the growth of existing pits is a stochastic process. This hypothesis is supported by the fact that a wide distribution of pit depths occurs in a single specimen subjected to a nominally uniform environment. In a study of the pit depth distribution evolution in mild steel, Marsh et al.[5] identified four factors having the potential to produce the wide distribution of pit depths observed on any given sample:

1) The pits will have different initiation times;
2) Many pits will cease to propagate following limited growth;
3) The morphology of the pits will vary, with some favoring more rapid mass and charge transfer, and hence faster propagation rates; and
4) Some pits will initiate at metallurgical features which may favor more rapid propagation, e.g. inclusions and grain boundaries.

Further support for the concept of stochastic pit growth is given by the data and analysis of Aziz[6] for the pitting corrosion of aluminum in tap water. Figure 2.11 -3 shows the pit depth distribution data of Aziz. When first exposed, a large number of pits initiate and start propagating. After a short time, many pits progressively stifle while only a portion of the population continues to grow, resulting in a backwards "J" shape to the low depth portion of the distribution (This finding supports the concept of permanent pit growth cessation introduced in Section 2.11.4) For those pits still growing, the random influence of the environment on propagation rates results in a bell-shaped distribution, which moves as a body toward larger depths. (This finding directly supports the concept of stochastic pit growth.) After much longer exposures, the mode, *i.e.* peak, of the distribution becomes stationary and only the deeper pits continue growing. These pits grow at a steadily decreasing rate (which supports the use of a nonlinear increase in pit depth with time introduced in Section 2.11.4), and the majority of the pits eventually stifle. These last two findings may result from the build-up of corrosion products within and over pits.
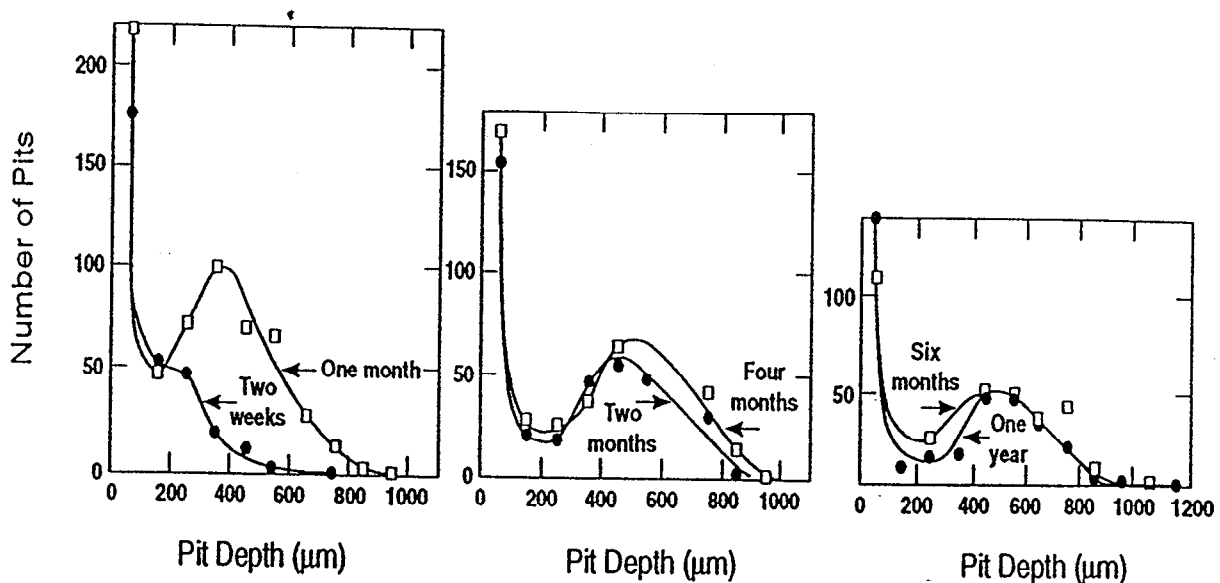
Figure 2.11 -3. The distribution of pit depths as a function of exposure time for Alcan 2S-O aluminum immersed in tap water. Data of Aziz[6].

2.11.3 The Initial Model

Stochastic pit initiation and growth

Over the past several years, a physically-based, phenomenological, stochastic model of pit initiation and growth has been developed[7-9]. This model is based upon the theory[10] that

small fluctuations in the local conditions (*e.g.* electrolyte chemistry, fluid flow rate, surface topography, near-surface microstructure) cause local breakdown of the passive surface film, resulting in the "birth" of metastable pits or "embryos". Many of these embryos become unstable when the local conditions change and repassivation, or "death", of the embryo results. Once a surviving embryo reaches a critical size or age (the two are assumed to be closely related), it becomes a permanent or "stable" pit and cannot die.

Monte Carlo computer codes have been developed to simulate the stochastic processes of embryo birth, death, and the establishment of a stable pit[7]. These codes establish a unit area that is divided into individual "cells" to represent a metal surface in contact with an aggressive environment. During each time step, a random number between 0 and 1 is generated for every cell that does not already contain an embryo or stable pit. If this random number is less than the user-prescribed birth probability, λ, a pit embryo is placed in that cell; otherwise the cell remains empty. Physically, λ corresponds to the probability that, over the area of one cell in a unit time, the local conditions will cause the passive film to break down, thereby initiating a microscopic pit embryo.

For each cell containing an unstable pit embryo, another random number is then generated. If this number is less than the input death probability, μ, the embryo dies and is removed from that cell. The death probability corresponds to the probability that a specific pit embryo, or breakdown in the passive film, will repassivate during a unit time. Pit embryo death has been linked physically, for example, with a reduction in the hydrodynamic boundary layer thickness, which causes a loss of the local concentration excursions needed to support the pit embryo[11].

The "age" of each surviving embryo, *i.e.* the number of time steps it has survived since birth, is incremented at each step and compared with the critical age, τ_c. If the age of an embryo equals τ_c, a stable pit is formed in that cell which is present for the remainder of the simulation. Physically, the critical age can be related to the ratio of the minimum stable pit depth to the velocity of pit embryo propagation[11]. The minimum stable pit depth is related to the surface roughness and the thickness of the hydrodynamic boundary layer, and the velocity of propagation depends on the electrochemical potential, aggressive ion concentration, and the nature of the alloy. Finally, note that all three of the pit initiation parameters (λ, μ, τ_c) can be related to experimentally measured quantities[7].

An example of the model predictions for pit initiation is shown in Fig.2.11 -4[7]. The parameters used to make this calculation (given in the figure) were chosen arbitrarily, so quantitative agreement with Fig. 2.11 - 2 is not expected. Qualitatively, however, the two distributions are similar, suggesting that the model treats pit initiation in a realistic way. Quantitative comparisons between the model predictions and pit initiation data have been given elsewhere[7] and support the same conclusion.
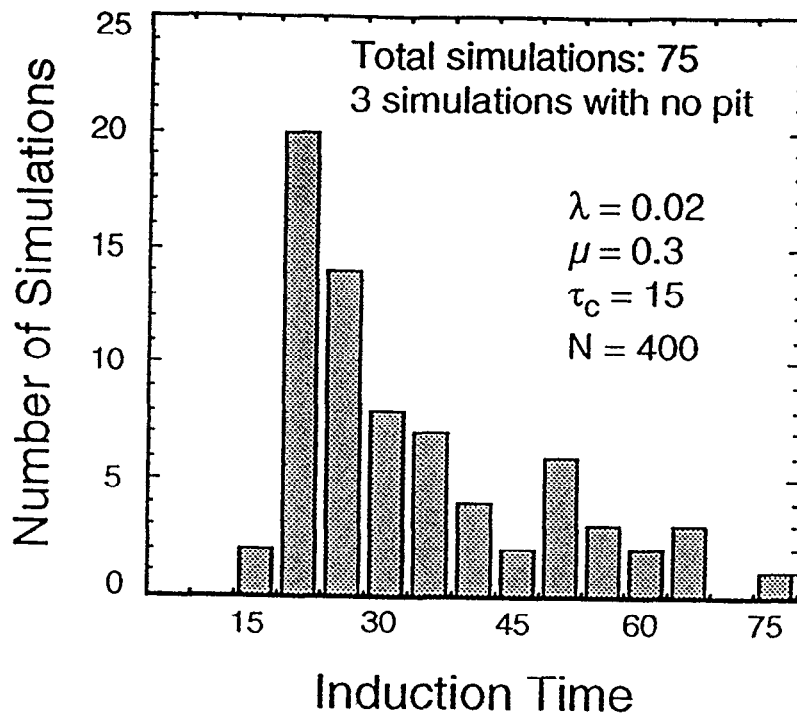
Figure 2.11 - 4. Model predictions of the distribution in stable pit induction times (arbitrary units). Three of the 75 simulations did not produce a stable pit within 75 time steps.

In the initial model, the effects of stochastic stable pit growth on the damage function evolution were included using a simple approach: growth of a stable pit during a particular time step occurs only if a randomly generated number between 0 and 1 is less than the prescribed growth probability, γ. Physically, γ corresponds to the probability that a pit will grow an increment in depth in one unit of time.

An example of the model predictions for stable pit growth under conditions of constant environment is given as a series of histograms in Fig.2.11 - 5. Each plot gives the number of pits (per unit area) at each depth for a particular exposure time, where time is given in number of time steps, Δt. (As discussed later, quantitative calculations for which exposure times and pit depths have physically meaningful units require experimental data to fit the parameters in the model.) For short times (10 steps) the distribution is narrow, with a large number of pits at low depths. As time increases, the total number of pits increases (40 steps) and the peak in the distribution occurs at an intermediate depth. The number of pits at very low depths is now less than at shorter times. At long times (100, 125 steps), the number of pits stays fairly constant and there are few (if any) pits at low depths. The distribution also begins to broaden and the number of pits at the peak of the distribution is less than at shorter times. The depth at which the peak occurs continuously increases with time. Many of these gross features are consistent with the data published in the literature, e.g. Fig.2.11 - 3. However, the linearly increasing maximum pit depth with increasing exposure time and the nearly

symmetric shape of the distribution are inconsistent with the available data, as described in Section 2.11.4.

The utility of damage function evolution predictions like those given in Fig. 5 for purposes of WP container performance assessment (PA) can be demonstrated as follows. Consider the units of pit depth in Fig. 2.11 - 5 to be millimeters, and consider a WP container 32 mm thick. For times of 10 and 40 steps all of the pits have depths less than the thickness of the container, so no release of radionuclides can occur as a result of pitting. Figure 5(c) shows that the time required for first penetration of the container is about 100 Δt, since at this time the first pit with a depth equal to 32 mm has developed. With further exposure to a time of 125 Δt, Fig. 2.11 - 5(d) shows that approximately 25 pits have calculated depths [3] 32 mm, and so will have penetrated a unit area of the container. While the results in Fig. 2.11 - 5 are only qualitative, quantitative predictions could be made by experimentally measuring pit depth distributions over a range of constant environmental conditions, and using the results to provide quantitative values of the model parameters for materials of interest.

Modeling the effects of environment

One major purpose of modeling pitting corrosion of WP containers is to extrapolate short-time "accelerated" test data to the extremely long service times. Since accelerated testing will require environmental conditions more aggressive than those expected in the repository, these extrapolations will require quantitative predictions of the effects of environment on pit initiation and growth rates. Simulating the effects of environment on pitting also will be required to explore container performance for various environmental scenarios, including the case in which the environment changes with time.
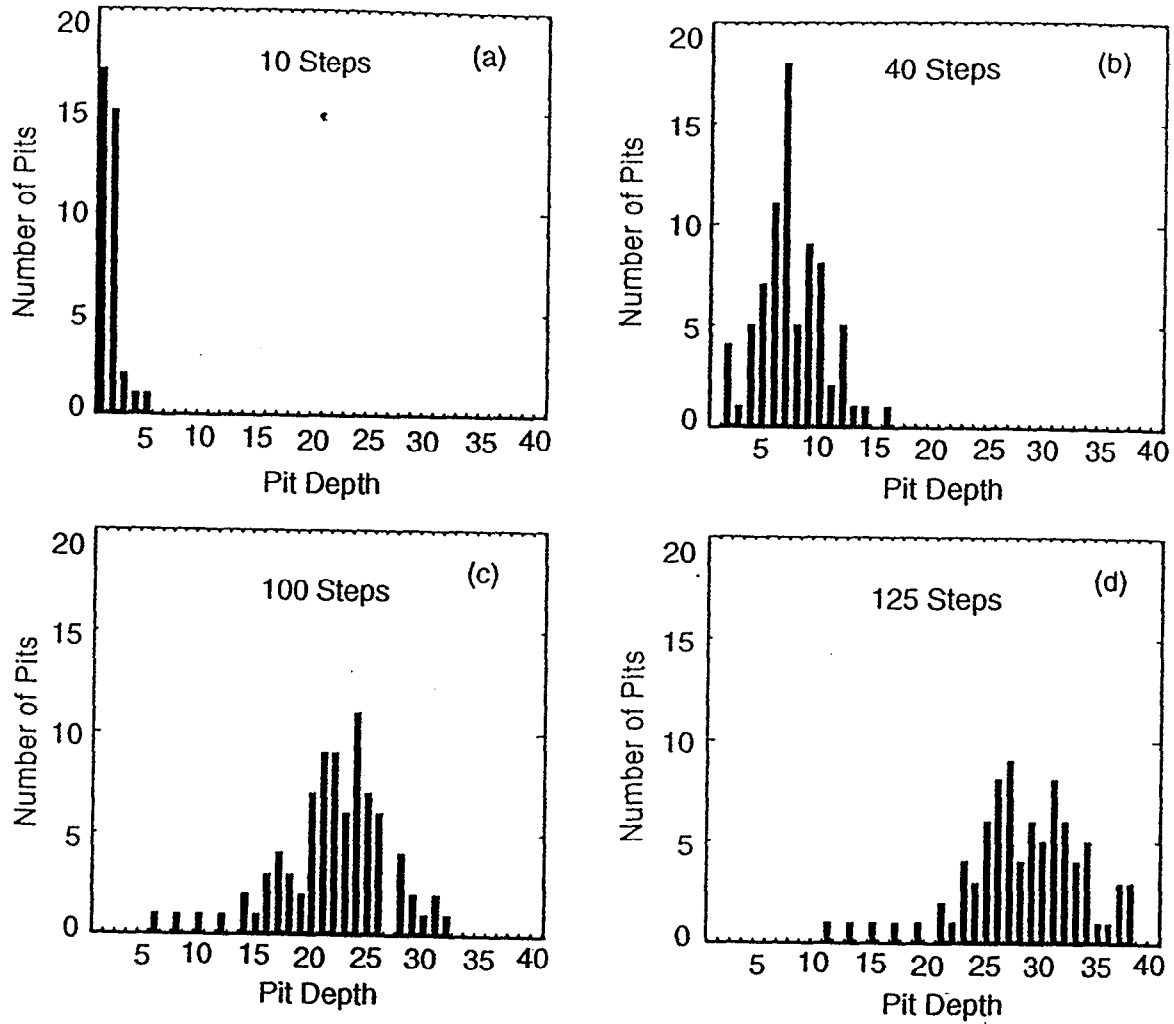
Figure 2.11 - 5. Evolution of the computed damage function histogram for times of (a) 10, (b) 40, (c) 100, and (d) 125 steps. An exponentially decreasing birth probability and a stochastic growth probability of 0.25 were used in the calculations[7]. Pit depths are in arbitrary units.

In the context of the stochastic pitting model, the goal is to model the environmental sensitivity of the stochastic parameters: λ, μ, τ_c, and γ. Rigorous development of such relationships has not yet been possible because it would require considerable experimental work. Therefore, simple but physically reasonable phenomenological expressions have been developed based on a variety of experimental data from the literature. The purpose of this exercise was to provide the means for qualitatively illustrating the potential power of the stochastic approach for predicting the pitting response to various environments. Future efforts should be aimed at improving the physical basis of these expressions, expanding their scope, and quantitatively exploring their predictive capabilities.

Three important environmental parameters have been included in the illustrative model: electrochemical potential, E, chloride ion concentration, $[Cl^-]$, and absolute temperature, T. Other variables, such as pH, oxygen concentration and the presence of other ions in solution, would need to be included in a complete analysis. Based on a wide variety of published experimental data, the following phenomenological expressions for the environmental dependence of the stochastic parameters were determined[7]:

$$\lambda = A_1 (E - B_1) \cdot \exp(C_1 \cdot [Cl^-]) \cdot \exp(-Q_\lambda / RT) \tag{1}$$

$$\mu = A_2 \cdot \exp(-C_2 \cdot [Cl^-]) \cdot \exp(-Q_\mu / RT) \tag{2}$$

$$\tau_c = A_3 \cdot \exp(-B_3 \cdot E) \cdot \exp(-C_3 \cdot [Cl^-]) \cdot \exp(+Q_\tau / RT) \tag{3}$$

$$\gamma = A_4 (E - B_4)^{B_5} \cdot ([Cl^-])^{C_4} \cdot \exp(+Q_\gamma / RT) \tag{4}$$

where the A's, B's and C's are constants, the Q's are activation energies and R is the gas constant.

Using Eqs. (1)–(4), predictions of the effects of E, $[Cl^-]$, and T on a variety of pitting phenomena have been made[7,8]. In general, the predictions are qualitatively consistent with published experimental data. Most importantly, it has been demonstrated[7] that this expanded stochastic model can predict the pit depth distribution evolution for continuously changing environmental conditions of the kind actually expected in the repository. Consider the simple, but plausible, environmental scenario shown in Fig.2.11-6[7]. Figure 2.11 - 7 shows the behavior of the stochastic variables computed by Eqs. (1)–(4) for this environmental history. Note how the simple environmental changes can cause complex changes in the stochastic variables, and thus the pitting response. This prediction suggests the need for sophisticated models, not just simple empirical laws, to predict the pitting response under realistic conditions. From the time evolution of the stochastic variables, the model can then predict the evolution of the damage function, Fig.2.11 - 8. Note how the complex environmental history has produced a pit depth distribution following an exposure of 115 steps that has a complex

shape compared to the simple shape given in Fig. 2.11 - 5. As described earlier, distributions like those shown in Fig. 2.11 - 8 can be compared with the thickness of the waste package container to assess its integrity. Thus, even for complex environmental histories, the model can predict when the container is first breached by a single pit and then how many pits per unit area will breach the container as a function of time for longer exposures. This information then could be used in a more complete PA model to predict radionuclide release rates.

Deficiencies of the initial model

The pit depth distributions predicted by the initial model for constant environmental conditions, *e.g.* Fig.2.11 - 5, properly exhibit an intermediate peak but incorrectly simulate a nearly symmetrical distribution. Data for a wide range of materials and testing conditions reported in the literature[5,6,12-16] show that such distributions actually have a positive skew. In other words, the peak in the distribution occurs toward small pit depths and a relatively long "tail" is exhibited at large depths, *e.g.* Fig. 2.11 - 3. While this feature of the data may seem to be a minor detail, efforts to more accurately model the tail of the distribution are justified because the deepest pits are the most significant in terms of waste package container degradation.

Related to the lack of a positive skew in the predicted pit depth distributions is the assumption that all stable pits continue to grow, albeit in a stochastic manner, throughout the entire simulation. As discussed in Section 2.11.2, a variety of data suggest that many small pits cease to grow early during exposure, probably due to a lack of available reactants, such as oxygen and electrons. Further, deep pits may cease to grow later in the exposure due to capping or clogging with corrosion products. The initial model could not simulate such behavior.

Despite the fact that pits grow to have a wide distribution of depths, indicating a probabilistic aspect to pit growth, many theories treat pit growth deterministically, typically as a problem in diffusion[17]. (Of course, the applicability of such theories to millimeter-scale pits is debatable.) These diffusion theories and a variety of experimental observations[6,17] suggest that the pit growth rate decreases as the exposure time and pit depths increase. Equation (5) is often used to phenomenologically describe these deterministic aspects of pit growth (for constant environmental conditions):
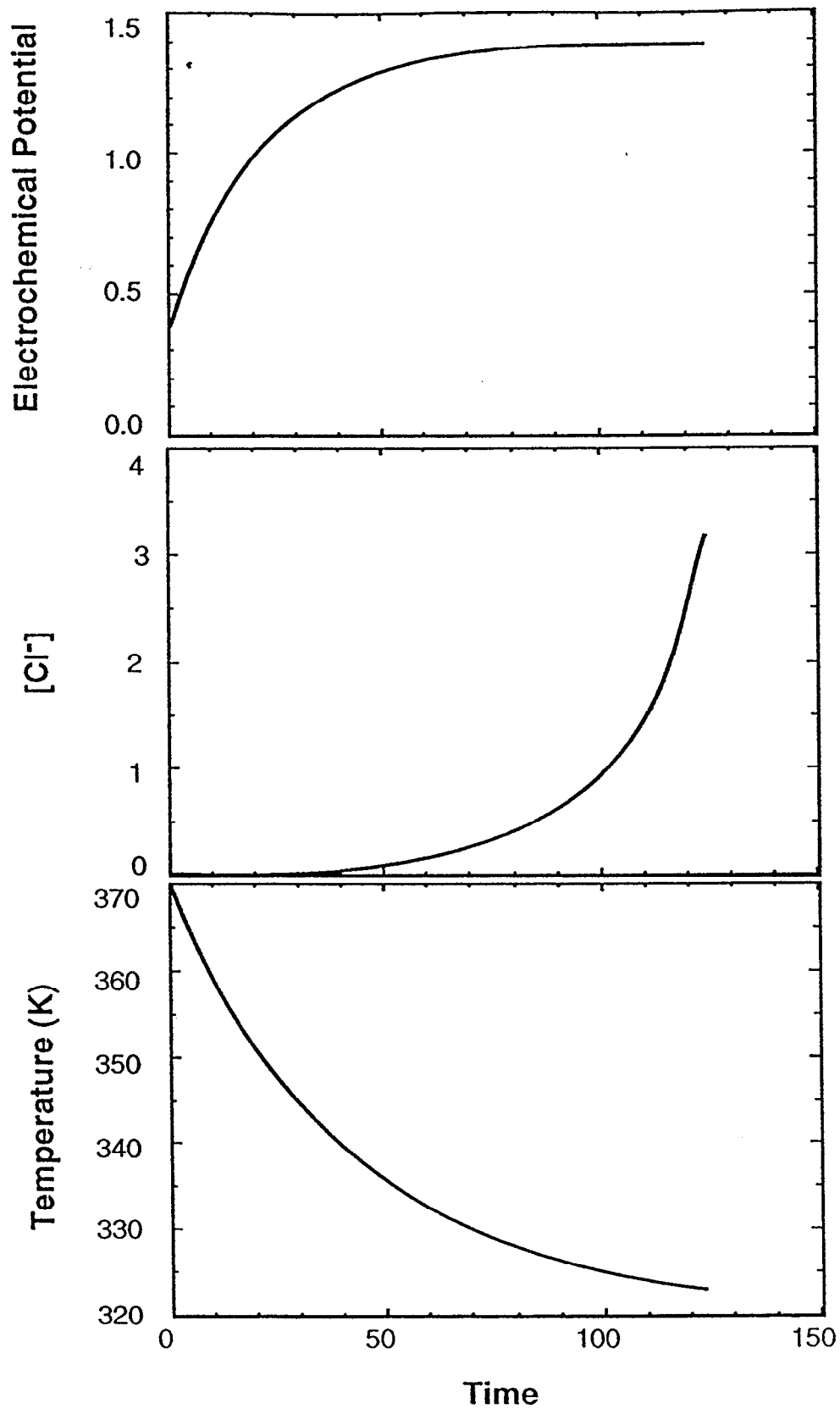
Figure 2.11 - 6. The hypothetical environmental history used to make the predictions given in Figs. 2.11 - 7 and 2.11 - 8. Time, electrochemical potential and chloride ion concentration are in arbitrary units.
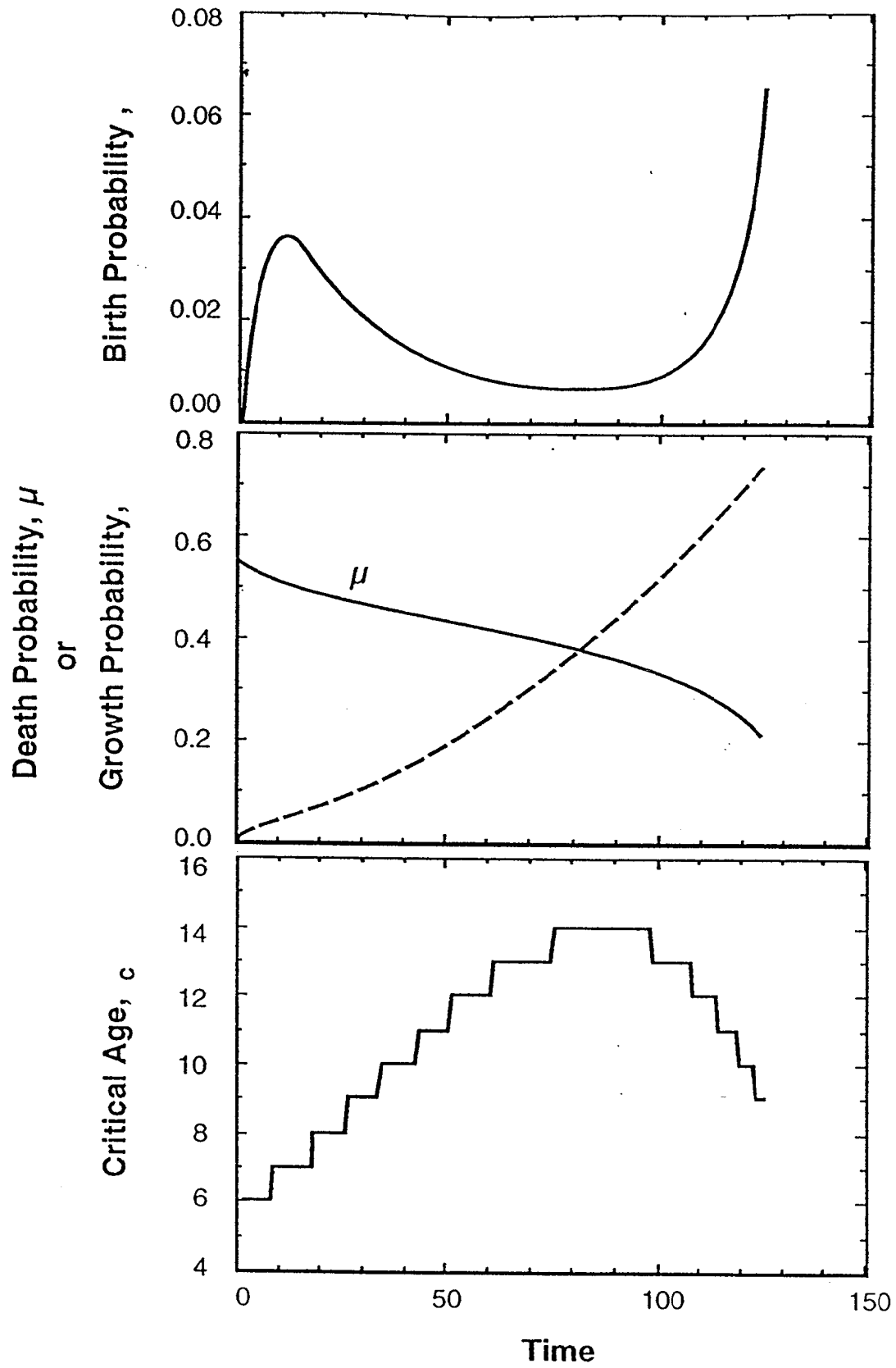
Figure 2.11 - 7. The time dependence of the stochastic parameters resulting from the environmental history given in Fig. 2.11 - 6.

2.11 - 12
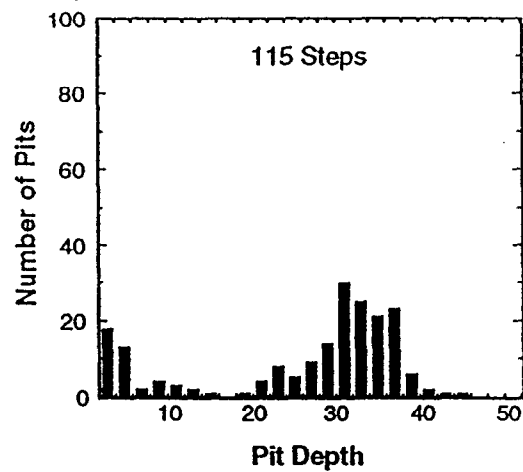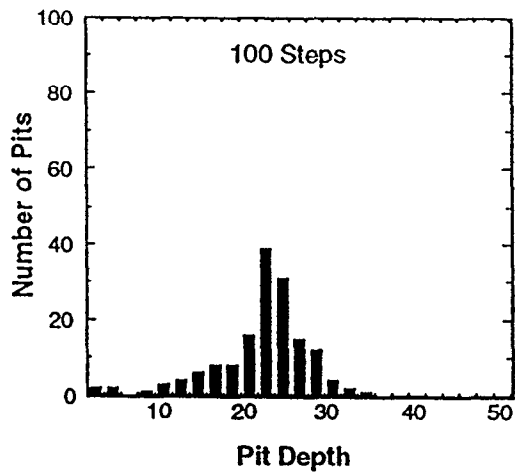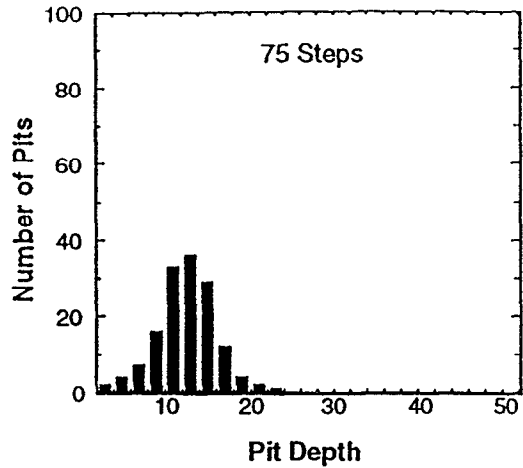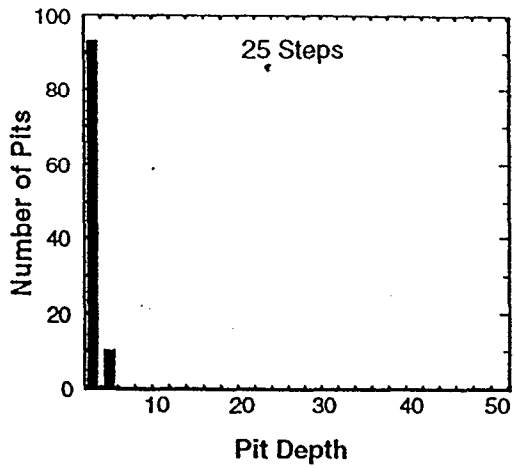
Figure 2.11 - 8. The damage function evolution resulting from the environmental history depicted in Fig. 2.11 -.6. Pit depths are in arbitrary units.

$$d = A t^p \;; p < 1 \;,\tag{5}$$

where d is pit depth, t is exposure time, and A and p are constants. Typically, $p < 1$ with values of 0.3 and 0.5 being quite common. However, the model presented in Section 11.3 predicts that the median and maximum pit depth increase linearly with exposure time for constant environmental conditions. This prediction stems from the assumption that the growth probability, γ, is independent of exposure time or pit depth, and the assumption that pit depth is directly proportional to the computed "age" of the pit[9].

Finally, while the physical basis for modeling stochastic pit initiation is solidly based on the theories and experimental results stemming from several careful investigations, the physical underpinnings of the stochastic pit growth model are more tenuous[7,9]. Therefore, it was desirable to improve the link between the pit growth model and accepted physical theories so that model extrapolations of laboratory data can be made with more confidence.

2.11.4 The Improved Model

Changes to the model

As discussed earlier, experimental evidence suggests that many pits cease to propagate following a limited amount of growth. To accommodate this observation, a new stochastic variable was introduced into the model: the probability that during any given time step a stable pit will *permanently* cease to grow, η. Again, a random number between 0 and 1 is generated at each time step for every growing pit, and if this number is less than or equal to η the growth of that pit is permanently halted.

To account for the nonlinear pit depth increase as a function of exposure time discussed in Section 2.11 - 3, the phenomenological relationship given in equation (5) was incorporated into the model using two different approaches. The first, or "preliminary," approach to including this deterministic aspect of pit growth involved a straight-forward extension of the model described in Section 2.11 -3. The "revised" approach involved a new interpretation of stochastic pit growth and included other changes to make the model more physically realistic.

In the preliminary approach, Eq. (5) was incorporated directly into the model with one slight modification. Instead of representing the exposure time, t is the pit "age," which is less than the actual exposure time for two reasons. First, it takes some "induction" time, τ, to initiate a pit following exposure (Section 2.11 -3). Second, pits are assumed to grow, or "age," stochastically with some probability γ, and may permanently cease to "age" with some probability η; *i.e.* pits do not age during all time steps. Thus, at the end of a simulation the pits have a distribution of "ages," from which the corresponding depths are computed using Eq. (5). Of course, Eq. (5) is not ideal for modeling purposes because it precludes easy treatment of variable environmental histories. However, it was worthwhile to use this equation in combination with the concepts of stochastic pit growth

and permanent growth cessation as a means to begin exploring models incorporating both the deterministic and probabilistic aspects of pit growth.

In the revised model, the use of exposure time as an explicit variable to describe a decreasing pit growth rate, Eq. (5), was eliminated. In addition to precluding the easy treatment of variable-environment exposures, the explicit use of exposure time is physically unrealistic since it is the increasing diffusion distance (*i.e.* pit depth), not exposure time *per se*, which causes the decrease in pit growth rate. The revised model also employs a new approach for simulating the stochastic aspects of pit growth. This approach was motivated by the interpretation of experimental pit depth distribution data by Marsh *et al.*[5]. These investigators suggested that the stochastic variation in pit growth rates stems from the variations in pit morphology and local metallurgical conditions which cause variations in the charge and mass transfer rates from pit to pit. Thus, pits grow continuously but at a variety of rates. The permanent pit growth cessation probability, η, also was included in the revised model.

To incorporate these two new concepts of stochastic pit growth into the model, Eq. (5) can be modified as follows:

$$^kd = {}^kA \, (t - {}^k\tau)^p \; ; p < 1, \tag{6}$$

where in this case t is the actual exposure time and the superscript k is used to distinguish among all the individual pits in the simulation. Note that each pit has its own induction time, $^k\tau$, and its own value of A. The stochastic variation in pit growth rates is simulated by randomly assigning a specific value of ^kA for each pit from a prescribed, possibly nonuniform, distribution. In the analysis performed here, it is assumed that the values of ^kA are distributed according to a normal, or Gaussian, distribution. Taking the time derivative of Eq. (6) and substituting for the quantity $(t - {}^k\tau)$ by inverting Eq. (6) gives an equation for the rate of pit growth that depends only on the depth of the pit, and not on the exposure time. Writing this equation in incremental form with Δt as the time step size gives:

$$\frac{\Delta^{\prime k} d}{\Delta t} = p \left({}^k A \right)^{1/p} \left({}^k d \right)^{p-1/p} , \tag{7}$$

where

$$\Delta^k d = {}^k d_i - {}^k d_{i-1} , \tag{8}$$

and the subscript i denotes the current time step. Thus, at any time step i in the simulation, the increment in pit growth can be written as a function only of the time step size, the pit depth at the previous time step, and the constants ^kA and p:

$$^k d_i = {}^k d_{i-1} + \Delta t \left[p \left({}^k A \right) \right]^{i/p} \left({}^k d_{i-1} \right)^{p-1/p} . \tag{9}$$

Calculations have shown that the pit depth distributions predicted using Eq. (9) are independent of time step size if the proper modifications are made to the input probabilities (e.g., λ, μ, η) to account for a change in Δt [7].

To implement Eq. (9), a method was established for producing random values of $^k A$ from a population that is normally distributed. An algorithm was identified[18,19] that produces random values from the standard normal distribution using a uniform random number generator, such as the one already implemented in the initial Monte Carlo code. Thus, for any value taken randomly from the standard normal distribution, Z, the value of $^k A$ with the corresponding cumulative probability is simply:

$$^k A = \sigma Z + \mu , \tag{10}$$

where σ and μ are the standard deviation and mean of the desired $^k A$ distribution, which are input prior to the simulation.

2.11.5 Model predictions

Figure 2.11 - 9 illustrates the capability of the new model in its preliminary form to simulate the complex time evolution of the pit depth distribution. For this simulation, the probability of initiating a new pit embryo was decreased exponentially with exposure time[7] such that no new pits were initiated for exposures greater than approximately 50 time steps. The parameters affecting the growth of these pits, γ, η, A and p, were chosen arbitrarily and are given in the figure. Following 100 time steps, Fig. 2.11 - 9(a), the distribution exhibits a peak at the lowest depths, followed by a decrease in the number of pits with increasing depth, and then a second local maximum. This gives the backwards "J" shape to the initial part of the distribution noted by Aziz (Fig.2.11 - 3). Experimentally, this portion of the distribution was attributed to the stifling of shallow pits. In the model, this same feature is caused by the permanent cessation of growth for many small pits through the parameter η. As the exposure time increases, the heights of the two peaks decrease somewhat as the distribution broadens, Fig. 2.11 - 9(b). The broad distribution of pit depths, particularly beyond the backwards "J" feature, was attributed by Aziz[6] largely to the randomly varying propagation rates for individual pits. This same characteristic is predicted by the preliminary model largely through the stochastic growth probability, γ. With further increases in exposure time, the two peaks remain stationary and only the deepest pits continue to grow, creating a long "tail" to the distribution, Fig. 2.11 -9(c). This same feature in the data of Aziz, Fig. 2.11 -3, is caused by the eventual stifling of most pits, so that only a few grow to large depths. Consistent with this finding, the growth cessation probability, η, causes most pits to stop growing after 500 time steps. Finally, note in Fig. 2.11 -3 that the maximum pit depth, d_{max}, increases ever more slowly as the exposure time increases. A similar phenomenon is

evident in Fig.2.11 -9. Following 100 time steps d_{max} = 3.5, while after a five-fold increase in exposure time d_{max} has less than doubled to 5.5, Fig. 2.11 -9(c). This prediction results partly from the use of Eq. (5) with p = 0.5. In addition, the rate of increase for d_{max} slows due to the use of η = 0.01. Consider that for an exposure of 500 steps only four of the initial 590 pits are still growing. This implies that the pits which early in the exposure were of maximum depth probably have permanently halted, requiring shallower pits to grow and become the deepest active pits at longer exposures. In summary, the complex pit depth distribution evolution exhibited in Fig. 2.11 - 3 is qualitatively predicted by the new preliminary model through the consideration of both the stochastic and deterministic aspects of pit growth.
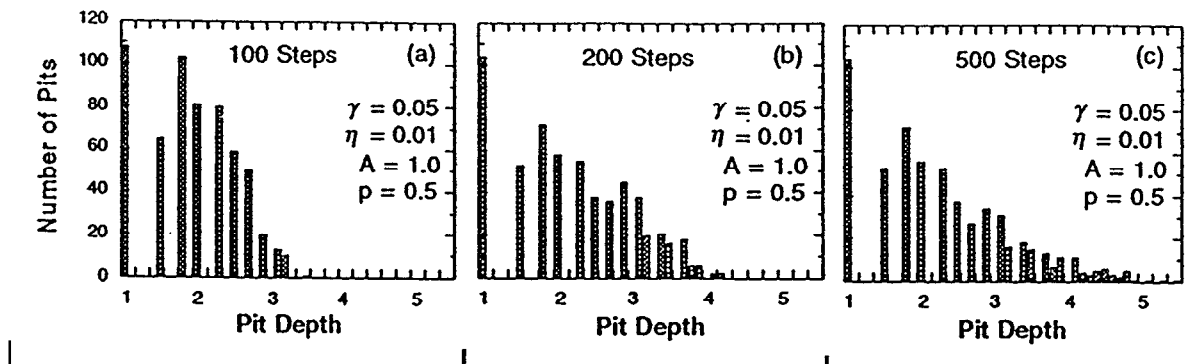
Figure 2.11 -.9. Distribution in pit depths computed by the preliminary model for the growth parameters given in the figure and exposures of: (a) 100 time steps, (b) 200 time steps, and (c) 500 time steps. Pit depths are in arbitrary units.

Of course, the evolution of the pit depth distribution is sensitive to the input parameters affecting pit growth. Calculations have shown that the shapes of the distributions during various stages of evolution are most sensitive to the relative values of the pit growth and cessation probabilities, γ and η. Experimental measurements of the pit depth distribution evolution for materials and environments of interest would be required to quantitatively determine values of γ, η, and the other model parameters.

Figure 2.11 - 10 presents the results of calculations similar to those shown in Fig. 2.11 - 9 but performed using the revised model. A permanent pit growth cessation probability of η = 0.01 and a time exponent of p = 0.5 again were used in these simulations. For relatively short exposure times, e.g. 50 time steps, Fig. 2.11 - 10(a) shows that the distribution of pit depths is nearly symmetric. In the revised model, this distribution in pit depths is largely caused by the distribution in A values, Eq. (10), since each active pit grows during every time step. Note that the backward "J" shape of the distribution at small pit depths present in the data of Aziz[6] and in the calculations presented in Fig. 2.11 - 9 is absent in Fig.2.11 - 10. Fortunately, this aspect of the distribution has little practical importance because the pits are small and don't grow. For intermediate exposures, Fig. 2.11 - 10(b) shows that much of the distribution moves as a body toward larger pit depths so that the distribution remains roughly "bell" shaped. However, it becomes somewhat skewed toward small pit depths with an increasingly long tail at large

depths. Similar features are observed in the data given in Fig.2.11 - 3 for pits beyond the backward "J." Finally, for relatively long exposures, Fig. 2.11 - 10(c) shows that the distribution has become nearly stationary, with only the deepest pits continuing to grow, making the tail at large depths more extensive. Again, this feature of the predictions is qualitatively consistent with that computed by the preliminary model and observed experimentally, Fig. 2.11 - 3.
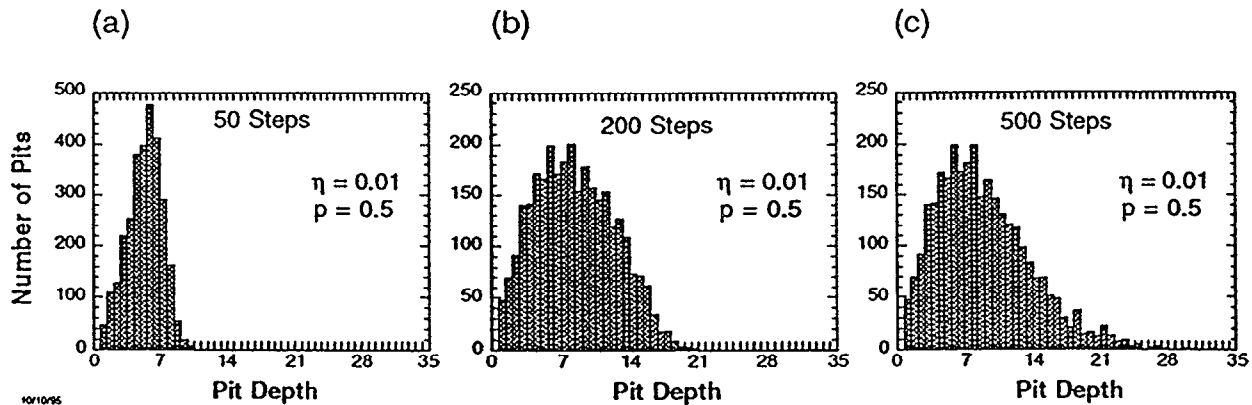

Figure 2.11 - 10. Distribution in pit depths computed by the revised model for the growth parameters given in the figure and exposures of: (a) 50 time steps, (b) 200 time steps, and (c) 500 time steps. Pit depths are in arbitrary units.

The new model, both in its preliminary and revised forms, is capable of simulating the nonlinear dependence of the maximum pit depth on exposure time (for constant environmental conditions). Figure 2.11 - 11 shows an example for the revised formulation using input values of $p = 0.5$ and $\eta = 0.001$. The plot with linear axes, Fig. 2.11 - 11(a), emphasizes the striking decrease in the pit growth rate with increasing exposure time and pit depth. The logarithmic plot in Fig. 2.11 - 11(b) shows that, as expected, the predicted time exponent equals the input value of p, so long as significant permanent pit growth cessation has not occurred. This latter phenomenon is what causes the computed maximum pit depth at 5000 steps to be somewhat below the line for $p = 0.5$.

In summary, the new model is capable of qualitatively reproducing the shapes of the pit depth distributions typically observed experimentally, including the presence of a long tail at large depths. The new model also predicts a nonlinear increase in maximum pit depth with increasing exposure time, consistent with a wide variety of data. These improvements stem from a combination of changes related to the stochastic and deterministic aspects of pit growth. Minor differences exist between the preliminary and revised versions of the new model in the details of their predictions regarding pitting damage (also see Section 2.11 -3). However, neither method is clearly superior to the other in the accuracy of its predictions, though the revised model has a stronger physical basis. Experimental data relevant to modeling pitting corrosion of waste package are required to make a final judgment regarding the suitability of the two methods.

(a)   (b)
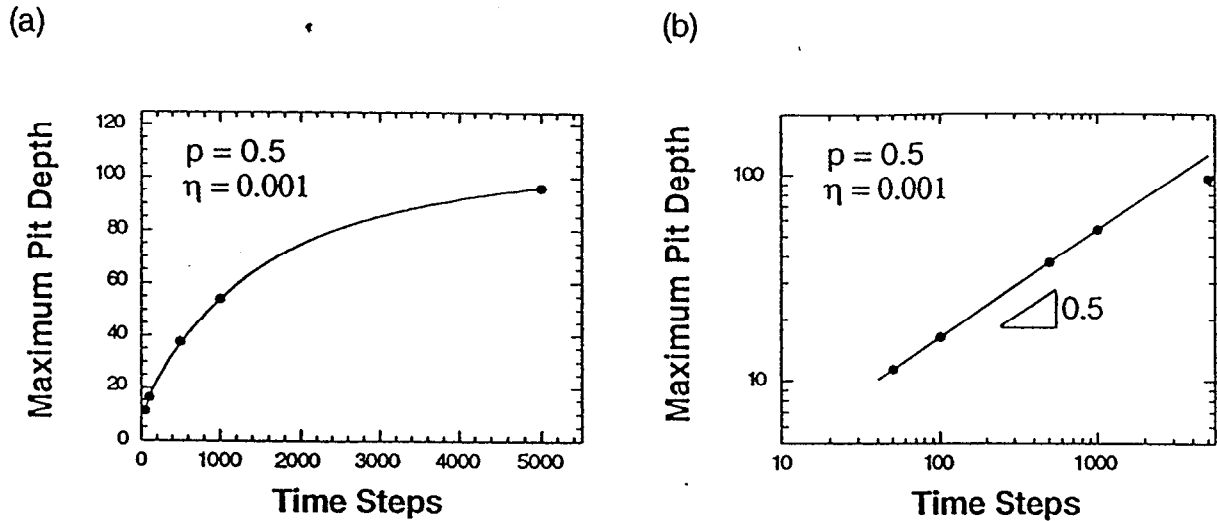
Figure 2.11 - 11. Revised model predictions of the time dependence of the maximum pit depth
are plotted on (a) linear and (b) double-logarithmic axes. Pit depths are in arbitrary units.

2.11.6. Dependence of Maximum Pit Depth on Surface Area Exposed

The method of "extreme-value statistics" (EVS) is commonly employed in the analysis of
experimental pit depth data[6,12-14]. EVS is particularly valuable for predicting the
commonly observed logarithmic increase in maximum pit depth with increasing
specimen or service component surface area[5,6,14,15]. In the context of waste package
container design and performance assessment, EVS analysis of laboratory data collected
on a limited number of small specimens might provide the means to predict the
probability of pits reaching significant depths (e.g. equal to the container thickness) over
the surface of an entire container, or many containers. Such a prediction should be
accurate so long as the extrapolated maximum pit depth exceeds the deepest measured pit
by no more than about a factor of three[6]. Fortunately, this provides an extrapolation in
exposed surface area of up to three orders of magnitude.

Given the utility and wide acceptance of EVS to analyze pitting damage, it is useful to
determine if the stochastic pitting model is consistent with this method. Therefore,
modifications to the Monte Carlo code were made which follow from the actual
experimental procedure described by Aziz[6]. First, an individual test coupon is simulated
by a single model "run" using a unique "seed" value to initiate the random number
generator[7]. Using a single set of input parameters, an N-run simulation is performed in
which each run begins with a different random number seed. This procedure corresponds
to the exposure of multiple, identical test coupons to the same corrosive environment, as
described by Aziz[6]. Analogous to the experiments, the surface area simulated is
proportional to the number of runs in the simulation, since one run represents a unit
surface area. Following each run within a particular N-run simulation, the maximum

the maximum computed pit depth is stored. Once all N runs have been completed, these values are sorted in ascending order, providing "data" analogous to those collected experimentally[6]:

$$d_1^{max} \geq d_2^{max} \; ... \; \geq d_m^{max} \; ... \; \geq d_N^{max} \; .\tag{11}$$

The cumulative probability that the deepest pit is less than or equal to d_m^{max} is then computed from these data as:

$$\Phi_m = m \, / \, (N + 1).\tag{12}$$

These probabilities from the Monte Carlo simulation are then analyzed using the most common expression for the expected extreme-value distribution[6]:

$$\Phi_m = \exp \left[-\exp \left(-y_m \right) \right] ,\tag{13}$$

where y_m is the "reduced variate." The reduced variate is defined as:

$$y_m = \alpha \left(d_m^{max} - u \right) ,\tag{14}$$

where u is the "mode" (highest point of the extreme-value distribution) and α is the "scale" parameter measuring the width of this distribution. The values of u and α are fit to the Monte Carlo "data," Eq. (11), as follows. First, Eq. (13) is solved for y_m, giving:

$$y_m = -\ln \left\{ -\ln \left(\Phi_m \right) \right\} ,\tag{15}$$

where Φ_m is computed from the Monte Carlo results using Eq. (12). For each value of Φ_m, a corresponding y_m is computed from Eq. (15). Then, the data pairs (d_m^{max}, y_m) are plotted on linear axes and fit to Eq. (14) using linear least squares analysis to determine α and u. Extrapolation of this fitted line provides predictions of the probability and exposure time required for the occurrence of a pit of any given depth[6].

(a)

(b)
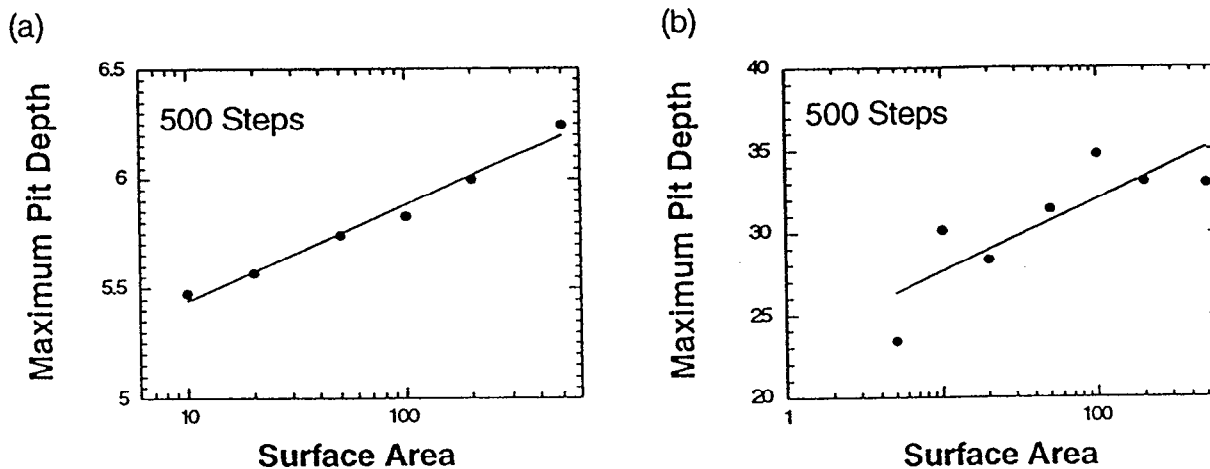
Figure 2.11 - 12. Predictions of the increase in maximum pit depth with increasing exposed surface area from (a) the preliminary model, and (b) the revised model. Pit depth and surface area are in arbitrary units.

In general, the stochastic model is consistent with the EVS theory. For example, it has been shown[9] that the d_m^{max} vs y_m plots predicted by the stochastic model are qualitatively consistent with those measured experimentally in several material–environment systems[6,12-14]. Most importantly, consistent with previous EVS analyses and data, the stochastic model predicts that the maximum pit depth increases logarithmically with increasing exposed surface area, Fig. 2.11 - 12. Thus, by performing simulations with identical input parameters and varying the numbers of runs, the effect of exposed container surface area on the maximum pit depth can be predicted by the stochastic model.

2.11.7 Experimental Validation

Modeling cannot progress without input from experimental data. Experimental data are required to fit the model parameters so that quantitative predictions can be made, to verify the accuracy of the model, to validate the basic model assumptions, and if necessary to re-formulate the model. Ideally, the process of modeling and testing is iterative, with these efforts taking place in parallel so that results from one can drive improvements in the other. Plans for experimental support of the stochastic modeling effort have been made[20-22] but funding constraints have limited the execution of these plans.

To date, the experimental validation of the models has been limited to a few preliminary measurements of the pit depth distribution evolution in Alloy 825. Briefly, these experiments involve exposing flat specimens to an aggressive aqueous environment. A constant electrochemical potential is applied to the specimens to induce relatively rapid pitting under controlled conditions. Each specimen is removed from the aggressive environment following a prescribed exposure time, and examined to measure the

can then be compared with model predictions to test the assumptions and equations used in the model.

Specifically, potentiostatic polarization experiments were performed on 1 cm^2 samples of Incoloy 825 immersed at 90 °C in 5% NaCl aqueous solution containing sulfuric acid (pH ~ 2.6). These data were acquired by the procedures discussed in Section 2.5 of this report. Using optical microscopy, the depth of each pit was measured by calibrated focusing and the pit diameters were measured with a filar eyepiece. (Note that pits with depths less than about 25 μm, of which there were many, were not measured). Examples of the measured pit depth and diameter distributions are given in Fig. 2.11 - 13. These distributions are qualitatively similar to the predicted distributions shown in Fig. 2.11 - 10 for relatively short exposures. In particular, there is a peak in the distributions at an intermediate depth or diameter. However, the long tail in the distribution at large depths (or diameters) that is predicted by the model for long exposures is not observed in the short-exposure distributions given in Fig. 2.11 - 13. Longer time exposures are required to test this prediction of the model. Table 2.11 - 1 gives a summary of the measured pit depth data gathered to date. Although these data are insufficient to draw many firm conclusions, it appears that increasing the applied electrochemical potential, E_{app}, increases the number of pits per unit area. The effects of exposure time and electrochemical potential on pit depths are not yet clear.
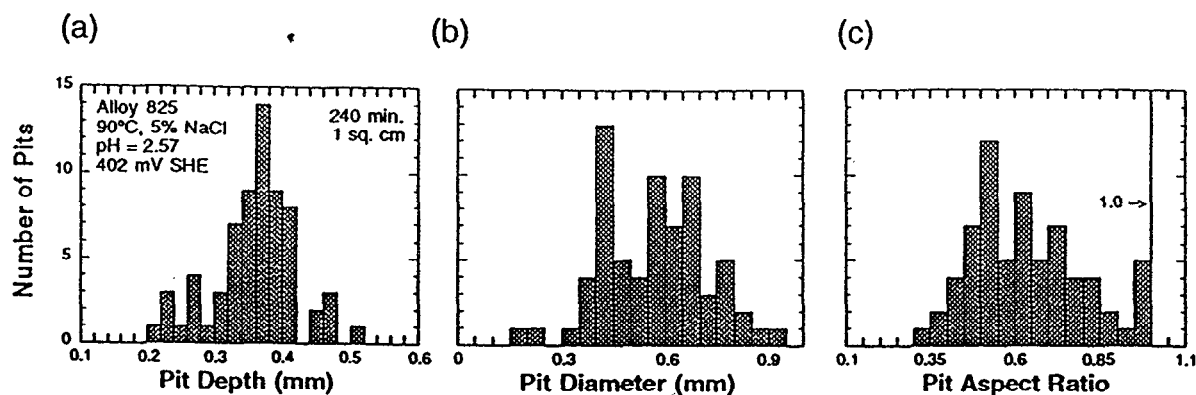

Figure 2.11 -13. Experimental distributions of (a) pit depth, (b) diameter, and (c) aspect ratio for Incoloy 825 immersed for 240 minutes at 90° C in pH 2.57, 5% NaCl solution and polarized at 402 mV SHE. Unpublished data of Henshall and Roy [23].

Table 2.11 - 1. Pit depth distribution data for 1 cm^2 samples of Incoloy 825 immersed in acidified brine (5% NaCl) at 90 °C. Data of Henshall and Roy [23].

E_{app} (mV SHE)	Exposure Time (min.)	pH	Number of Pits	Maximum Depth (mm)	Median Depth (mm)
372	480	2.67	1	0.361	0.361
382	120	2.66	6	0.653	0.449
382	232	2.64	34	0.899	0.621
392	218	2.51	21	0.822	0.681
402	240	2.57	68	0.505	0.363

Figure 2.11 -13(c) shows the distribution in pit aspect ratios, defined as the pit depth divided by the diameter. If the aspect ratio is less than one (broad, shallow pits), automated pit depth measurement techniques may be viable for future work, or the pit diameter could be used as a conservative measure of damage. The data given in Fig. 2.11 - 3(c) reveal that all pits have an aspect ratio less than one for this experiment, though testing under somewhat different conditions revealed aspect ratios of up to 2. Again, more data are required to make a firm conclusion regarding pit aspect ratios in Alloy 825.

2.11.8 Summary and Conclusions on Pitting Corrosion Model

A phenomenological, stochastic model of pit initiation and growth has been developed in support of waste package container design and performance assessment. This model can simulate the time evolution of the distribution in pit depths on a metal surface exposed to an aggressive environment. A review of the initial model revealed it to be capable of realistically simulating stochastic pit initiation. This model also includes simple phenomenological relationships describing the environmental dependence of the stochastic parameters. Therefore, it can simulate pit initiation and growth under variable-environment histories, such as those anticipated in the repository.

Recent improvements to this model have focused on pit growth and the time evolution of the pit depth distribution. These improvements include the capability to model permanent pit growth cessation, methods to deterministically predict a nonlinear increase in maximum pit depth with increasing exposure time (for constant environmental conditions), and a more physically realistic treatment of stochastic pit growth. These improvements have resulted in predictions that are qualitatively more consistent with a variety of experimental data in the literature, for example the development of pit depth distributions with a positive skew and a long tail at large pit depths. Further, this model has been shown to be consistent with extreme-value statistical methods for predicting the logarithmic increase of maximum pit depth with increasing exposed surface area.

A critical need has been identified for generating experimental data for candidate container materials exposed to repository-relevant environments. These data are required to quantitatively assess and further develop the model. Preliminary pit depth distribution data for Alloy 825 (Incoloy 825) have been presented. These data are qualitatively consistent with stochastic model predictions of a peak in the pit depth distribution at intermediate depths, and show that this alloy is susceptible to pitting under aggressive conditions.

2.11.9 Future Work on Modeling the Performance of the Inner Barrier Material

A waste package degradation model abstraction workshop was held in January 1997 in preparation for the total system performance assessment (TSPA) models being developed for the viability assessment (VA) in 1998. As a result of that workshop, some restructuring of the models that would describe the performance of the inner barrier material is proposed. The approach outlined in the Metallic Barriers SIP proposed that models be developed for each mode of corrosion and that these individual models be "summed" (in proportion to the extent that each corrosion mode would be operable) to establish a damage function for the inner barrier. In rethinking that approach, it appears that several corrosion modes can be operable simultaneously and interactively, and thus these modes should be modeled as coupled processes as well.

Corrosion of the inner barrier is sequential to corrosion and penetration of the thick outer barrier material. Corrosion products from the extensive amount of material penetrated will significantly condition the water. Thus, the environment that the inner barrier is exposed to is very much altered from the geochemically conditioned water that was significant in initiating the outer barrier corrosion.

Assuming a carbon steel outer barrier, copious amounts of iron-rich corrosion products will be formed, and these are expected to be principally in the +3 oxidation state. Depending on how the two barriers are fabricated, there may or may not be space between them that can act as a creviced region. The combination of a crevice and ferric ions is aggressive toward some of the candidate materials for the inner barrier, causing attack in the crevice and possibly pitting attack on areas away from the crevice. In addition, the galvanic contact between the two electrochemically dissimilar metals imposes an electrolytic current between the metals that adds other modes to consider, at least while some of the outer barrier remains. Hydrogen is generated on surfaces, particularly at low pH areas in the crevice. Insoluble corrosion products from the outer barrier also act to restrict diffusion of chemical species and promote crevice effects, and additionally provide a wedging effect as a source of localized stress. Thus, stress corrosion cracking and hydrogen embrittlement are additional potential corrosion modes. Lastly, microbiological activity can acerbate these effects. Iron-oxidizing bacteria, acid-producing bacteria, and anaerobic kinds of bacteria, such as metal reducing and sulfate reducing types, can also affect the local chemistry and the corrosion attack.

While corrosion models have been developed for individual corrosion modes (like the work described in the previous sections for pitting corrosion), combining models and treating the fundamental reactions (anodic dissolution, mass transport, cathodic reduction) as they apply on each metal and in the creviced and uncreviced regions as multiple coupled processes is also necessary to provide an integrated process corrosion model for abstraction and prediction of the performance. This is obviously a chemically complex case, but this proposed approach did receive a positive response at the workshop, and it will be pursued.

References to Section 2.11

1. H. Fontana and N. Greene, "Corrosion Engineering", 2nd Edition, McGraw-Hill, pp. 39-57 (1967).
2. D. Shoesmith, "Modelling to Predict the Corrosion Behavior of Nuclear Waste Containers," presented at the *Forum for the Use of Nickel Alloys for Radwaste Containers*, Tucson, AZ, Feb. 22-23 (1995).
3. R. W. Andrews, "TSPA-95 Objectives and Approach: Focus on Waste Packages/EBS Conceptual Models," presented at the NWTRB Full Board Meeting, Las Vegas, NV, Apr. 19-20, (1995).
4. T. Shibata and T. Takeyama, "Stochastic Theory of Pitting Corrosion," *Corr.* 33 (1977) 243-251.
5. G. P. Marsh, I. D. Bland, and K. J. Taylor, "Statistical Study of Pit Propagation in Carbon Steel Under Nuclear Waste Disposal Conditions," *Br. Corros. J.* 23, 157-164 (1988).
6. P. M. Aziz, "Application of the Statistical Theory of Extreme Values to the Analysis of Maximum Pit Depth Data for Aluminum," *Corros.* 12, 495-506 (1956).
7. G. A. Henshall, "Modeling Pitting Corrosion Damage of High-Level Nuclear-Waste Containers using a Stochastic Approach," *J. Nucl. Mater.* 195, 109 (1992).
8. G. A. Henshall, "Stochastic Modeling of the Influence of Environment on Pitting Corrosion Damage of Radioactive-Waste Containers," in *Scientific Basis for Nuclear Waste Management: XVIII,* T. Murakami and R.C. Ewing, eds., MRS, Pittsburgh, PA, p. 679-686 (1995).
9. G. A. Henshall, "A Phenomenological Approach to Simulating the Evolution of Radioactive-Waste Container Damage Due to Pitting Corrosion," in *Scientific Basis for Nuclear Waste Management: XIX,* W. M. Murphy and D. A. Knecht, eds., MRS, Pittsburgh, PA, pp. 613-619 (1996).
10. D. E. Williams, C. Westcott and M. Fleischmann, "Stochastic Models of Pitting Corrosion of Stainless Steels: I. Modeling of the Initiation and Growth of Pits at Constant Potential," *J. Electrochem. Soc.* 132, 1796-1804 (1985).
11. D. E. Williams, C. Westcott and M. Fleischmann, "Stochastic Models of Pitting Corrosion of Stainless Steels: II. Measurement and Interpretation of Data at Constant Potential," *J. Electrochem. Soc.* 132, 1804-1811 (1985).
12. J. E. Strutt, J. R. Nicholls, and B. Barbier, "The Prediction of Corrosion by Statistical Analysis of Corrosion Profiles," *Corros. Sci.* 25, 305-315 (1985).
13. H. F. Finley, "An Extreme-Value Statistical Analysis of Maximum Pit Depths and Time to First Perforation," *Corros.* 23, 83-87 (1967)

2.12 Materials Recommendations

The Metal Barrier SIP identifies three activities (E-20-90, -91, and -92) associated with recommendations of materials for the multi-barrier waste package container. These include the development of selection criteria, the selection process itself, and development of specifications for the selected material. Work is proposed to work closely with the waste package design group in these activities. In most instances, the selection criteria divide into a group of engineering considerations (cost, fabricability, weldability, previous experience) and performance considerations (mostly corrosion properties, but some interest in metallurgical stability and mechanical properties).

The updated candidate list for the waste package container, as well as those for the other EBS materials, was published in 1995 [1]. Since that time, work has not progressed at LLNL on quantifying selection criteria. Recently, the waste package design team has requested a re-examination of Alloy 625, also known as Inconel 625 (UNS N06625), a Ni-Cr-Mo, alloy as a candidate material for the inner barrier. Their request was made on the basis of perceived improved weldability of Alloy 625 compared to other candidate alloys in this class of material. A report from the design team is in preparation that addresses their reasons for including it among the candidates. Alloy 625 contains 8 - 10% Mo, compared to 12.5 to 14.5% Mo in Alloy C-22, 14 to 17% Mo in Alloy C-4, 6 to 8% Mo in Alloy G-3 and only 2.5 - 3.5 % Mo in Alloy 825. Thus, from a testing point of view, addition of Alloy 625 provides an intermediate composition that will be useful. Plans are being made to acquire test specimens of this material in several configurations for the different testing activities described in previous sections of this report. While Alloy 625 is often used in corrosive environments, some of the minor alloying additions improve its strength at somewhat elevated temperatures. This may cause some concerns with the long term phase stability, and this will be evaluated along ageing studies proposed for this (and the other Ni-Cr-Mo) candidate materials as part of Metal Barrier SIP activity E-20-67.

Reference for Section 2.12

R. D. McCright, Updated Candidate List for Engineered Barrier Materials, UCRL-ID-119442 (October 1995)

3.0 Basket Materials in Spent Fuel Waste Packages

(input to this section of the report was provided by Richard Van Konynenburg)

3.1 Functions of Waste Package Basket Materials

Evaluation of materials that could be fabricated into baskets for spent fuel waste packages was begun in FY-94. The basket provides internal partitioning between spent fuel assemblies. The three specific functions of the basket is to provide:

1. Structural support
2. Heat conduction
3. Nuclear criticality control

The design of the internal structure in nuclear spent fuel waste packages is evolving. One design uses square tubes arranged in a close-packed array, each tube incorporating neutron absorbing material. Future designs may make use of flux traps (spacing apart of spent fuel assemblies to reduce nuclear reactivity) and may have differing quantitative needs for mechanical integrity, strength, thermal conductivity, and neutron absorption. However, these properties will continue to be the important ones. Because of the very large waste packages designed to hold multiple assemblies (for example 12 to 24 PWR assemblies), the long-term criticality control function takes on great importance. The heat conduction function is primarily of interest in the early part of the repository operation and containment period.

Evaluation of the basket material is complicated by the fact that some spent fuel is expected to arrive at the repository already canistered from operations at the reactor site or, possibly, at some interim storage facility. It is an important repository operational question whether these spent fuel packages can remain intact and be placed inside the waste package for disposal or whether these packages will need to be re-opened and the spent fuel assemblies (and any structural and criticality control hardware) then placed inside the waste package. Other spent fuel is expected to arrive at the repository site in an uncanistered form, and will be placed within a basket grid and within a disposal container at the repository surface facility. Thus, many aspects of the design and material selection for the internal criticality control structure depend on co-operation between individual organizations in the waste management operation.

A Scientific Investigation Plan (SIP) to evaluate basket materials was written, as SIP-CM-02 in March 1995, and five general activities were described. The five are: (1) Literature Review and Analyis, (2) Scoping Experiments, (3) Long-Term Corrosion and Properties Evaluation, (4) Performance Modeling, and (5) Materials Recommendations. This SIP generally parallels the efforts and arrangments of activities of the Metallic Barrier SIP. The results of the scoping tests on candidate materials are described in the next sections.

3.2 Choice of Environment for Scoping Corrosion Tests

The design environment inside intact canistered and uncanistered spent fuel waste packages is intended to be dry, inert gas. Achievement of this environment will depend on success in drying, pumping out, backfilling, and sealing these canisters and packages. However, given the likelihood of eventual containment failure, most likely by corrosion of the waste package containers, the environment inside such a breached container must be considered. One of the current design assumptions[5] is that containment could fail for as many as 1% of the waste packages in the first 1,000 years. The federal regulation establishing the requirement for criticality control (10 CFR Part 60.131(b)(7))[6] does not explicitly specify a time limit, but the current design assumption[5] is that criticality control will be required for 10,000 years. For comparison, the half-lives of the dominant fissile nuclides in the spent fuel are 24,100 years for ^{239}Pu and 704 million years for ^{235}U.[7]

When containment failure occurs, gaseous and liquid species in the surrounding environment could enter the waste packages. Since inundation by water is considered unlikely for the repository horizon at Yucca Mountain,[8] the most probable species that would enter are the constituents of moist air. If moist air were the only intruder, repository criticality would not be of concern. However, prudence dictates that we anticipate that significant quantities of liquid water might enter at least some of the packages. In order for this to occur, it would have to take place by liquid transport via fracture flow rather than by evaporation and condensation onto the packages, because the packages will always be at higher temperatures than their environment, because of nuclear decay heat. Liquid transport from the geologic environment would mean that the solutes present in vadose water would also enter the packages. An example of the ground water present in the rock of the repository horizon (Topopah Spring tuff) is that obtained from Well J-13. Its analysis is shown in Table 1.[9]

One of the current design assumptions[5] is that the centerline temperature in the waste packages containing spent nuclear fuel will not exceed 350°C. Because the pressure in the repository will be about one atmosphere, liquid water cannot be present in a failed waste package until its temperature has dropped below about 100°C, depending on the presence of hygroscopic salts, some of which can raise this temperature limit somewhat.

It is not possible to accurately predict when a given waste package will fail, what the temperature will be at that time, and when liquid water might be available to enter a failed package. It is also therefore not possible to accurately predict what the radiation dose rates will be at the time these events occur. In the presence of these uncertainties, a variety of scenarios are envisioned. Consideration of worst cases is appropriate so that modeling and prediction of degradation rates can be extrapolated to expected conditions.. Perhaps the worst case would be early containment failure, while there is still significant heat output from strontium-90 and cesium-137. In this case only humid atmospheric gases could enter the package initially, because the temperature would be above the boiling point.

In this worst case the temperature might be sufficiently high and the oxygen sufficiently plentiful that the spent fuel cladding would fail, and the UO_2 fuel would be oxidized to U_3O_8, which would result in splitting of the cladding and crumbling of the pellets into powder. In this case the gases and later, liquids entering the waste package would be exposed to alpha and beta radiation in addition to the gamma radiation that would be emitted by intact fuel, and the dose rate could be in the range of hundreds of grays per hour.[10,11] Upon cooling below the boiling point, in the worst case liquid vadose water could then enter the package, bringing in its solutes. This case would involve significant radiolysis.

As can be seen in Table 3.1 J-13 well water contains 129 mg/L of bicarbonate, and has near-neutral pH. If water having this composition entered a failed waste package at near current ambient temperatures, the bicarbonate would initially buffer the pH near neutral. However, if sufficient acid were produced by radiolysis, the buffer would be overcome, and the pH would drop.

In less extreme scenarios, containment would be maintained until sufficient cooling occurred that the UO_2 would not oxidize and crumble. The air and water that entered would then be subject only to gamma irradiation, and the dose rates would be much lower because of decay of 30-year half-life ^{137}Cs, the dominant gamma emitter. In such a case, radiolysis might not be a significant factor. Because of the uncertainly involved in predicting the course of events, scoping tests were performed using a corrosion environment that contains significant concentrations of the chemical species known to be produced by irradiation of an air--water system, that are also known to be important in corrosion. Reviews of radiation chemistry in moist air and moist air--water systems have been presented.[12,13]

Barkatt et al.[14] reported the results of experiments in which an air--deionized water system was gamma-irradiated at room temperature. The observed radiolytic species were nitric, formic, and oxalic acids and hydrogen peroxide. For a total dose of 6.2×10^4 Gy over a 3-day period at 25°C, the concentrations of these species, respectively, were 78, 46, 30, and 16 micro- moles per liter. This dose is orders of magnitude smaller than what could be reached in an early-failing waste package over a period of hundreds of years. The nitric acid is formed by radiolysis in the gas phase, and condenses into the liquid phase. The hydrogen peroxide is formed in the liquid phase. The formic and oxalic acids are formed from dissolved CO_2 in the liquid phase, but only after the pH has been lowered to about pH 4 by nitric acid production.[13] In order to be able to perform scoping tests conveniently, at relatively low cost, and in a short time, the effects of irradiation are simulated by ordinary chemical means. In so doing, any effects of transient, free radical effects are ignored. The concentrations of radiolytic species are much higher than those observed by Barkatt et al., to make possible a batch-type experiment that would show observable results in a short time, and to account for the fact that the repository time-scale of interest is several orders of magnitude longer and the resulting worst-case doses are orders of magnitude higher than those in the Barkatt et al.

.In addition to radiolytic species, chloride ion is included, since it is present in J-13 well water and is known to be important in corrosion of many metals. The corrosion medium is formulated as a buffered-pH solution. The presence of the weak acids (formic and oxalic) with pK values of 3.75 and 4.27, respectively, at 25°C,[15] lends itself to this, and the establishment of a buffer provides a controlled-pH environment so long as it is maintained, and an indicator of significant chemical reaction if it is overcome.

The test temperature was comfortably set below the boiling point to facilitate control, but high enough to produce significant reaction rates. The repository temperatures will span a range from well above boiling down to ambient over the course of time.

3.3 Selection of Candidate Basket Materials

Ideally, one would like to have a single material that could perform all the functions listed above at reasonable cost and with good long-term corrosion performance. However, as is often the case, these various requirements are not satisfied by a single substance, and compromises must be made. For structural support, metals are preferred, and in particular those that have significant strength at the peak temperature of 350°C. High thermal conductivity would suggest aluminum or copper, of the commonly used metals. Chemical elements with high neutron absorption cross sections include lithium, boron, silver, cadmium, gadolinium (and other lanthanides), and hafnium. Materials best able to withstand the projected corrosion environment would include stainless steels, high-nickel alloys, zirconium alloys, and some ceramics. Of the metals mentioned here, aluminum and copper are the least costly. Of the elements with high neutron absorption cross sections, the least soluble in water over a wide pH range is hafnium.

In the presence of these conflicting properties and requirements, a wide variety of candidates were chosen, taking into account the functions of the basket, past experience with materials in similar applications (reactor control rods and neutron absorbers for pool storage of spent fuel, shipping casks, and neutron shielding),[16-18] the requirement for "reasonable" cost,[19] and the need for good corrosion performance. Candidates under consideration by MPC designers were included, as were some developmental materials and some ceramics based on naturally occurring minerals, expected to have high durability under repository waste package conditions.

The candidates that were tested are listed in Table 3.2 The aluminum- and copper-based materials provide the high thermal conductivity of the base metal and incorporate a form of boron for neutron absorption. Since boron exhibits very low solid solubility in both aluminum and copper, it is present as a dispersed phase. In the case of aluminum and its alloys, addition of boron produces borides, namely AlB_2 and others. In the case of alloying with copper, boron exists as the element. In both aluminum and copper, boron can also be incorporated as boron carbide. Samples representing all of these approaches have been included. Boral™ and Boralyn™ are commercial products. The others are developmental. The "A•B"™ material was originally developed for light armor applications.

The boron-alloyed stainless steels are commercial products. The Böhler material is melted and rolled, and contains the boron as elongated precipitates of mixed metal borides. The Neutrosorb PLUS™ is made by a powder metallurgy process, and its mixed metal borides are more nearly spherical in shape, more uniform in size, and more homogeneously distributed. In both cases, the borides are chromium- and iron-rich, with a small amount of nickel, as determined by scanning electron microscopy--energy dispersive x-ray specroscopy (SEM-EDS).

The Zircadyne 702™ is a commercial product composed of essentially pure zirconium, but including the hafnium that occurs naturally in the ore with zirconium. Hafnium is a good neutron absorber, and is separated from the zirconium when the latter is used to make zircaloy cladding for reactor fuel. However, leaving the hafnium in would be beneficial for a basket material, and the cost of the zirconium is actually lower if the separation is not performed and the hafnium remains.

Boron carbide and hafnium oxide samples were tested to determine the dissolution of these neutron absorbers as bulk ceramic materials. The yttria is added to the hafnium oxide to stabilize the high-temperature tetragonal crystal structure. Gadolinium is a strong neutron absorber, and it was incorporated as monazite (gadolinium phosphate) because of the known chemical durability of natural monazite. Zircon and zirconolite were tested as hosts for hafnium because of their known durability in the natural state as well.

3. 4 Description of Scoping Corrosion Tests

The vessels used were Pyrex™ 1000-ml three-neck flasks (see Fig. 1). One port was fitted with a Pyrex condenser to capture evaporated water and return it to the vessel. A second port was fitted with a thermometer. The third was used for filling and was capped with a Pyrex plug. Teflon™ seals were used, with no grease. Glassware was cleaned before the tests by rinsing with 10% sodium hydroxide solution, followed by rinsing with 1 M nitric acid, followed by rinsing with distilled water.

The composition of the corrosion medium was intended to be as follows:

> 0.01 M formic acid (methanoic acid, $HCOOH$)
> 0.01 M sodium formate ($NaCOOH$)
> 0.02 M sodium oxalate ($Na_2C_2O_4$)
> 0.01 M nitric acid (HNO_3)
> 0.01 M sodium chloride ($NaCl$)
> 0.01 M hydrogen peroxide (H_2O_2)
> in distilled water

With this formulation, the hydrogen ion from the strongly ionizing nitric acid will associate with about half of the oxalate to form oxalic acid, and the formic and oxalic acids, together with their salts, will buffer the pH. This solution was used, as intended,

for all but samples #1 through 5. For samples #1 through 5, the formic acid was inadvertently left out of the solution. Although formate was still present, the pH buffering was not as robust for these samples, as evidenced by comparison of the final pH of solution #5 (the first control) with that of solution #28 (the second control).

Approximately 700 ml of solution was used in each test vessel. Vessels were weighed before and after filling and at the end of tests to determine water loss. Each vessel was heated using a heating mantle, in which its bottom was nested. Temperature control was accomplished by manual adjustment of Variac transformers. The temperatures were maintained at $90\pm5°C$ for the test duration of 96 hours, except for sample #19, which was terminated at 90 hours, after extensive corrosion. The thermometers were calibrated in an ice bath and in boiling distilled water. The solutions were kept mixed by free convection, driven by the heating mantles. The pH of each solution was measured at room temperature before and after the test, using a calibrated pH meter. For solutions #1 through 5, the initial pH was pH 4.06. For the others, it was pH 3.80 to pH 3.82.

Table 3.2 - Candidate Basket Materials Tested

- Aluminum (Alloy 1100) with dispersed aluminum boride (Alboron™)

- Aluminum (Alloy 6061) with dispersed aluminum boride (Alboron™)

- Aluminum (Alloy 6351) with dispersed aluminum boride (Alboron™)

- Aluminum with finely dispersed boron carbide (Boralyn™)

- Aluminum - boron carbide composite (Boral™)

- Aluminum oxide - boron carbide ceramic (A•B™)

- Copper with dispersed elemental boron

- Copper with dispersed aluminum oxide (Glidcop A-15™) and elemental boron

- Copper with dispersed boron carbide

- Copper with dispersed aluminum oxide (Glidcop A-15™) and boron carbide

- Austenitic stainless steel (type 304L) (control without boron)

- Austenitic stainless steel with dispersed borides made by melting (Bohler Bros. A976™)

- Austenitic stainless steel with dispersed borides made by powder metallurgy—base metal (Carpenter Technology Neutrosorb PLUS™)

- Austenitic stainless steel with dispersed borides made by powder metallurgy—welded (Carpenter Technology Neutrosorb PLUS™)

- Zirconium—hafnium (Teledyne Wah Chang Zircadyne 702™)

- Boron carbide (hot pressed)

- Hafnium oxide with 5 wt. % yttrium oxide (hot pressed)

- Gadolinium phosphate (monazite, hot pressed)

- Zirconium silicate containing hafnium (zircon, hot pressed)

- Calcium zirconium titanate containing hafnium (zirconolite, hot pressed)

Note: most of the metallic materials were supplied by the manufacturers noted in the description. The ceramic materials were hot pressed in our own laboratories.
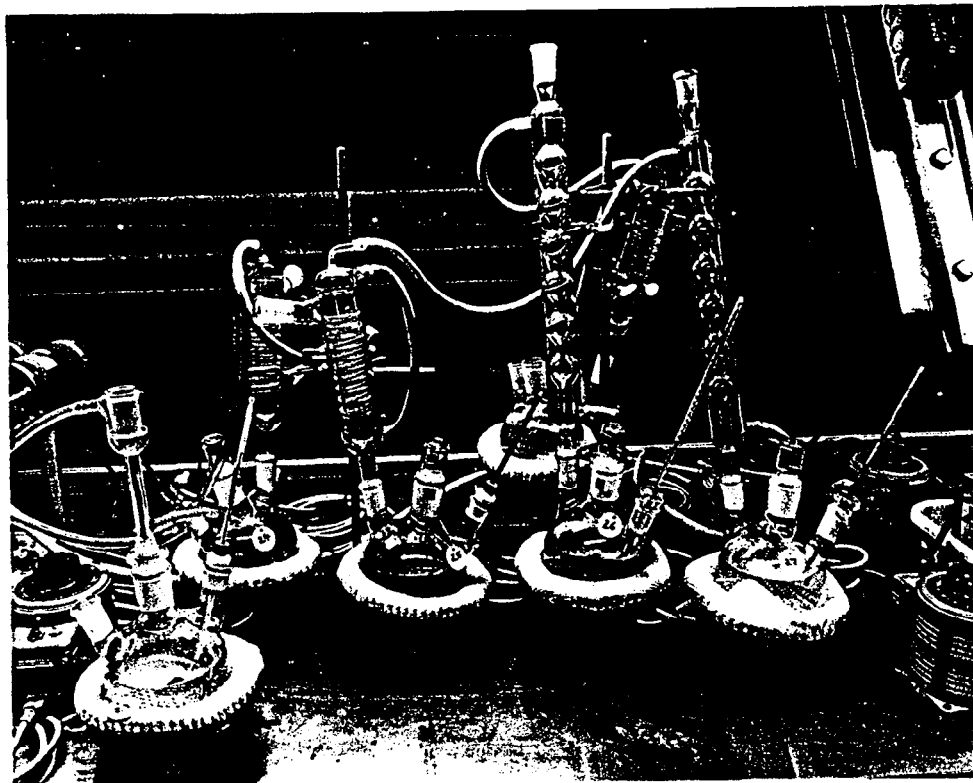
Figure 3.1. Corrosion Test in Progress

Unfiltered samples of each solution were chemically analyzed before and after the tests, using ion chromatography and inductively-coupled plasma optical emission spectrometry (ICP-OES). Iodometric titration was performed to determine peroxide, but suffered from interferences in some of the solutions. Observed precipitates were analyzed by X-ray diffraction. Metallography and SEM-EDS were performed on some of the samples initially. Each sample was sanded smooth using 600-grit paper and then was ultrasonically cleaned using acetone, methanol, and distilled water in succession. Samples were weighed before and after the tests (after cleaning in the case of metal specimens except the stainless steels and alloy 702) using a calibrated electronic balance with a precision of ± 1 mg. Samples were examined by metallograph after cleaning. Cleaning of the metal samples was performed according to ASTM Standard Practice G1-90.[20]

3.5 Test Results and Discussion

During the tests, it was observed that for all four copper-based samples, the solutions turned bright blue during initial warmup. For the welded Neutrosorb PLUS sample (#19), the solution initially became yellow-green in color, then abruptly changed to turbid brown. Then a brown precipitate dropped out over a period of hours, and the solution was clear again. The solutions remained clear for all the other samples. The aluminum metal-based samples and the copper-based samples evolved gas bubbles, indicating hydrogen evolution.

The corrosion and pH results are given in Table 3.3, and the final solution compositions are shown in Table 3.4. Weight losses of the solutions were found to be less than 4%. Photomicrographs of samples #3 and 19 are shown in Figs. 2-3. XRD analysis of the precipitate from sample #19 indicated hematite (Fe_2O_3) as a major constituent and halite (NaCl) and sodium oxalate ($Na_2C_2O_4$) as minor constituents.

Considering the first control solution (#5), it can be seen that the initial concentrations of formate, oxalate, nitrate, and chloride were essentially preserved, and the pH moved from pH 4.06 initially to pH 4.73 at the end. Boron pickup from the Pyrex vessel amounted to only 0.22 mg/ml or 2.0×10^{-5} M. As noted earlier, the formic acid was inadvertently left out of solutions #1 through 5, which include the first control. Had it been put in as intended, the initial pH would have been pH 3.80 to pH 3.82, and the final pH would have been pH 3.88, as observed for control solution #28. Considering the two control solutions together, the analyses demonstrate that the solution is sufficiently thermally stable for the time period used, that the pH buffer is effective for the time and temperature used, and that boron dissolution from the Pyrex vessels is minimal. For the sample in the first batch that did not undergo significant corrosion (#1), the omission of formic acid in the first batch is not significant because the pH buffer was not seriously challenged, and formic acid is not a chelating agent. For those that did corrode significantly (#2-4), one might expect even more corrosion if the buffer had been more robust.

Table 3.3. Corrosion and pH Results

Sample No.	Sample	Mass Loss (g)	Corrosion Rate (mm/y)[A]	Final pH
5	Control #1	-	-	4.73
2	1100Al-4.3 wt.%^{10}B	0.070	1.9[B]	7.13
8	6061Al-0.6 wt.% ^{10}B	0.124	2.4[B]	6.85
9	6351Al-0.5 wt.% ^{10}B	0.088	2.6[B]	7.03
7	Boralyn	0.133	1.6[B]	6.80
3	Boral	0.061	1.8[B]	7.32
23	A•B	0.025	0.60	4.08
24	Cu-1.5 wt.% B	0.263	2.4	4.14
25	GlidCop-1.5% wt.% B	0.240	2.0	4.14
4	Cu-1.8 wt.% B$_4$C	0.146	1.8	5.11
10	GlidCop-1.8 wt.%B$_4$C	0.088	1.4	4.07
20	304L SS	0.003	0.01	3.99
26	Bohler A976 SD	0.011	0.041	4.16
22	Neutrosorb PLUS-base	0.007	0.06	4.49
19	Neutrosorb PLUS-welded	0.125	0.88[B]	6.37
1	Zircadyne 702	0.003	0.06	4.26
14	B$_4$C	0.001	0.05	3.88
18	Hf0$_2$-5 wt.% Y$_2$0$_3$	0.000	0.00	3.88
16	Gd-monazite	0.003	0.2	3.88
17	Zircon-5 wt. %Hf0$_2$	0.002	0.08	3.88
13	Zirconolite-5 wt.%Hf0$_2$	0.029	1.2	3.88
28	Control #2	-	-	3.88

[A] Yearly rates are intended for comparative purposes only. They are linearly extrapolated from 96-hour tests.

[B] Pitting was observed on these samples. Rates do not represent uniform corrosion.

Table 3.4. Final Solution Compositions
(in units of 10^{-4} M)

Sample Number	Formate	Oxalate	NO_3^-	Cl^-	B	Al	Si	P
5	91	190	93	93	0.20	<0.03		
2	93	200	90	94	4.39	31		
8	170	200	80	90	0.98	52		
9	150	180	90	90	0.40	38		
7	170	200	70	90	0.23	52		
3	97	190	89	92	0.90	31		
23	181	199	98	96	4.12	1.35		
24	199	234	97	97	0.42			
25	195	232	94	95	0.30	0.13		
4	85	180	97	95	0.31			
10	160	200	100	100	0.27	<0.03		
20	170	200	99	100	0.06			
26	150	190	93	95	0.13			
22	120	190	110	110	0.12			
19	72	150	96	94	0.17			
1	93	200	90	92				
14	170	210	100	90	0.10			
18	180	200	100	100				
16	160	200	100	90				0.23
17	160	200	90	90			0.37	
13	170	270	100	100				
28	190	190	82	94				

Sample Number	Ca	Ti	Cr	Fe	Ni	Cu	Y	Zr	Gd	Hf
5										
2										
8										
9										
7										
3										
23										
24						48.5				
25						47.7				
4						29.6				
10						18.7				
20			0.025	0.021	<0.03					
26			0.35	1.56	0.27					
22			0.019	0.94	0.19					
19			2.38	7.25	2.37					
1								0.022		
14										
18							0.002			0.005
16									0.020	
17								0.024		0.003
13	0.11	0.14						0.02		0.002
28										

Table 3 - 1 Composition of Well J-13 Water (ref. 9)

| Element or Ion	Concentration (mg/L)
Na	46.
Si	29.
Ca	13.
K	5.
Mg	2.
B	0.13
Al	0.05
HCO_3^-	129.
SO_4^{2-}	18.
NO_3^-	9.
Cl^-	7.
F^-	2.

pH 7.4
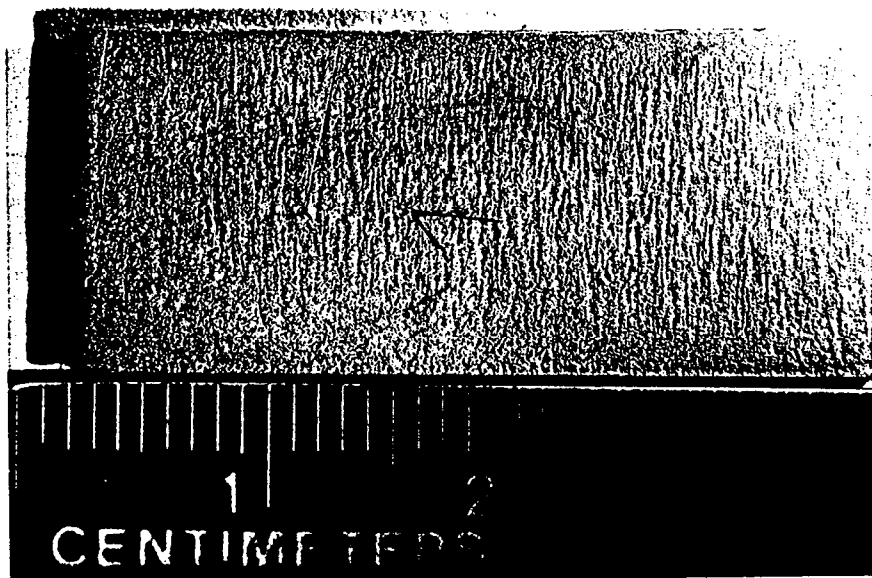
Figure 3 -2. Boral Sample (#3) after Corrosion and Cleaning
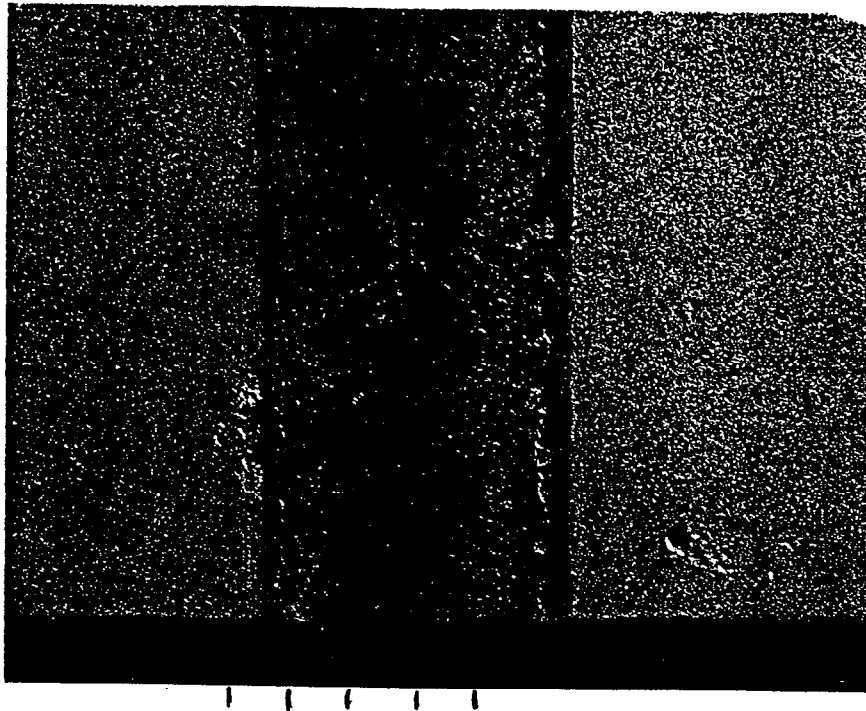
Figure 3 - 3. Weld on Neutrosorb PLUS Sample (#19) after Corrosion
(1-mm divisions on scale at bottom)

Turning to the aluminum metal-based samples (#2, 8, 9, 7 and 3), it can clearly be seen that considerable oxidation of aluminum occurred. The samples were pitted, exhibiting "equivalent" uniform corrosion rates of about 2 mm/y. Aluminum dissolved in the solution, hydrogen gas (presumably) was evolved, and the pH buffer was overwhelmed. The boron concentration in the solution was observed to increase, except in the case of Boralyn. The aluminum observations are consistent with the known behavior of aluminum in acid solutions, as discussed in a previous unpublished paper.[21] For samples #2, 8, and 9, it is understandable why the boron concentration in solution rose, since the boron is primarily in the form of borides in these samples,[22,23] and most borides are soluble in acid solutions.[24] As can be seen from sample #14, however, bulk boron carbide did not dissolve significantly in 96 hours under these experimental conditions. The increase in dissolved boron in the case of Boral (#3), which contains boron primarily as the carbide, must therefore be due to soluble B_2O_3, which is included at small concentrations by the manufacturer[25] in order to assist in passivating the aluminum when the material is used in spent fuel pools. In Boralyn (#7), the B_4C particles are reported by the manufacturer to be coated with a proprietary material.[26]

The A·B sample (#23) performed somewhat better than the aluminum metal-based materials in terms of weight loss, presumably because the aluminum is already oxidized in this material, but the boron loss to the solution was high.

The copper-based samples (#24, 25, 4, and 10) exhibited corrosion rates comparable to those of the aluminum-based samples, but did not overcome the pH buffer. The B_4C-containing copper-based samples (#4 and 10) did not release significant amounts of boron to the solution, again consistent with the bulk B_4C behavior. GlidCop A-15 (#25 and 10) showed somewhat better corrosion resistance than did the pure copper (#24 and 4). The observations with the copper-based samples are consistent with the known behavior of copper in oxidizing acid solutions.[28]

The stainless-steel-based samples (#20, 26, 22, and 19) performed well except for the weld on sample #19, which exhibited knife-line attack along its edge as well as attack on the body of the weld (See Fig. 3). The structure of the weld zone on sample #19 was found by SEM-EDS to consist of dendritic austenite surrounded by a eutectic structure composed of austenite and boride phases, as described by Robino and Cieslak.[28] The corrosion attack appeared to have occurred preferentially on the austenite phase. This is consistent with the low boron concentration observed in the solution and the known resistance of chromium boride to attack by acids.[24]

The chemistry of the solution for sample #19 is complex. Probably the initial yellow-green color of the solution was due to ferrous iron. It can be expected that this would have formed initially during corrosion of the austenite. Oxalic acid is known to stabilize iron in the ferrous state, and oxidations by hydrogen peroxide are generally slow in acid solution.[29] However, ferrous iron eventually will react with hydrogen peroxide to produce (brown) ferric iron, hydroxide ion, and hydroxyl free radical via the Fenton reaction. The hydroxyl free radical in turn will rapidly decompose formic and oxalic acids. Furthermore, ferric iron is a catalyst for the decomposition of hydrogen peroxide into water and oxygen. Hydrogen ions are reduced to hydrogen gas during the corrosion of iron, and the result is an increase in pH. At higher pH ferric iron is less soluble, accounting for the precipitation of hematite (ferric oxide).

The zirconium-hafnium alloy (#1) also performed well, as would be expected considering the low solubility of both metals at the pH used, even allowing for the complexing effect of oxalate on zirconium.[29] Considering that this sample was tested in the batch of solution without the formic acid addition, its solution maintained its pH even better than the control in this batch (#5).

The remaining ceramic samples (#14, 18, 16, 17, and 13) had little impact on their solutions and showed little or no weight loss, with the exception of #13, zirconolite. Its small weight loss was probably due to dissolution of residual starting material that remained unreacted during hot pressing. The elevated oxalate concentration value is within the measurement uncertainty, which was high for this particular sample, and is not considered significant.

Boron carbide is known to be difficult to dissolve. According to Samsonov et al.,[30] boron carbide is stable with respect to acids. Mineral acids, taken individually, practically

do not decompose it under normal conditions. For example, nitric acid oxidizes boron carbide only at relatively high temperatures and under the condition of a continuous return to the reaction mixture of the oxides of nitrogen that are volatilized upon heating."
Gmelin reports that B_4C is stable in the cold against the acids HCl, H_2SO_4, HNO_3, HF, and $HClO_4$ and their mixtures, and fairly stable when hot. Only in 1:1 diluted acids does B_4C show a very slight solubility.[31] Boron carbide has been known to dissolve under neutron and gamma irradiation in reactor cooling water at about 350°C when it has been exposed as a result of failure of control rod cladding.[18] This is consistent with the facts that boron carbide is highly thermodynamically unstable with respect to reaction with oxygen to form boron oxide and carbon dioxide, neutrons produce (n, alpha) reactions which cause atomic displacements in boron carbide, radiolysis of water produces oxidizing conditions, and boron oxide is soluble in water. At 25°C, the free energy of the oxidation reaction is -2,715 kJ/mole.[15]

The hafnium oxide sample was the only one for which no weight change was detected. Only 0.09 ppm of Hf was found in the solution. This is consistent with its very low solubility[32]. The monazite and zircon samples showed barely detectable weight changes. The silicon observed in the solution used with the zircon sample (#17) may have come from the Pyrex vessel or from unreacted SiO_2 in the sample.

No special efforts were made to produce high quality ceramics for this scoping study. Of the ceramics fabricated by us (hafnium oxide, gadolinium monazite, zircon, and zirconolite) the first two were most readily formed by hot pressing. Zircon would better be made by pre-reacting before hot pressing. Making high-quality single-phase zirconolite requires intimate mixing of starting materials on a very fine scale. The excellent performance of these materials in spite of incompletely reacted samples demonstrates their high chemical durability.

3.6 Summary and Conclusions on the Survey of Candidate "Basket Materials"

The desirable properties for waste package and MPC basket materials are reasonable strength, high thermal conductivity, high neutron absorption, easy fabricability, good corrosion performance, and low cost. Of these properties, corrosion performance is uniquely important for long-term criticality control in a geologic repository.

Radiolysis of air and vadose water in a failed waste package over long times could produce significant quantities of several acids and hydrogen peroxide. Short-term scoping corrosion tests of a variety of candidate materials in a solution containing these substances at 90°C showed that both aluminum- and copper-based materials are vulnerable to significant corrosion under these conditions, as expected. Boron-containing stainless steel materials performed well in the absence of welds. The single welded sample tested underwent significant corrosion. Other welded boron-containing stainless steels or the same material welded by a different process or heat treated differently may not show vulnerability to corrosion. Further testing will be required if designs call for welding these

materials.Zirconium-hafnium alloy performed well in the corrosion medium used, as was expected.

Ceramics, including boron carbide, hafnium oxide, gadolinium monazite, zircon (containing hafnium), and zirconolite (containing hafnium) all performed well, even though the samples of the latter two materials were not fully reacted during their fabrication.

The most reliable protection against loss of neutron absorber from waste packages over the long term in a geologic repository is low   solubility of the absorber element used, under the conditions expected. Using this criterion, hafnium is superior to both gadolinium and boron.[31] If boron is to be used, it would be preferable for it to be either in the form of boron carbide or in the form of high-chromium metal borides that are surrounded by a corrosion resistant metal. Boron carbide is highly thermodynamically unstable with respect to reaction with oxygen to produce boron oxide and carbon dioxide, boron oxide is soluble in water, and dissolution of boron carbide has been found to occur in neutron- and gamma-irradiated reactor cooling water at temperatures near 350°C. The rate of dissolution under repository conditions is expected to be low, but cannot be quantified at present. Non-chromium metal borides are generally soluble in acid solution, but higher chromium borides have been found to be resistant to attack.

Future efforts will be directed toward developing better understanding of the long-term corrosion behavior of boron carbide and boron-containing stainless steels under the expected range of conditions, since these materials represent a compromising balance between low-cost but less corrosion resistant materials (such as the Al-base materials) and the highly corrosion resistant but expensive materials (such as Hf). It appears that a significant electrochemical potential difference exists between the boride phase and the austenite matrix, and testing is proposed to characterize these differences. Some of the same techniques used for studying localized corrosion and galvanic corrosion, discussed in Section 2.0 for the Metallic Barriers work, will be used.

Since the time of this survey, it has been pointed out by one of the manufacturers that anodized Boral would be expected to show significantly higher corrosion resistance. Anodized material was not available at the time the survey test was performed. Although anodization improves the corrosion resistance of aluminum in oxidizing environments, like nitric acid, anodization would not appear to offer much increase in the corrosion resistance to chelating agents, like oxalic acid. However, it is intended to re-test the material in the anodized condition to make the evaluation more thorough. A full report is in preparation on the survey. This report will give additional details.

An activity plan has recently been completed [33], and this plan links the scoping work discussed above with planned new work. The new work will focus primarily on boron-stainless steel. Because some of the scoping work indicated an electrochemical effect between the boron-rich phases and the austenite matrix, we have recently attempted to make single metal borides (particularly iron boride and chromium boride) and mixed

borides, corresponding to the structures and stoichiometry observed in the commercial specimens. Electrochemical polarization curves (similar to those described in Section 2.5) were determined, and it appears that the borides are more noble than the austenite matrix and that the chromium borides are more noble than the iron borides. This work is continuing.

References for Section 3.0

1. Van Konynenburg, R. A., McCright, R. D., Roy, A. K., and Jones, D. A., "Engineered Materials Characterization Report," UCRL-ID-119564, Lawrence Livermore National Laboratory, Livermore, CA 94550 (December 1994).

2. TRW Environmental Safety Systems, Inc., "Multi-Purpose Canister (MPC) Implementation Program Conceptual Design Phase Report, Vol. IIA-MPC Conceptual Design Report, Doc. No. A20000000-00811-5705-00002, Rev. 00, TRW, Vienna, VA (September 1994).

3. TRW Environmental Safety Systems, Inc., "Initial Summary Report for Repository/Waste Package Advanced Conceptual Design,"Doc. No. B00000000-01717-5705-00015, Rev. 00, TRW, Vienna, VA (August 1994).

4. Van Konynenburg, R. A., "Waste Package Basket Materials, Scientific Investigation Plan," SIP-CM-02, Lawrence Livermore National Laboratory Yucca Mountain Project, Livermore, CA (March, 1995).

5. TRW Environmental Safety Systems, Inc., "Controlled Design Assumption Document (CDA)," Doc. No. B00000000-01717-4600-00032 Rev. 00A, TRW, Las Vegas, NV (June, 1994).

6. U. S. Nuclear Regulatory Commission, Final rule, federal regulation 10 CFR Part 60, Code of Federal Regulations, U.S. Government Printing Office, Washington, D. C. (1995).

7. Lederer, C. M., and Shirley, V. S., Table of Isotopes , Seventh Ed., John Wiley and Sons, New York (1978).

8.National Research Council, "Ground Water at Yucca Mountain: How High Can It Rise?," National Academy Press, Washington, D.C. (1992).

9. Harrar, J. E., Carley, J. F., Isherwood, W. F., and Raber, E., "Report of the Committee to Review the Use of J-13 Well Water in Nevada Nuclear Waste Storage Investigations," UCID-21867, Lawrence Livermore National Laboratory, Livermore, CA (January, 1990).

10. Lundgren, K., "Radiation Levels and Absorbed Doses Around Copper Canisters Containing Spent LWR Fuel," SKBF KBS Technical Report No. 82-11, SKB, Stockholm, Sweden (1982).

11. Christensen, H., and Bjergbakke, E., "Radiolysis of Ground Water from Spent Fuel," SKBF KBS Technical Report No. 82-18, SKB, Stockholm, Sweden (1982).

12. Reed, D. T., "Progress in Assessing the Effect of Ionizing Radiation on the Anticipated Waste Package Environment at the Yucca Mountain Potential Repository Site," Proceedings of Nuclear Waste Packaging, Focus '91, American Nuclear Society, La Grange Park, IL (1991).

13. Van Konynenburg, R. A., "Radiation Chemical Effects in Experiments to Study the Reaction of Glass in an Environment of Gamma-Irradiated Air, Groundwater, and Tuff", UCRL-53719, Lawrence Livermore National Laboratory, Livermore, CA (May 1986).

14. Barkatt, Aaron, Barkatt, Alisa, and Sousanpour, W., "Gamma Radiolysis of Aqueous Media and Its Effects on the Leaching Processes of Nuclear Waste Disposal Materials," Nucl. Technol. 60, 218 (1983).

15. Dean, J. A., Ed., Lange's Handbook of Chemistry, Thirteenth Ed., McGraw-Hill, New York, (1985).

16. Tipton, C. R., Jr., Ed., Reactor Handbook, Vol. 1, Materials, Second Edition, Interscience Publishers, New York (1960).

17. Ursu, I., Physics and Technology of Nuclear Materials, Pergamon Press, New York (1985).

18. Gupta, C. K., Materials in Nuclear Energy Applications, Vol. II, CRC Press, Boca Raton, FL (1989).

19. Nuclear Waste Policy Act of 1982, Pub. Law 97-425, 96 Stat. 2201, codified at 42 U.S.C. 10101 et seq.

20. American Society for Testing and Materials, "G1-90, Standard Practice for Preparing, Cleaning, and Evaluating Corrosion Test Specimens,"Annual Book of ASTM Standards, ASTM, Philadelphia, PA (1995).

21. Van Konynenburg, R. A., "Corrosion Considerations in Choosing MPC Basket Materials," unpublished white paper dated December 7, 1994, Lawrence Livermore National Laboratory, Livermore, CA.

22. Massalski, T. B., Binary Alloy Phase Diagrams, Second Edition, Vol. 1, p. 123, ASM International, Metals Park, OH (1990).

23. Personal communication with Marvin Wachs, Eagle-Picher Industries (August 24, 1995).

24. Trotman-Dickenson, A. F., Exec. Ed., Comprehensive Inorganic Chemistry, Vol. 1, pp. 727-8, Pergamon Press, New York (1973).

25. Personal communication with Bruce Jansen, AAR Advanced Structures (August 23, 1995).

26. Personal communication with Robin Carden, Alyn Corp. (August 23, 1995).

27. Uhlig, H. H., and Revie, R. W., Corrosion and Corrosion Control, Third Ed., John Wiley and Sons, New York (1985).

28. Robino, C. V., and Cieslak, M. J., "High-Temperature Metallurgy of Advanced Borated Stainless Steels," Met. and Mat. Trans. A, 26A, 1673-1685 (1995).

29. Cotton, F. A., and Wilkinson, G., Advanced Inorganic Chemistry, Fifth Ed., John Wiley and Sons, New York (1988).

30. Samsonov, G. V., Markovskii, L. Ya., Zhigach, A. F., and Valyashko, M. G., "Boron, Its Compounds and Alloys", AEC-tr-5032 (Book 1) U. S. Atomic Energy Commission, Washington, DC (1960), translated from a publication of the Publishing House of the Academy of Sciences of the Ukranian S.S.R., Kiev (1960).

31. Amberger, E. and Stumpf, W., "Boron, Supplemental Volume 2: Elemental Boron and Boron Carbides," Gmelin Handbook of Inorganic Chemistry, K. Buschbeck, Ed., Springer-Verlag, Berlin (1981), p. 189.

32. Pourbaix, M., <u>Atlas of Electrochemical Equilibria in Aqueous Solutions,</u> Pergamon Press, New York (1966).

33. Van Konynenburg, R. A. Yucca Mountain Project Activity Plan, Scoping Experiments; Long-Term Corrosion Testing and Properties Evaluation of Candidate Waste package Basket Materials, AP-CM-002.2/02.3, Lawrence Livermore Laboratory, 1996.

4.0 Backfill, Packing and Invert Materials

(this section contains excerpted input provided by Annemarie Meike and William Glassley)

Backfill materials may be used to engineer a number of effects including controlled radionuclide release and enhanced containment lifetime. In this context, backfill and packing are used interchangeably. Controlled radionuclide release may be achieved by a number of different processes. These include the provision for:

(1) solid surface area for radionuclide sorption and retardation (example: zeolites as an ion exchanger plus ion sorber),
(2) chemical conditions that retard dissolution and thus the release of certain radionuclide species (example: for neptunium, a conditioned backfill that creates chemically reducing conditions),
(3) chemical species that react with certain radionuclides (example: Ca $^{14}CO_3$) to form precipitates, a barrier to water flow, or radionuclide transport by advective flow, and
(4) low saturation and connectivity conditions that control diffusive transport

All of these provisions need to be considered over a range of temperatures since, at elevated temperatures, some may be more effective; others, less effective.

It is important to note that backfill may have beneficial and non-beneficial effects on performance of the EBS. For example, the presence of backfill raises the waste package container surface temperatures. The beneficial effects would be to prolong the dry-out period and the period of no microbial activity, and the duration of the low temperature oxidation degradation mode on the metal container (See Section 2.3). As a consequence, degradation can be minimized provided the container temperature does not become too high and cause excessive oxidation.

In FY-96, the YMP is conducting a number of studies to determine whether a backfill should be incorporated into a repository design strategy that could be applied to Yucca Mountain. In this assessment, it is important to show that the backfill repository design significantly outperforms a design in which no backfill is used. The Systems Engineering WBS is in the process of assembling a report on use of backfill materials in the repository. Much of the material presented below on using a chemically conditioned backfill will also appear in that report.

4.1 Chemical Modeling of Backfill Additives

Thermodynamic databases are available for chemical modeling of a conditioned backfill.. It is possible that the appropriate choices of conditioned backfill may promote container lifetime by buffering pH to the alkaline range. However, some aspects of the presence of a backfill may not be beneficial. For example, backfill may produce conditions such as micro-environments in which crevicing or pitting of the metal surface is favored. The

backfill may also form a substrate for the migration and re-entry of microbes once environmental conditions favor their propagation. Furthermore, the backfill may provide a medium for capillary or wicking effects, drawing water to the container surface and enhancing corrosion.

The purpose of applying sophisticated modeling capabilities to backfill material design is to determine whether the designed engineering functions are satisfied. For instance, it is critical to demonstrate that the timing of chemical conditioning effects coincides with the need for that effect. Chemical effects that control radionuclide release must be in effect after the containers are breached. The models are also used to define bounding conditions and degrees of uncertainty. Modeling can assist in the identification of issues critical to the effectiveness of the material to perform the desired function.

The chemical modeling effort centered on a backfill comprised of magnetite, lime, and quartz sand in a molar ratio of 80:15:5. The purpose of the magnetite is to reduce the E_h of the environment, while that of the lime is to buffer the pH to the alkaline region. Quartz sand is considered an ideal backfill medium, because compared to crushed Topopah Spring tuff, it has no internal porosity and would therefore not likely act as a wick to attract water.

The EQ3/6 geochemical code was used to estimate the pH, Eh, mineral assemblage, and water chemistry as a function of time. This code is based on the thermodynamic properties of the various reacting species. The OS3D/GIMRT reactive transport code was used to simulate chemical changes in an aqueous fluid as it moves through a porous medium. This code therefore provides a model of the time dependent evolution as a function of flow rate, thermal gradient, and water chemistry. Three aqueous chemistries were used in the simulation: one fluid was J-13 well water, which is believed representative of the groundwaters associated with the repository horizon; the second fluid was one approximating the chemical characteristics of groundwater that equilibrates with concrete used in repository construction; and third, a brine equilibrated with concrete, the salts in the brine being the result of repeated evaporations of groundwater due to heat generated in the repository.

Physically, the exposure of the waste packages to oxygen, carbon dioxide, and other atmospheric gases is limited by two possibilities. Either the drifts are ventilated mechanically or naturally through rock fractures or the drifts are "closed" and unventilated. This distinction is important, because in the ventilated system the gas composition and fugacities remain constant and in the unventilated system they change with time due to reaction with the backfill. In the transport models, two cases were used. In one case, the precipitated minerals remained in the system and continued to react with the aqueous phase. In the other case, they were allowed to leave the repository system.

4.2 Conclusions from the Simulations Studies on Chemical Additions to Backfill

Several combinations of conditions were run using the two codes. The simulations demonstrated that a backfill composed of quartz sand, magnetite, and lime will not control oxygen fugacity of pH unless the drifts are completely sealed. Even then, the chemical conditioning effects would be minor, and would probably not achieve the engineering goals. Substituting elemental iron (as a powder) for magnetite gave essentially the same results. All of the chemical evolution takes place and the conditioners are expended within a matter of decades, which is insignificant with respect to the repository time frame. Given the other potentially negative effects of backfill, it is concluded that these additives to backfill may not add any beneficial effects, but may add complexity to the EBS and, consequently, increase uncertainty. Other chemical additives, particularly certain other metal oxides and sulfides, have been considered, and from a thermodynamic sense, they may be functional over long time periods. However, they are much more costly than iron or lime, and in the case of the metal sulfides, would provide a medium for microbiological activity.

This work on chemical conditioning of backfill materials was reported in a much larger report on the feasibility of using backfills in the Yucca Mountain repository[1]. That work should be consulted for more details about the calculated chemical effects and their change with time.

4.3 Future Work

The rather strong negative demonstration that chemical additives to backfill will not be effective when they are needed curtails further work in this area. Attention is expected to be turned, in FY-97, toward the invert material and what its formulation should be. Use of concrete and cementitious material as part of the invert (and also as part of the drift support structure) will likely condition the near-field environment around the waste package in the short term, but the long-term effects are what matters. Work is proposed (in conjunction with WBS 1.2.3) on determining the thermal and chemical stability of concrete materials using both experimental and modeling approaches. This work is described in an activity plan, which is in preparation.

Reference for Section 4.0

(1) M. A. Balady, Engineered Barrier System Performance Requirements Systems Study Report, BB0000000-1717-5706-00001, rev.00A, Civilian Radioactive Waste Management system, Management and Operating Contractor, draft report, August 1996.

5.0 Non-Metallic Materials

(input to this section of the report is based on information originally generated by Keith Wilfinger)

At various times, the YMP has considered an alternative waste package design where one of the barriers is a ceramic or other non-metallic material. Ceramic materials offer an important advantage in their chemical similarity to minerals in the host rock so that arguments on their long-term stability are based on thermodynamics rather than kinetics, as is the case for all of the candidate metallic materials. A report was prepared in 1995 [1] that summarized the benefits and limitations of non-metallic barriers and the state of the technology in manufacturing these barriers to the dimensions of a waste package. Since that time, the YMP sponsorship of the work has been discontinued, but at the time of this writing (late August 1996), there are plans to revive the effort.

Some excerpts have been taken from the Wilfinger report in order to present the status of a non-metallic barrier. Most of the evaluation has centered around ceramic materials. The evaluation considered using ceramic materials as a coating applied to a metal barrier and using ceramic materials (and other non-metals such as graphite) as a self-supporting liner as part of a multiple barrier waste package. In both instances, the intent was to combine the best feature of chemical inertness of the ceramic with the fracture toughness of the metal.

5.1 Concerns with Ceramic Materials

All ceramic engineering materials are brittle compared with the candidate metals. Ceramics do not undergo measurable plastic deformation under load at the expected repository temperatures. Ceramics can be deformed only fractionally before exceeding their elastic limit, leading to typically catastrophic fracture. Fracture strength and impact resistance are therefore of greater importance for ceramic packages than for metals, hence the emphasis on using both classes of materials in a waste package design. In order to provide resistance to slow crack propagation during long periods under static loading, a high fracture toughness is necessary. In a combined metal-ceramic package, the metal will provide support to the ceramic. However, the strength of ceramics should not be discounted, because of improved material properties and high toughness microstructures developed in recent years. Also, ceramic materials can be pre-loaded for fracture resistance. Thermal treatment and differences in thermal expansion between components can be used to put a ceramic liner in compression, thereby making it very resistant to fracture, which is inherently a tensile process. It would then be possible for corrosion processes to open gaps in the metal without exposing the waste form.

Another concern is porosity. Some ceramics are quite porous, depending on the specific forming route and temperature. Ideally, the fabricated material should have no connected porosity and be crack free. This is necessary to prevent inward penetration of water (or water vapor) and outward migration of gaseous or ionic radionuclides. Generally, if a

material is 94% of theoretical density or greater, the porosity is isolated rather than continuous. But even isolated porosity should be avoided, because of its small adverse effect on heat transfer and its much larger adverse effect on mechanical properties.

Joints or seals (such as those on a liner) must provide similar protection as the rest of the ceramic. The number of such joints and closures should be minimized, since each presents a potential weak spot in the barrier system. The report went on to discuss various ways of joining ceramics (such as using compatible metal brazes). However, joining is one of the main limitations in making a stand-alone ceramic barrier. The problem is eliminated if a ceramic coated product is used.

Although many ceramic materials are expected to be chemically inert in the repository environments, preference is given to a ceramic with a simple formulation, natural analogs, and only a single continuous phase. The ceramic also needs adequate thermal conductivity to maintain design limiting temperatures (e.g. 500°C centerline glass temperature and 350° C spent fuel temperature) inside the container.

From engineering considerations, ceramics must be fabricable in the desired form using conventional techniques or by a reasonable adaptation of existing technology. Production of fully dense monolithic ceramics in the required sizes is presently uncommon. Quality control on a production basis is another concern. Cost must also be given its due. Given sufficient time and investment, any single object can probably be produced, but the process must be economically and technically reasonable for manufacturing large numbers of parts.

5.2 Candidate Materials

The report considered a number of materials: alumina, zirconia, silicon carbide, silicate materials, spinel (magnesium aluminate), glass-ceramics (also a group of silicates), graphite, and titania.

Alumina, especially in the alpha phase, is attractive as a candidate material since it "matches" many of the minerals found in welded tuff. Alumina is well characterized and can be formed into relatively large, dense, and impervious objects. Pieces of alumina can be joined by brazing, using a bonding glass, or by diffusion bonding. When quenched rapidly, as in thermal spraying, alumina retains a metastable gamma structure that can subsequently be annealed to form the alpha phase. Alumina is chemically stable in moderately acidic conditions.

Partially stabilized zirconia (PSZ) consists of relatively large grains of stabilized cubic zirconia containing sub-micron precipitates of metastable tetragonal zirconia. Stabilizing additions are yttria, calcia, magnesia or rare earth oxides. The advantage of PSZ is that the unstabilized tetragonal precipitates can be induced to transform martensitically to the less compact, stable monoclinic structure when stressed, thereby creating a counter-stress that opposes crack propagation. Zirconia is also chemically resistant to acidic

environments. Micron scale zirconia can be incorporated in an alumina structure to act in much the same way as the precipitates in PSZ. This can allow some of the improved properties of a toughened ceramic without paying the full cost penalty of using zirconia alone.

Silicon carbide is light-weight, very strong, tough, refractory ceramic that is chemically resistant to both caustic and acidic environments. It is protected by an SiO_2 "skin" when exposed to oxidizing environments. Unfortunately, sintered silicon carbide is rather difficult to densify.

Silicate materials also have a natural analog in the welded tuff mineral assemblage. Many silicate materials are manufactured and contain other oxides, as in mullite (alumina and silica), forsterite (magnesia and silica), and cordierite (magnesia, alumina and silica). Most silicates tend to have a significant vitreous (glassy) component and a low thermal conductivity. Additions of alumina, magnesia, and boria make for a more refractory and chemically resistant glass. The presence of a glassy phase offers considerable advantages in ease of forming dense, impervious ceramics. However, a glassy phase can also reduce mechanical strength and toughness, more or less in proportion to the amount of glass. "Glass-ceramics" are a sub-class of the group of silicates, but exhibiting some unique properties. Early in their processing, glass-ceramic materials are completely glassy, and as such may be worked using conventional glass handling techniques. The finished shape is then crystallized by proper heat treatment, resulting in a fine-grained, polycrystalline ceramic with virtually no porosity and little or no residual glass. After crystallization, many glass-ceramics are at least twice as strong as glasses of the same composition. However, with present technology, it would be difficult to fabricate a thin-walled glass container in the required size for a waste package liner and then support it while it undergoes heat treatment.

Titania is a light, moderately strong, chemically inert and moderately refractory polycrystalline ceramic. However, it is more expensive than alumina and has a slightly higher thermal expansion. Some aluminum titanate compositions have been developed and these have a low overall thermal expansion.

Commercial graphite consists of crystalline graphite in an amorphous carbon matrix. Current technology allows it to be molded and extruded in large sizes. On the negative side, commerical graphite is both typically porous (generally around 80% dense) and structurally weak. Graphite can be rendered gas tight and impermeable, but this requires a large scale chemical vapor deposition process to fill the pores with silicon carbide.

Spinels are structurally similar, mixed oxide ceramics. One spinel in particular, magnesium aluminate ($MgAl_2O_4$), may be useful in the context of a waste package. In most respects, the properties of this spinel resemble those of aluminum oxide. It differs from alumina in one very important way, however; it is not subject to the $\gamma \rightarrow \alpha$ transition after thermal spray. This makes the spinel less subject to cracking during high temperature annealing than an alumina coating.

5.3 Candidate Processes

The state of technology in the ceramic processing industry was reviewed in the report, and the report lists several manufacturers of make ceramic products. The report discussed several ways of making and joining ceramic pieces to produce a monolith which could function as a liner for one of the barriers. The report also discussed ways of applying a ceramic material as a coating on one of the metal barriers. Two approaches were recommended for further study:

1. A self-supported, impervious ceramic liner could be put between metallic shells. The liner would be cold isostatically pressed, green machined blocks that would then be sintered and diffusion bonded. Closure would be accomplished mechanically, in conjunction with a thermal sprayed outer coating to develop an acceptable seal. Metallizations and brazes could be used instead, but credit for performance would then be limited to the properties of the closure material.

2. A thermal spray coating could be applied to a metal container, producing a relatively thin, dense layer that should prevent it from corroding under repository conditions. Magnesium aluminate spinel offers most of the benefits of alumina in this application, but is not subject to thermal transformation. This type of construction probably poses the least overall risk of failure. Modern thermal spray techniques could also allow the fabrication of free standing or coated ceramic waste container using a single basic process and may allow a seamless method to accomplish final closure.

5.4 Prospect and Plans for Thermally Sprayed Ceramics

The thermal spray technique to apply a ceramic coating onto a steel (or other metal) container appears the most feasible approach, since it largely overcomes the limitations imposed by joining pieces of ceramic. The thermal spray could be performed remotely on a filled waste container.

Thermal spray coating are formed by spraying a metal container with ceramic powder melted in an electric arc (plasma spray) of flame (flame spray, HVOF, D-Gun techniques). The molten droplets spread and cool rapidly when they impact the substrate, creating a continuous, solid layer. Thermal spray techniques allow the formation of polycrystalline coatings that are more refractory than enamels, since the substrate does not have to be heated to the melting point of the ceramic. The application can be made thicker by making multiple passes over the same area, allowing it to be used either inside or outside the metal structure. In general, thermal-sprayed ceramic coatings have been typically porous, achieving a maximum of about 90% of theoretical density. These coatings would be subject to penetration by moisture. Recently, with the advent of high velocity oxyfuel (HVOF) and detonation (D-gun) type sprayers, manufacturers have claimed densities in the range of 98-100% of theoretical density. Lower melting formulations tend to have the lowest porosity, but at the expense of a reduction in

material properties. Although zirconia can be thermally sprayed, it typically does not approach full density because it is so refractory. The density of all thermally sprayed coatings can be improved by careful control of feedstock and spraying conditions, but complete melting of the sprayed particulates is a requirement for the densest coatings.

A potential problem is brought about by the rapid quenching of the sprayed droplets, sometimes resulting in metastable phases. Alumina, for example, does not generally solidify to the α-structure on rapid cooling, but rather forms the transitional γ-phase. This results in greatly reduced thermal conductivity. Subsequent transition to the α form results from reheating above 1000 °C, leaving a more compact structure than the γ-phase. Post coating heat/pressure treatments are sometimes used to densify thermally sprayed ceramic coatings, but the substrate properties determine the maximum temperature to which the coated object can be heated. These operations would prove challenging to perform in a remotely-operated facility. In most applications, coatings are considered "thick" when they exceed one millimeter. However, thermal sprayed structures up to 80 mm thick have been made successfully. Robotic systems can be constructed to apply coatings to the interior or the exterior of large vessels. Sealing of an interior coating remains an issue, but an exterior coating on a metal vessel could be made to provide a "seamless" closure. Some manufacturers claim to be able to deposit α-alumina rather than the usual γ.

Plans for making and evaluating thermally sprayed coatings have been formulated for FY-97. These include making laboratory-scale plasma sprayed alumina and magnesium aluminate spinel coatings on carbon steel and then measuring the porosity, mechanical properties, and bonding to the metal substrate. The coated products would then be exposed in a suitable aggressive medium to determine their corrosion resistance. Also, physical and mechanical properties important to evaluating the integrity and durability of the coating will be measured. These properties include the porosity of the coating and the impact energy needed to break the coating.

Reference for Section 5.0

[1] K. Wilfinger, "Ceramic Package Fabrication for YMP Nuclear Waste Disposal", LLNL report UCRL-ID-118660, June 1995.

Acknowledgments